Shape Characterisation of Sheet Metal Assembly Variation with a View to Quality Assessment and Dimensional Control

Timothy Ian Matuszyk

April 2008

A thesis submitted for the degree of Doctor of Philosophy
of the Australian National University

To my family

Declaration

The work in this thesis is my own except where otherwise stated.

Timothy Ian Matuszyk

Publications

- Matuszyk, T, I., Cardew-Hall, M, J., and Rolfe, B, F. (2006). Observing dimensional variation in an automotive sheet-metal sub-assembly. In *Proceedings of the Society of Automotive Engineers 2006 World Congress, April 3-7, 2006-01-1635, Detroit, Michigan.*

- Matuszyk, T, I., Cardew-Hall, M, J., and Rolfe, B, F. (2007). The effect of clamping sequence on dimensional variability in sheet-metal assembly. In *Proceedings of the International Conference on Manufacturing Automation, May 28-30, National University of Singapore.*

- Matuszyk, T, I., Cardew-Hall, M, J., and Rolfe, B, F. (2007). The effect of clamping sequence on dimensional variability in sheet-metal assembly. *Journal of Virtual and Physical Prototyping.* 2(3):161-171.

- Cardew-Hall, M, J., Matuszyk, T. I., and Rolfe, B. F. (2008) Local shape characterisation of sheet metal assemblies. In *6th CIRP International Conference on Intelligent Computation in Manufacturing Engineering, July 23-25, Naples, Italy.*

- Matuszyk, T, I., Cardew-Hall, M, J., and Rolfe, B, F. (2008). The kernel density estimate/point distribution model (KDE-PDM) for statistical shape modeling of automotive stampings and assemblies. *Journal of Robotics and Computer-Integrated Manufacturing.* (review pending).

- Matuszyk, T, I., Cardew-Hall, M, J., and Rolfe, B, F. (2008). Experimental comparison of sheet metal assembly clamping sequences. *Journal of Manufacturing Science and Engineering*. (review pending).

Acknowledgements

I d like to thank my family for being so supportive: my grandpa Stefan, my dad Eugene, my mum Dina, my sister Leanne, my brother Andre, my father-in-law Soo-san, my mother-in-law Ok-yeon, my sister-in-law Hyun-joo, my brother-in-law Joo-hyung, and in particular I would like to thank my loving wife Kyung-ah for her support during my studies and life in general.

I d like to thank my academic supervisors Professor Michael Cardew-Hall and Dr Bernard Rolfe for giving me such a fantastic opportunity and for their much valued guidance.

I d like to thank all the University people who helped me out in some way over the years: Jeremy Smith in particular for helping me out during my time down at Geelong; Dr Shankar Kalyanasundaram for the handy APAC quota; Professor John Duncan for assisting me with the analytical examples; Greg Burgess and Dr Keith Lovegrove for resolving the scanner troubles; Rob Gresham, Ben Nash, and Dave Tychsen-Smith for their technical expertise; Dr Matthew Doolan for his technical advice and proof reading; Dr Teddy Mantoro, and Andrew Wilkinson; Helen Shelper, Pam Shakespeare, Marie Katselas, Kitti Whitworth; Srinivas Shridharan, Dave Ferrari, Oday Jerew, Bijaya Paudyal, Sawat Paitoonsurikarn, Kumar Kc, Huan Zhang, Piya Siangsukone; Bob Forrester, Professor Stephen Roberts, Professor Qinghua Qin, Erasmo Scipione, Ian McRobert, John Smeltink, Victor Pantano, Josephine Farmer, Paul Pounds, Mark Euston, Milli Styles, James Sinclair, Linden Coot, and many others.

I d like to thank all of the people down at Ford of Australia who helped support this work: my industry supervisor Reinhard Muecke for his much valued guidance and for making the industry trials happen, Brendon Boyd and Andrea Cavallaro for their supervision early on in the project; the various plant managers who supported the STAMP program - Andrew Higginbotham, Dave French, and Ben Rumble; the Technical Inspection team - Peter Jenkinson and Chris Wickens for finding the time for my studies, Glenn Rush, Peter Ilijevski, and Mark Vials for performing the measurements,

and Gary Williams, Andrew Hill, Petar Miletic, John Clark, and Martin Trewhella; Vinko Saric, Santosh Nadig, and John Robertson for arranging sheet metal for my experimental trials; Neil Blick and Shridahr Padaki for using manual CMM s for my first measurement study; Scott Randall and Darren Scott for getting my final trials done; the front-cross afternoon shift staff - Yolanda, Kevin, Beryll and Gill; the US people who hosted me during my 2006 visit - Janice Gall, Doug Heerema, and Jim Darkangelo; Paul Dunn and Mike Marshall for introducing me to the plant; Jasna Pavic for her work and help with the front cross; Graham Hughes for his technical support; David Law and Peter Caddy for giving me access to the iges files; Ken McCarthy and Tony Chick for their training courses; and also Trevor Bennion, Marina Krasic, Brenden Eeles, Joel Bird, Victor Schielke, Chris Wilson, Gerard Kolotelo, Jemma Wayth, Suzanne Hurst, Richard Stoljinski, Peter Hutchinson, Ralph Smith, Geoff Hughes, Barry Hunter, Adrian Dowdell, Darko Kraljevic, Wally Lakey, Barry Johnston, Vic Sesar and many others.

I d also importantly like to thank the Australian Research Council for their funding (ARC Linkage Grant #LP0560908).

Abstract

Sheet metal assembly is a complex process involving component-to-component and component-to-tooling interactions. A key characteristic of sheet metal assemblies, the flexibility of components, means that variation does not stack-up according to the additive theorem of variance that applies to rigid bodies. Instead, components can be bent and distorted into conforming or non-conforming shapes by assembly interactions. This characteristic of flexibility also means that in comparison to rigid body assembly, additional aspects of the assembly process, such as clamp sequence and weld sequence, can influence the way in which variation propagates. Through a detailed understanding of the influence of assembly processes on variation propagation, manufacturers can adjust their processes to target particular quality assessment criteria: in this thesis, it is firstly demonstrated how assembly processes such as clamping sequence can be altered to control different variation patterns (and therefore quality) in sheet metal assemblies.

However, in order to truly optimise a sheet metal assembly process for dimensional control, there must be a well defined quality assessment framework from which to select the best processes. The most commonly adopted measures of assembly quality are based on the mean and standard deviation of a set of assumedly statistically independent measurement points. Such approaches are perhaps not the best measure of assembly quality. This is primarily due to their inability to adequately capture a key characteristic of assemblies: correlated variation patterns.

This thesis proposes that assembly quality cannot be simply assessed by the mean and variance of a set of assumedly statistically independent measurement points, and that correlated variation patterns in the form of bows, buckles, twists and ripples also form a large part of assembly quality perceptions. Two key methods were therefore developed to better characterise assembly variation: the multivariate statistical shape model, and the local shape descriptors. These shape charaterisation measures overcome key limitations of existing univariate quality measures including an inability to capture correlated variation patterns, monitor non-normally distributed data, interpret high dimensional data, and measure local variation patterns of different sizes or scales. Through addressing these limitations, the proposed shape characterisation methods

provide significant advancements in the ability of manufacturers to accurately measure variation and discriminate between differing levels of assembly quality, and are particularly well suited for the interpretation of high dimensional measurement data made available by optical co-ordinate measuring machines. The new shape characterisation methods therefore provide a framework for achieving new levels of quality assessment, with a view to the ultimate goal of developing optimal dimensional control strategies for sheet metal assemblies.

Contents

Chapter 1

Introduction

1.1 Dimensional variation in sheet metal assembly

Success in the automotive industry is largely dependent on creating high levels of customer perceptions of vehicle quality. This can be seen through the inattentiveness of US automotive manufacturers to quality in the 70 s and 80 s that resulted in significant growth of higher quality overseas manufacturers (Keller, 1989). In 1990, Wu and Hu claimed:

> The dimensional quality of an automobile body determines the functionality, fitness and customer perception of the quality of the vehicle.

While obvious initial observations such as large flushness gaps or poor closure fits can adversely affect customer perceptions of vehicle quality, there are additional issues to consider stemming from dimensional variation. A 1998 CONSAD study identified how increased dimensional quality of vehicles leads to production cost savings via improved labor productivity and reduced waste, and creates ongoing maintenance savings through a reduced likelihood of warranty claims. Dimensional control of the body assembly process is therefore a vital area of focus for manufacturers as they aim to establish and maintain high levels of customer perceptions of quality of their vehicles, and ultimately remain competitive in an increasingly competitive landscape. In its broadest sense, this thesis is aimed at providing a framework of tools that will enable manufacturers to implement smarter assembly approaches for the control of dimensional variation. Before proceeding to detail the contributions of this thesis, it is first important to contextualize the key problems at hand. In this section, an introduction to variation and tolerances, the sheet metal assembly process, and important characteristics of assembly variation propagation (or stack-up) will be presented. Later sections will then move on to address the key motivational factors and aims of this thesis.

1.1.1 Variation and tolerances

Variation is an unavoidable, natural part of manufacturing processes, but it can be controlled to differing levels depending on the manufacturer s understanding of the process and the amount of resources they are willing to use in this effort. The process of deciding what levels of variation are allowable in a finished product is based upon functionality, desired quality level, manufacturing capability, and cost of manufacture, and is often an iterative process requiring ongoing revisions. In terms of dimensional variation, tolerances are the criteria against which products are assessed; they are the dimensional variation limits stating the maximum allowable variation of a product if it is to meet design specifications. The process of assigning tolerances as described by Daniel in 1998 is illustrated in Figure 1.1. Firstly, dimensions are assigned for a product after which initial tolerances are specified based on functional requirements. Tolerances are then verified to see if they are achievable. If the specified tolerance is achievable then these tolerances will form variation guidelines for production. If tolerances are not achievable, then the tolerances need to be revised, and/or the design or process needs to be improved.

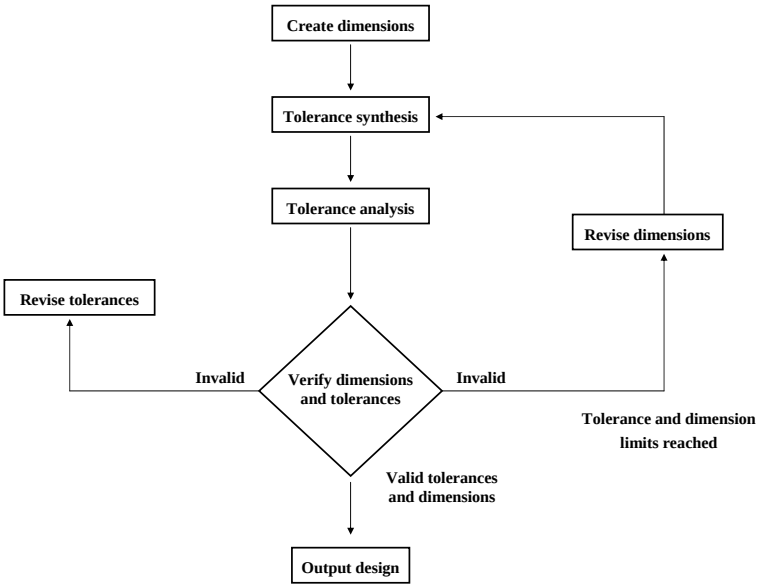

Figure 1.1: The process of allocating tolerances for process monitoring guidelines (Daniel, 1998).

The study of how variation accumulates through the assembly process is necessary in order to accurately assign tolerances. Without proper assignment of tolerances,

manufacturers might waste valuable resources in attempts to meet unreachable quality targets, or conversely the quality of products might suffer due to overly loose tolerancing criteria. Tolerance stack-up in rigid component assemblies can be calculated through the additive theorem of variance (Glancy and Chase, 1999). This law does not generally apply to flexible component assemblies, such as stamped sheet metal assemblies, due to the ability of components to distort into conforming or non-conforming shapes (Takezawa, 1980). Sheet metal assembly therefore presents additional challenges in the assignment of accurate tolerances due to the complex tolerance stack-up resulting from flexible component deformations and interactions.

1.1.2 The sheet metal assembly process

Sheet metal assembly is an iterative process, where stamped panels are joined together to form sub-assemblies, sub-assemblies joined together to form assemblies, until the final Body-In-White (BIW) structure is created. The joining process can be broken down into four key stages: *place*, *clamp*, $fasten/weld$, and *release* (Chang and Gossard, 1997). The *place* cycle refers to the locating and positioning of components on an assembly fixture by a set of locating pins and rest surfaces. The *clamp* stage refers to the application of clamps to hold the workpiece in place for the assembly process. The *weld* stage involves a series of resistance spot welds that join the components together. Finally, the fixture clamps are released, with the newly built assembly ready for the next assembly cycle. This assembly process is illustrated in Figure 1.2.

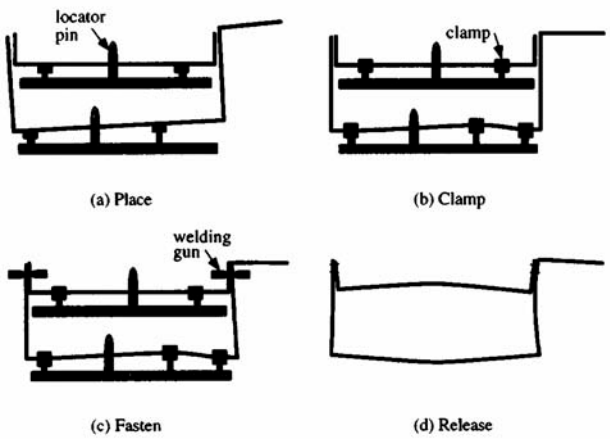

Figure 1.2: The *place*, *clamp*, $fasten$, *release* cycle (Chang and Gossard, 1997).

As stated earlier, due to the flexibility of assembly components, tooling to part and part to part interactions can bend and distort assembly components. The *place*, *clamp*, $fasten$, *release* cycle (PCFR) presented in Figure 1.2 also illustrates this behaviour.

1.1.3 Automotive sheet metal build approaches

The approach to sheet metal assembly differs significantly between car manufacturers as there is not an established and proven best method. The two most common methods used in industry are the Net Build and Functional Build approaches. The Net Build approach involves first evaluating the quality of individual components based on strict conformance to specification requirements. Under this approach, the main assumption is that the quality of an assembly will ultimately be optimised if the quality of the individual components is maximized. The Functional Build approach is where components are approved based on their ability to produce an acceptable assembly, and not solely on their conformance to original part print specifications (Hammet et al., 1999). This approach is mainly applied to sheet metal assemblies, where studies have shown that unacceptable parts can be assembled into acceptable assemblies and vice-versa (Majeske and Hammett, 2000). Some manufacturers therefore use the Functional Build approach to deal with an inability to accurately understand and predict tolerance stack-up in sheet metal assemblies.

1.1.4 A simple assembly model

In order to illustrate key differences in variation propagation between rigid and non-rigid component assembly, two simple analytical examples are compared. Both examples consist of a two component assembly. One feature is monitored on each component, with the standard deviation of the measured features (or measurement points) given as 1 mm. The standard deviations of the components are then compared to the standard deviation of the corresponding assembly measurement point for each example assembly.

Rigid component assembly

Rigid component variation stack-up can be modelled by the additive theorem of variance. Here, the variation of an assembly measurement point is equal to the root-sum-of-squares of the variation of its components. A simple two piece assembly is illustrated in Figure 1.3.

The width of the final assembly is equal to the sum of the widths of each block.

$$d_3 = d_1 + d_2 \tag{1.1}$$

Assuming the two random variables d_1 and d_2 are statistically independent, the assembly mean and variance can be calculated from equation (1.3).

$$\mu_3 = \mu_1 + \mu_2 \tag{1.2}$$

$$\sigma_3^2 = \sigma_1^2 + \sigma_2^2 \tag{1.3}$$

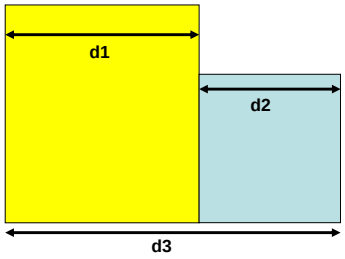

Figure 1.3: A simple two block assembly.

Given that the standard deviation for each block is 1 mm, the final assembly standard deviation σ_3 can be calculated. It can be seen that for rigid component assemblies, assembly variation is greater than the variation of its components, but less than the sum of the variation of the individual components.

$$\sigma_3 = \sqrt{\sigma_1^2 + \sigma_2^2} = \sqrt{1^2 + 1^2} = 1.4mm \tag{1.4}$$

Non-rigid component assembly

In order to model variation stack-up in non-rigid component assemblies, the flexibility of the assembly components must be captured. In this section, a simple two piece cantilevered beam assembly model is used to illustrate variation propagation in non-rigid assemblies. This is a similar approach to the models presented by Liu and Hu in 1995. The analytical model is representative of the two piece assembly presented in Figure 1.4, which is similar to assemblies investigated in later chapters. The top hat is 1000 mm long, the flanges are 25 mm, height is 50 mm, and the top channel width is 65 mm. The bottom plate is 135 mm wide and 1000 mm long for this example. Sheet metal thickness is 0.85 mm for both parts. Note that the assumption of small deformations are assumed for this model.

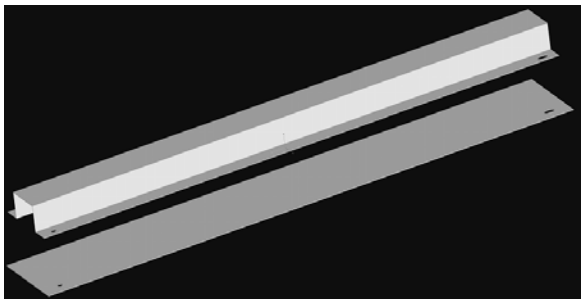

Figure 1.4: Hat section and bottom plate.

The analytical model of the above assembly is described as follows. Consider a case where the top hat and bottom plate both have a uniform curvature, resulting in some displacements (d_H and d_P) from the nominal design at either end. Due to symmetry of the assembly, two cantilever beams half the length of the assembly illustrated in Figure 1.4 are adequate representations of the setup. The assembly process involves a *place*, *clamp*, *fasten*, *release* cycle (PCFR). Figure 1.5 represents the first stage in the assembly cycle, where the parts are located for assembly.

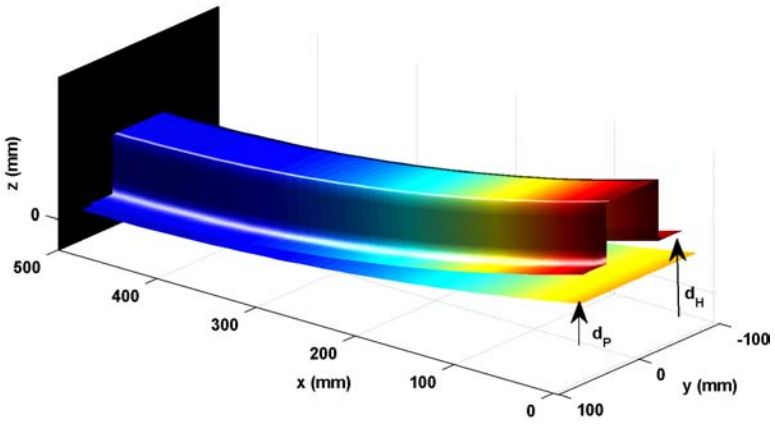

Figure 1.5: Hat and plate with initial uniform bows resulting in end displacements.

The second stage of the assembly process, *clamp*, can be modelled as follows. Consider a moment applied at the end of the top hat to make it lie flat in the nominal position. This moment can be seen to simulate the application of a number of clamps along the length of the hat to hold/position the assembly for the welding process. Similarly, a moment can be applied to the bottom plate. The moments required to make a beam lie flat can be calculated using a basic mechanics equation (Craig, 1999):

$$M_y = \frac{2EI_y d}{l^2} \tag{1.5}$$

where M_y = Moment, E = Young s modulus, I_y = second moment of area, d = initial end deflection, and l = length of the cantilever beam (500 mm). Note that the y subscripts denote that moments and second moments of area are calculated about an axis of rotation parallel to the y axis. Moments for the top hat and bottom plate are therefore calculated as follows:

$$M_{yH} = \frac{2EI_{yH} d_H}{l^2} \tag{1.6}$$

$$M_{yP} = \frac{2EI_{yP} d_P}{l^2} \tag{1.7}$$

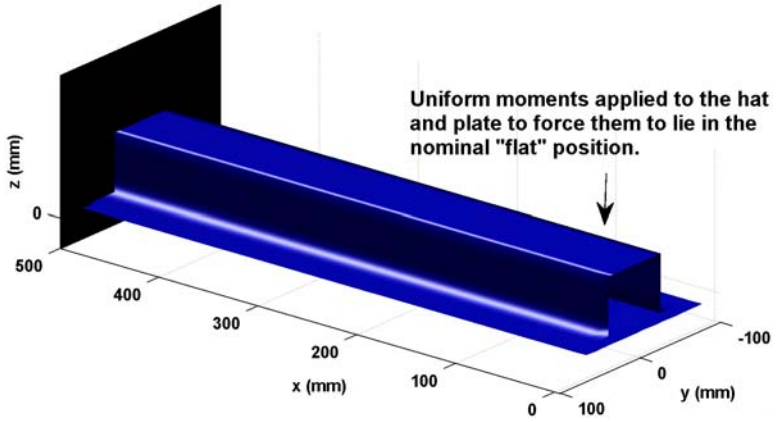

Figure 1.6: Moments applied to the hat M_{yH} and plate M_{yP} to force them into the flat nominal position. This is equivalent to the *clamp* stage in the assembly cycle.

Once the two beams lie flat, the third stage of the assembly process, $fasten$, is performed. Here the two parts are fused together along their length, which can be seen to represent a series of spot welds along the length of the beams. The final stage of the assembly process is *release*. This process can be represented by applying an equal and opposite moment to the newly fused assembly presented in Figure 1.6. According to equation (1.5) we have:

$$M_{yA} = (M_{yH} + M_{yP}) = \frac{2EI_{yA}d_A}{l^2} \tag{1.8}$$

By substituting equations (1.6) and (1.7) into equation (1.9) and re-arranging, we can calculate final assembly spring-back d_A.

$$d_A = \left(\frac{I_{yH}}{I_{yA}}\right) d_H + \left(\frac{I_{yP}}{I_{yA}}\right) d_P \tag{1.9}$$

Substituting in second moment of area values for the hat ($I_{yH} = 9.93 \times 10^{-08} m^4$), plate ($I_{yP} = 6.91 \times 10^{-12} m^4$), and final assembly ($I_{yA} = 1.58 \times 10^{-07} m^4$), we have an expression relating initial component deflection to final assembly deflection.

$$d_A = \left(6.28 \times 10^{-1}\right) d_H + \left(4.37 \times 10^{-5}\right) d_P \tag{1.10}$$

Assuming the two random variables d_A and d_P are statistically independent,the assembly mean and variance can be calculated from equation (1.9).

$$\mu_A = \left(6.28 \times 10^{-1}\right) \mu_H + \left(4.37 \times 10^{-5}\right) \mu_P \tag{1.11}$$

$$\sigma_A^2 = \left(6.28 \times 10^{-1}\right)^2 \sigma_H^2 + \left(4.37 \times 10^{-5}\right)^2 \sigma_P^2 \tag{1.12}$$

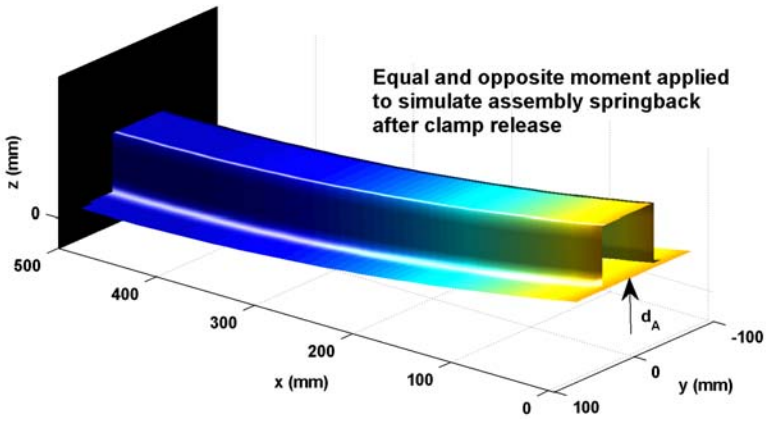

Figure 1.7: The sum of the moments used to clamp the hat and plate flat are applied (in the reverse direction) to the newly fused assembly to give the amount of spring-back. This is equivalent to the *release* stage of the assembly cycle.

Given that the standard deviation for the components σ_H and σ_P are set to 1 mm, the final assembly standard deviation can be calculated.

$$\sigma_A = \sqrt{(6.28 \times 10^{-1})^2 + (4.37 \times 10^{-5})^2} = 0.628mm \tag{1.13}$$

It can be seen that the standard deviation of the final assembly is less than the standard deviation of its components. This is in contrast with the non-rigid assembly example presented earlier in this section, where assembly variation was greater than the standard deviation of its components. This highlights a key characteristic of sheet metal assembly: that variation can be absorbed by the assembly process. This result supports the findings of Takezawa (1980). This example therefore highlights additional difficulties that flexibility of sheet metal components present in terms of variation or tolerance stack-up analysis. It can also be noted that variability in the plate has a very small influence on final assembly variability, which is why plate variation is ignored in later chapters.

1.2 Problem statement

The previous sections have introduced the sheet metal assembly process and illustrated how the flexibility of components means that traditional tolerance analysis techniques are non-applicable to sheet metal assemblies. It has been shown how variation can be absorbed by the sheet metal assembly process due to the flexibility of components: this is not the only implication of the flexibility of components. Depending on the way a workpiece is clamped or welded, it can distort in different ways. Studies have shown that aspects of the assembly process such as clamp and weld sequence can affect the

way in which variation propagates through the assembly process (Liu and Hu, 1995b; Hoffman and Santosa, 2003). The goal of robust process design is to select a string of procedures that will minimize final assembly variability. For sheet metal assembly, additional process factors such as weld and clamp sequence need to be considered to truly achieve an optimal process for dimensional control.

There are many ways of investigating sheet metal assembly processes, including direct experimentation, and more time and resource effective mechanistic simulation approaches (Hu et al., 2001). There are also approaches for designing and optimizing assembly processes for specified dimensional quality criteria, such as generalized assembly laws (Shiu et al., 2000), previous process knowledge (Chen et al., 2006a), and more advanced process optimization techniques (Liao, 2003a). However, in order for these techniques to be effectively applied for the purposes of dimensional control, there must be a well defined quality assessment framework from which to select the best processes. For example, if measures of assembly quality are not well defined or cannot adequately describe the quality of an assembly, then it is difficult to truly design a process that optimizes for assembly quality and maximizes customer quality perceptions.

Traditionally, univariate measures of a series of measurement points such as mean and standard deviation are used to assess the dimensional quality of assemblies. A major limitation of such assessment tools is their inability to capture a key characteristic of assembly variation: the correlation between regions on a surface, or geometric covariance (Merkley, 1998). Figure 1.8 illustrates how points on a surface tend to move in a correlated fashion. When using univariate methods, quality assessments are therefore made on a flawed representation of the variation in an assembly. The advent of optical measurement devices that allow the rapid measurement of entire free-form surfaces exposes further flaws of univariate measures of quality. For one, traditional quality assessment methods do not lend themselves well to the interpretation of such high dimensional data sets. While monitoring 10 process run charts for 10 measurement points is manageable, applying this approach to 1000 s of measurement points would prove too difficult. Also, due to the assumption of statistical independence univariate quality measures cannot adequately capture local features on manufactured surfaces, such as bumps and ripples, which could impact negatively on the quality perceptions of customers (see Figure 1.8).

The limitations of the traditional univariate dimensional quality assessment methods is therefore the key motivating factor for this thesis. This leads us to the focus of the research to be presented, which is to address the limitations of current univariate measures of assembly quality by proposing new ways of representing assembly variation to allow for more detailed and systematic assessment of quality. The integration of such an approach with process investigation tools will then provide an improved framework for the selection of optimal processes for dimensional control.

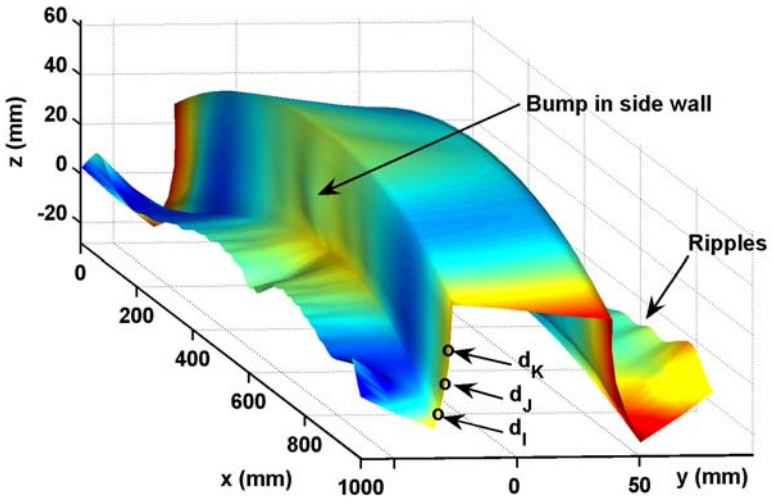

Figure 1.8: An example manufactured shape with variation (FE simulation with magnified displacements). See how points d_I, d_J and d_K tend to move in a correlated fashion. Also, note local features such as bumps and ripples which can detract from quality perceptions of the product.

1.3 Proposed approaches

The approaches presented in this thesis can be divided into a number of key sections: the influence of processes on assembly variation, characterizing assembly variation, and a view to optimal process design for dimensional control.

1.3.1 The influence of processes on assembly variation

One key component of this thesis is the demonstration of how certain aspects of sheet metal assembly (in this case clamping sequence) can be refined to create processes that are more robust to assembly variation. It essentially illustrates a way of utilizing available tools such as experimentation and simulation to optimize a process for particular quality assessment criteria. Processes are investigated with a non-linear contact finite element assembly model, along with a concurrent experimental assembly jig.

1.3.2 Characterizing assembly variation

As stated earlier, univariate measures of quality such as mean and standard deviation are limited in their ability to account for key behavioural characteristics of sheet metal assembly variation. This thesis presents two key approaches for the characterization of sheet metal assembly variation that are aimed at addressing the limitations of previous univariate representations of assembly variation and quality: the multivariate shape model, and local shape descriptors.

Multivariate shape model

The ability to effectively model dimensional variation of stampings and assemblies is an important tool for manufacturers to investigate, assess and control quality levels of their products. Statistical Process Control (SPC) and Six-Sigma approaches use the assumptions of statistical independence and normally distributed data to create quality process control guidelines which are predominantly used in industry. These approaches are limited in their ability to characterize correlated variation modes, deal with high dimensional data sets, and accurately estimate the overall shape distribution. In this thesis, a combination of the Point Distribution Model, which is based on Principal Components Analysis, and Kernel Density Estimation, is used to develop a multivariate statistical shape model (the KDE-PDM) that addresses the limitations of previous statistical models. The KDE-PDM s capabilities make it particularly suited to variation monitoring and diagnosis of high dimensional measurement data sets made available by optical measurement devices, and some suggestions for its implementation are also presented.

Local shape descriptors

The emergence of optical measurement devices such as laser scanners and photogrammetry have allowed for rapid and detailed inspection of entire free-form surfaces. Instead of measuring 10 critical points on a sub assembly, it is now possible to capture 1000 s of measurement points. This quantity of inspection points is creating new possibilities for the analysis and assessment of dimensional quality. Correlated variation modes and localized features such as deformations in the form of ripples and bumps can now be captured. In order to make use of this new measurement data for the purposes of quality assessment, there are two key issues that need to be addressed: firstly, a way of characterizing local shape features with a set of numerical descriptors needs to be established, and secondly, the relationship between such a local shape characterization framework and customer quality perceptions needs to be developed. This thesis seeks to address the first issue by presenting a set of example numerical descriptors that are able to distinguish between differing manifestations of manufacturing variation in sheet metal assemblies. Techniques used include: surface curvature energy, scale energy bands derived from the continuous wavelet transform, and a curvature threshold approach for automatic local feature identification. Some suggestions as to how relationships could be established between the shape descriptors and quality perception are also presented.

1.3.3 A view to optimal assembly process design

This thesis presents methods for investigating assembly processes, and new approaches for more accurately representing and describing assembly variation. In order to take full advantage of these tools, they must be combined within an integrated and synergistic framework for the analysis, assessment and selection of optimal assembly processes for dimensional control. A framework for the integration and implementation of the approaches presented in this thesis, along with existing research and analysis methods, is therefore proposed.

1.4 Thesis overview

Chapter 2 outlines some background literature to provide some context and motivational factors for this thesis.

Chapter 3 presents a series of measurement studies conducted on a production case study. The chapter serves to highlight key behavioral characteristics of sheet metal assembly, and serves as a practical introduction to the field of sheet metal assembly.

Chapter 4 proceeds to investigate the influence of clamping sequence on the propagation of variation through a simplified single stage assembly. Here the finite element method is used to reveal the extent to which selection of clamping sequence can influence final assembly variability.

In Chapter 5, experimentation is used to illustrate the ability of different clamping sequences to result in different mean assembly shapes. The finite element assembly approach is also validated against the experimental results, and then further applied to illustrate the ability of different clamping sequences to result in different final assembly variability. Finally, generalized clamp design guidelines based on experimental and simulation observations are proposed and applied to the example assembly with promising outcomes.

Chapter 6 presents a multivariate approach for statistical shape modelling of automotive stampings and assemblies. The approach provides improvements over current methods in its ability to deal with high dimensional data sets, represent correlated variation modes, and provide accurate estimates of the underlying shape distribution.

Chapter 7 presents an approach for the characterization of localized shape features on stamping and assemblies. The advent of optical measurement devices have allowed for the rapid capture of thousands of data points across free-form surfaces. Now that

such measurement devices can capture local features such as bumps and ripples, this chapter proposes a set of formalized numerical descriptors for such features.

Chapter 8 firstly seeks to tie the range of approaches presented thus far in the thesis together within a quality assessment framework for dimensional control. It then concludes the thesis by summarizing the contributions this thesis has made towards the areas of quality assessment and process design for sheet metal assemblies, and also proposes future avenues of research.

Chapter 2

Background

2.1 Introduction

This chapter firstly provides a review of literature into some key areas of automotive body assembly design and dimensional control: Virtual assembly, Process diagnosis, and Knowledge-based design. While methods proposed by previous research do provide powerful process monitoring and design aids for manufacturers, an accurate measure of assembly variation is required to provide a true quality objective for these methods to target. This leads to the second key section of this chapter, which begins with an introduction to current univariate measures of assembly variation that are commonly used by industry to provide quality targets for assembly and process design for dimensional control. This is followed by the statement of a number of key limitations of the current univariate measures of assembly variation and quality, which hinder the ability of current research methods to assist manufacturers in their aims of reaching true quality objectives. These key limitations provide the main motivation behind the work to be presented in this thesis, which is aimed at developing new ways of characterising variation to allow for improved discrimination and assessment of assembly quality with a view to optimal process design.

2.2 Virtual assembly

There are two key ways of investigating assembly processes. The first is experimental or production trials, which is favourable as it is a physical process that is being evaluated. However, such an approach can be rather costly and time consuming. The second approach is to use computer simulation tools to mimic the physical process, which allows for fast and cost effective virtual prototyping (with a trade-off in accuracy). Such tools are becoming increasingly important as manufacturers aim to remain competitive by reducing process variation to produce continually higher quality products (Taguchi,

1986), and reducing lead times in efforts to get new products to the marketplace earlier (Watanabe and Ane, 2004). Two main simulation approaches for modelling assembly variation propagation are finite element based models that take into account the flexibility of assembly components, and multi-station models which seek to represent variation propagation through the entire assembly process. Both of these tools are powerful methods that can assist engineers in both process and product design. The following sub-sections will present a range of different approaches for virtual assembly identifying how it is used for the analysis of variation propagation and tolerance allocation. They will then proceed with methods for utilising virtual assembly capabilities for process optimisation.

2.2.1 Finite element models

In Chapter 1, the difference between variation propagation in rigid and non-rigid assemblies was illustrated. Finite element methods have become a popular tool for the analysis of sheet metal assemblies, as they capture the key characteristics of flexibile components, therefore providing an accurate representation of the physical process. A selection of approaches for the mechanistic modelling of non-rigid assemblies will be reviewed in this section.

One of the first approaches for mechanistic modelling was presented by Liu and Hu (1995a). They used one dimensional beam elements to explore variation characteristics of two and three piece assemblies. Tooling variation, part variation, sheet metal thickness and assembly sequence were areas investigated. The study revealed important characteristics of sheet metal assembly, such as which variation sources are dominant under particular conditions. Liu and Hu (1997b) extended the use of their beam assembly model to explore assembly variation in simple two-piece beam assemblies for different join types: Lap joints, butt joints, and butt-lap joints. The influence of part and tooling variation was investigated for a range of sheet metal thickness combinations, with each of the join types exhibiting different assembly variation characteristics. This modelling approach displayed the potential of mechanistic modelling as an analysis tool for non-rigid assemblies.

Shiu et al (1997) decomposed entire body structures into beam models for non-rigid assembly analysis. Beams were connected at end nodes, with joint-to-joint forces acting along the length of the joint beams, and locating/assembly forces applied at beam end nodes. They used this model to explore the deformation of assemblies due to particular faults such as mis-location. Shiu et al (2002) later extended the application of their beam-based model as a tolerance allocation tool. In this approach, they initially specify the desired tolerances for Key Product Characteristics (KPC s), which are the functional tolerance requirements of the final product. Then, using the mechanistic beam model, they calculate the maximum allowable tolerances for Key Control Char-

acteristics (KCC s), which are the manufacturing requirements that satisfy the KPC s. They later used this model to develop a minimised cost approach for assigning both deterministic and stochastic tolerances (2003).

In 1997, Chang and Gossard demonstrated the application of the finite element method for flexible assembly variation analysis on a front end assembly. They used the place, clamp, fasten, and release cycle to describe the key steps of the assembly process. The steps can be described as follows: place refers to the components being located; clamp is where the locating clamps are applied to hold the work-pieces in place; fasten spot welds the components togethe; release refers to the release of the assembly from a fixture jig, at which point spring-back occurs (see Section 1.1.2). They also implemented a similar cycle to represent the assembly being loaded onto a fixture for measurement. They were among the first to use detailed shell element models for the analysis of more realistic assembly geometries. The previously mentioned beam based models could only represent simplified approximations of body panels.

Hoffman and Santosa (2003) presented a simple model of welding and clamping of sheet metal. In their model, two sheets of slightly different shape are joined at two weld points, with each piece represented as a simplified beam model. The beam model is made up of rigid bars linked together by torsional springs. With this model they illustrated the characteristic of welding sequence dependence in sheet metal assembly. This characteristic of welding sequence dependence was investigated by a more detailed FEM implemented in commercial software ANSYS, by Hu et al (2001). They combined linear elastic and contact simulations to capture the effects of deformation induced interaction between assembly components, as they saw the potential for this behaviour to greatly influence the final shape of an assembly. Through utilizing more advanced numerical simulation tools than earlier approaches, a more accurate representation of the physical process could be achieved. They explored the use of their FE modelling approach on alternative welding sequence patterns for a three-piece dash panel assembly. Three different welding sequences were explored and compared to physical experiment data, with promising levels of correspondence for the two measured critical points.

A popular approach for variation analysis of flexible sheet metal assemblies is the method of influence of coefficients proposed by Liu and Hu (1997a). This method utilises several key assumptions such as small deformations and linearity in order to allow the derivation of a single response matrix to relate component to assembly shapes. The method requires two FEM simulation runs: one to calculate the component responses to assembly forces (such as clamping and welding), and another to calculate the assembly spring-back after tooling forces are released. The primary advantage of this method over direct FE simulation (Chang and Gossard, 1997; Hu et al., 2001) is significantly decreased computation time for stochastic modelling approaches, however, the approach was unable to capture non-linear assembly characteristics such as deformation

induced contact and friction. Dahlstrom and Linkvist (2007) developed an approach that seeks to retain the advantages of the method of influence of coefficients , while being able to capture deformation induced interactions. Deformation induced contact can significantly influence the way in which variation propagates through the assembly process, and approaches that neglect such behaviour can lead to erroneous assembly predictions. Here, a contact search finds expected regions of deformation induced contact, and then a linear model for the reaction forces and distances of the expected contact nodes is calculated.

Soderberg et al. (2006) used FE techniques to develop robustness analysis software for compliant assemblies. The software provides a way for designers to predict the sensitivity of locating designs to variability, and to determine approaches that can satisfy a particular level of robustness (resistance to variability in components). The integration of advanced FE methods within more accessible design tools increases the value of such approaches as they can be more readily harnessed for design improvements. Gerth (2006) explored the concept of a virtual functional build. This involves detailed measurement of components using laser scanners or photogrammetry, from which virtual FE meshes are created. These are then used as inputs to finite element assembly models, in this case the commercial software VisVSA, to determine whether the components produce assemblies that are within tolerance limits. This virtual build approach was important as it used realistic model inputs for the FE assembly tool, whereas previous approaches have used estimates of input component shapes. Furthermore, previous studies have often neglected extensive experiential or production validation, whereas this approach could readily facilitate the comparison of simulated and actual production results. It is vital that simulation tools provide a realistic representation of the physical process if they are to be truly beneficial as a design aid.

Fan et al. (2007) studied the thermo-mechanical influence of resistance spot welding on assembly variation. The commercial software SYSWELD was used to study different welding sequences for a two piece assembly. Thermo mechanical behaviour was considered through localised modelling of the weld zone which is then imported to a global model. It was revealed that different weld sequences applied to identical components can result in different final assembly shapes, and experimental validation shows sufficient correlation. While this method corresponds closely to the physical process in comparison to previous approaches, it is also computationally far more demanding. As with other computationally intensive FE simulation approaches, the application of this method is limited as it is not readily combined with Monte-Carlo approaches for the estimation of tolerances

As seen through the range of methods described in this section, mechanistic simulation of sheet metal assembly has taken on many forms. To summarize the approaches, linearised models are advantageous as they are computationally less demanding and can

therefore be more readily combined with stochastic modelling for variation propagation modelling. However, linearized approaches can miss important behavioral aspects of the physical process such as deformation induced contact and contact due to the initial placement of components in fixtures, although some progress has been made in attempts to capture such behaviour (Soderberg et al., 2006). Nonlinear approaches can provide more realistic representations of the physical system, such as deformation induced contact, however they are computationally demanding. It could be expected that in some cases, linear models would be sufficient, and in other cases nonlinear approaches more appropriate due to the specific contact conditions: new approaches could take a hybrid approach to assembly modelling and adapt simulation techniques to the particular case to reach an accuracy to computational effort compromise. Later in this thesis, a nonlinear contact assembly approach implemented in a commercial code will be used to simulate a single station process due to the closer representation of the physical system.

The mentioned finite element models for sheet metal assembly simulation provide valuable tools for the prediction of variation propagation. However, in order to make best use of these tools, an accurate and well defined measure of quality must exist that can then be targeted in quality control efforts. This thesis will propose a range of shape characterisation methods that can provide an improved and less subjective definition of assembly quality, allowing research methods such as finite element assembly models to target true quality objectives. These concepts will be developed further in later sections.

2.2.2 Multi-station models

The previous section discussed finite element methods for single station assembly simulation, which importantly captures the flexibility of assembly components. Sheet metal assembly is an iterative process involving many sub-assembly stations between initial stampings and the final BIW, so multi-station assembly analysis forms an important piece of the virtual assembly toolset. This section discusses some key approaches for multi-station assembly variation modelling.

There are many well established methods for the analysis of variation or tolerance propagation in mechanical assemblies based primarily around vector-loop equations (or assembly functions). Root-sum-of-squares (RSS) approaches use a first order approximation to derive a linear propagation model and are popular due to their ease of use (Gao et al., 1995). The inability of RSS approaches to deal with non-linear input and output distributions has led to the proposal of higher order taylor series approximations for more accurate depictions of tolerance propagation (Shapiro and Gross, 1981). A second order method proposed by Glancy and Chase (1999) combined finite difference approximations of partial derivatives, the Method of System Moments for estimating

nonlinear system outputs (Cox, 1979), and nonlinear distribution fits, to allow for the approximation of nonlinear assembly tolerances. Another perhaps more straightforward method of variation or tolerance propagation analysis in complicated nonlinear assemblies is the Monte Carlo method, which involves running thousands of random inputs to the assembly function to estimate final distributions. A drawback of this method is obvious time constraints, although there are advancements that have been made to reduce computational effort of such approaches (Huang et al., 2004; Wu et al., 2006).

A more recent and increasingly popular form of modelling variation propagation in multi-station assemblies has been referred to as the state space modelling approach. It uses established control theory methods to describe the positioning of each component throughout each stage of the assembly process, and is often combined with Monte Carlo simulation for variation or tolerance analysis. A state space modelling approach was presented by Jin and Shi (1999) to determine the variation propagation throughout all steps in multi-stage assembly. Part orientations were transformed according to particular manufacturing stage conditions. Tooling error, such as locating pin deviations, part error, and re-orientation are the key sources describing the positioning of parts throughout the stages of the model. State space modelling of assembly variation propagation has become popularly known as the Stream of variation theory (Hu, 1997). Xiong et al. (2002) present a statistical variation analysis model for multi-station assembly that is implemented in IDEAS. As with the state space modelling approach, this is achieved by a series of transformations of assembly components at each assembly stage. These approaches have provided valuable tools for the investigation of variation propagation and tolerance allocation in multi-station models, however, they have only focused on rigid component assemblies which limits the predictive accuracy for sheet metal assembly.

Camelio et al. (2003) presented a method that combines state space modelling techniques for multi-station variation propagation analysis with mechanistic variation analysis. Linearized mechanistic variation simulation analysis (Liu and Hu, 1997a) was incorporated into the discrete step model at the assembly stage. At each assembly step, parts are located, clamped, welded and released according to the mechanistic variation model, and this is cycled for each step. Part, fixture and welding gun variation are considered in this final model. The limitations of this model include: model complexity as the number of assembly stations increase, there is no consideration of non-linear behaviour (such as deformation induced part-to-part and part-to-tool interactions), and it is discontinuous for variables such as fixture positioning. This means that a new model must be developed for alternative welding sequences. However, the combination of multi-station assembly and flexible component modelling provides a key advancement in virtual process investigation.

While multi-station modelling for rigid component assemblies is well developed, the application of multi-station modelling to sheet metal assembly presents additional challenges through the need to capture the flexibility of components. The combination of linearized finite element simulation with multi-station models is practically achievable, however, linear mechanistic simulation approaches are not as accurate as non-linear contact models. Advancements in the field of sheet metal assembly could involve developing computationally reasonable methods for capturing nonlinear contact behavior in flexible assemblies. For example, the linearised contact assembly approach proposed by Soderberg (2006) could be integrated into the multi-station approach. For the purposes of this thesis, virtual multi-station modelling is not considered due to the adoption of computationally intensive nonlinear mechanistic simulation models, and to make the experimental set-up more manageable. Moreover, a natural extension to the research presented later in this thesis is to extend the virtual analysis of multi-station models using the shape characterisation tools developed for stampings and single station assemblies.

As with the mentioned finite element models, multi-station simulation approaches for sheet metal assembly provide valuable tools for the prediction of variation propagation and can be used to identify more optimal assembly approaches. However, in order to make best use of these tools, a well defined measure of quality must exist that can be targeted in quality control efforts. This thesis proposes a range of methods that can assist in providing improved quality objectives for multi-station analysis.

2.2.3 Process optimisation

A key goal of automotive manufacture is to control variability of the final product and maximize customer quality perceptions. The previous sections have focused on describing a range of tools that can be used for virtual investigation of automotive body assembly processes. This section looks into the application of these virtual simulation tools for the selection of more optimal assembly and process designs for dimensional control. Aspects of the assembly process that have been the focus of optimisation techniques include fixture configuration, clamping schemes and positioning, weld locations, and assembly sequences.

Optimum fixture positioning for the minimization of assembly variability has been explored (Camelio et al., 2004b). Here, they combined finite element assembly modelling with non-linear programming methods to determine optimal fixture configurations. Variation sources explored included component and tooling variability. Liao (2003b) presented a method for minimising the dimensional variation in the workpiece, including variation induced by gravity, by optimising clamp and fixture locations using a genetic algorithm. Yi et al. (2005) utilise the EAVS software package to undertake a clamp shimming optimisation study. Shimming of clamps is often undertaken in prac-

tice to fine tune the assembly process and minimise assembly deformation. Optimal shim amounts were determined by minimising an objective function based on the final assembly mean deviations. Liao (2006; 2007) has also proposed methods for clamp shimming selection for improving dimensional quality. Genetic algorithms for the optimisation of spot weld locations in order to maximise dimensional build quality of sheet metal assemblies has also been explored by Liao (2003a; 2005). The advantage of this method over previous approaches was that it can provide optimisation for any number of welding points as opposed to a fixed number.

Optimisation approaches have also been extended to multi-station processes. Zhang and Ni (2003) also look into an adaptive process for robust process design that considers product structure, connection type and assembly sequence. It has been shown that different join types can alter the way in which variation propagates through assembly processes (Chen et al., 2006b). This characteristic has been used to formulate an adaptive joint design approach in consideration of different assembly sequences (Cao et al., 2007). Here, joins are selected (via a genetic algorithm) to provide the optimal in-line adjustability for key product characteristics given a particular assembly sequence. While these presented optimisation techniques can be quite effective in the identification of more optimal processes, a limitation of such tools is the significant computational effort required.

Application of genetic algorithms for process optimization appear to be the most widely adopted due to their ability to consider aspects such as clamp and weld sequence. Also, genetic algorithms can be less likely than other optimisation methods to have issues with local maxima, and can also exhibit more rapid convergence (Gershenfeld, 1998). The extension of genetic algorithms to consider more aspects of the assembly process such as assembly sequence, cycle time (Xie and Hsieh, 2002), and shop fit-out costs would be an area of future advancement. A limitation of optimisation methods is that they do require specific expertise or knowledge of the user, and even with more efficient optimisation techniques, significant computational loads can be expected. Section 2.4 will develop approaches that can be used to limit the need for optimisation methods for the selection of robust processes.

As stated with the virtual assembly tools, optimisation techniques require an accurate definition of assembly quality to target, otherwise the effectiveness of such techniques will always be limited. This thesis proposes a range of techniques that can enhance the effectiveness of optimisation methods through providing improved quality objectives.

2.3 Process diagnosis

The previous section has discussed virtual assembly tools that allow for rapid simulation of assembly processes. This section will discuss research into automotive assembly process monitoring, which forms an essential piece of quality control operations. Research has focused strongly on the identification of outlier events, fault patterns, and variation sources. While traditionally statistical process control has formed the basis of process monitoring within the automotive industry, research has focused heavily on the use of multivariate techniques to take into account the correlation between measurement points on an assembly. Some key approaches are presented in the following.

Identifying faults in the assembly process, such as mis-location, has developed as a focus of much research. The concept behind these methods is firstly to theoretically determine a set of patterns that relate to particular fault types. The next step is then to identify the primary fault patterns of production measurement data, and to compare them to the pre-determined fault patterns for problem identification and resolution. Ceglarek and Shi (1996) studied rigid body assembly processes with single faults using principal regression analysis. By setting up a geometric relationship between locating features and measurement points on a part, they created linear theoretical fault models that could be represented by a diagnostic vector (an eigenvalue/eigenvector pair). Locating pin error causing rotation of a work-piece is one example of an error. PCA was then applied to production data, with the key variation mode extracted. A minimum distance classifier was then used to determine which theoretical fault type the dominant variation mode represented. In 1996, Yang also used PCA to decompose assembly process data into key variation patterns, with a key focus on the geometrical interpretation of the patterns. In 2002a, Ding et al. used the state-space modelling approach to explore fault detection in multiple assembly stations through measurement data obtained only after the end assembly station. Similarly, predetermined fault patterns were compared with PCA patterns found in measurement data for fault classification.

Designated components analysis, a fault identification approach presented by Camelio et al. (2004a), defines a set of linear fault patterns based on product and process information. These fault patterns or components do not necessarily need to be orthogonal, which was a requirement and limitation of traditional PCA-based methods. Non-orthogonal patterns are transformed into an orthogonal basis via Gram Schmidt orthonormalisation, where components can be translated or scaled but not rotated. The ability of the method to diagnose multiple faults revealed that dependant fault types are more diagnosable than independent fault types, and that locator faults are easily diagnosable whereas clamp faults are not. In 2000 Rong et al. investigated a method for identification of faults in non-rigid beam assemblies. Through decoupling the inversed stiffness matrix of a beam structure, diagnostic or displacement vectors which

represent a single fault occurrence were determined. Independent diagnostic vectors were identified from the inversed stiffness matrix. It was shown that if a single fault occurs in a process that corresponds to one of the pre-determined diagnostic vectors, the first principal component (or eigenvalue eigenvector pair) of the measurement data can be matched to that fault via hypothesis testing, even in the presence of measurement noise. This technique was successfully applied to an industry case study.

Investigations have shown that sensor placement can have a large influence on the diagnostic capability of multivariate process monitoring tools. Khan et al. (1999) looked into optimal sensor placement strategies for the discrimination of pre-classified fixture fault errors for single station assemblies. Stream of variation theory has also been applied to formulate fault detection strategies for multi-station assemblies (Ding et al., 2002b). Here, the theoretical assembly models were used to experiment with different sensor placement strategies to test their effectiveness in diagnosing particular faults. Camelio et al. (2005) also explored an approach for determining sensor placement for effective fault diagnosis in sheet metal assembly. Initially, FEA is used to determine response patterns to particular faults. Then an effective independence algorithm (efi) is applied that starts with all feasible sensor locations, and progressively eliminates those having the least contribution to the linearly independent manifestation of the fixture faults .

Another method seeking to extract diagnostic information about fault manifestations from large quantities of multivariate process measurement data is presented by Apley and Shi (2001). Rather than assuming that fault types correspond to the orthogonally set Principal Components that correspond to the most amount of variation in the data, this model seeks to discover the patterns of physically occurring faults. The method is closely related to factor analysis. While this approach seeks to align itself with actual variability occurrences, the method requires much judgement from the user, and a less subjective refinement of this approach would prove useful. Apley and Zhang (2007) have presented a method for visualizing nonlinear variation patterns in multivariate manufacturing data, which was not possible with existing approaches. The method uses an unsupervised learning approach to provide a visual diagnostic tool for process monitoring. The approach involves using principal components analysis for dimensional reduction, principal curve estimation to learn the nonlinear variation pattern, and a recovery of the estimation variation pattern to the original dimensional space. Visualisation of physically occurring variation patterns can allow for a more intuitive interpretation of variation sources.

Guzman et al. (2004) took another approach to the use of multivariate statistics as a tool for assembly variation analysis. A dimensional slow build study was used to gather data of corresponding points throughout different assembly stages. A technique called partial least squares regression was applied to compare assembly stages and identify the

influence of input part variation modes on subsequent assembly stage variation. In the experiment presented, the technique was used to identify which assembly stages have the greatest influence on variability. The method is similar to Principal Components Analysis (PCA), except that the change of basis for the input components is selected to describe as much of the assembly variation as possible. A major advantage of this method is its ability to handle a large number of potential explanatory variables as well as a large number of response variables with a relatively small amount of observations. Yue et al. (2007) developed a number of product-oriented sensitivity indices which enable manufacturers to pinpoint key variation sources from theoretical multi-station assembly models. The indices measure the variation influence of a pattern, an individual part, and/or component, and components at a particular station to the dimensional quality of a final assembly.

Lian et al. (2002) explored the use of several data analysis techniques in order to provide more information about variability in sheet metal assembly. Correlation analysis and maximal tree methods were applied to segment large multi-dimensional data sets into small and large variation groups, while PCA was used to discover multivariate principle variation patterns. A decision tree method was proposed for the application of these techniques along with process knowledge in a systematic diagnostic support system. This approach was successfully applied in an experimental analysis of a rear end panel assembly, with a missing weld diagnosed as the cause of excessive variation.

This section has presented a range of process diagnosis methods which emerged from the need to determine more information than what can be derived from univariate SPC-style process monitoring approaches. With SPC, a process can be identified as out of control, but little information can be directly obtained with regards to what the cause of the out-of control condition is (ie, was it an operator loading error, is a locator broken, or was there a mean shift in the stampings?). Multivariate tools capture can capture correlated variation patterns, providing more detailed information about the nature of the out-of-control condition, and can be used to identify particular fault modes which can be related back to their root cause. Supervised fault identification approaches are perhaps the easiest to formulate however, these methods require an a-priori knowledge of fault patterns, which is not always possible. Efforts have therefore been made to implement unsupervised pattern identification methods to uncover unknown faults (Apley and Zhang, 2007). Future development of unsupervised pattern learning methods presents an avenue for future research.

While the mentioned multivariate tools have provided powerful process diagnostic tools, none of these methods appear to take full advantage of the advanced density estimation techniques that are available which could create further diagnosis capabilities. The multivariate shape model which is presented later in this thesis creates new possibilities in terms of density based unsupervised learning methods for sheet metal

assembly process diagnosis and control.

2.4 Knowledge-based design

Previous sections have discussed virtual methods for simulation and design of assemblies and processes, and approaches for improved process monitoring, diagnosis and control. As the application of these techniques evolves over the duration of many product cycles, it is likely that there will be expertise developed that can assist with the design processes of new products. As the name suggests, knowledge-based design involves drawing upon past knowledge of similar design cases to assist in the development of new products. Such approaches can lead to a quicker design process and more optimal design outcomes, as designers can access a wealth of stored process knowledge (Chapman and Pinfold, 1999).

In 2000 Shiu proposed a minimum stress criterion approach to minimise dimensional variation in sheet metal assemblies. In a simplified structural beam analysis of an automotive body-frame, they identified a relationship between internal stress and dimensional variability. They also showed that the welding sequence can affect the overall internal stress in assemblies, and suggested generalised welding approach guidelines that minimise the internal stress through the trial of various beam-based and finite element simulation assembly approaches. A joint design guideline for the minimisation of stress was also presented. The development of these guidelines can be seen as an early example of utilising previous process knowledge, which in this case was derived from virtual assembly studies, to assist in the selection of robust processes for future designs. Such generalised laws are more easily adopted by industry as there is less need for computationally intensive analysis as with the optimisation techniques presented in section 2.2.3.

The integration and application of knowledge based systems to the complex environment of automotive assembly is not a trivial task. Manarvi and Juster (2004) presented a generalised framework for combining process knowledge, virtual analysis techniques and databases as a tool for more efficient allocation of tolerances. This framework allows for designers to have easy access to the many resources available to assist with the tolerancing process within a structured toolset. Gerth and Baron (2003) present the Integrated Build (IB) approach to automotive body manufacture, which is an evolution of Functional Build approach discussed in section 1.1.3. For the IB approach, planning, implementation, design, and manufacturing launch are considered in parallel to allow for expanded opportunities for design adjustments and process reworking. The software package ADRIAN was developed to allow design engineers and draftsmen to perform preliminary mechanical analysis, with the aim of increasing design speed and enabling the investigation of more design alternatives (Bylund, 2005). This fits in with

the IB concept as design loops can be conducted in parallel at previously disjoint stages of the design process.

Chen et al. (2005) presented an object-oriented hierarchical case representation scheme for automotive panels in order to provide a means of arranging previous knowledge within a case-based reasoning environment. In 2006a Chen et al. proceeded to propose a case based reasoning framework for automotive body assembly process design. Here, knowledge retrieved from previous similar assembly cases was integrated with tools for initial solution generation, dimension chain generation, joint design selection, assembly sequence generation, and tolerance analysis and optimization. The demonstration of a knowledge based engineering system for automotive body structures to assist in finite element mesh generation has also been presented (Chapman and Pinfold, 2001). Knowledge databases have also been proposed to assist in stamping process design and dimensional control (Gresham et al., 2001; Smith et al., 2004). Here, information relating to previous processes and problem remedies are archived with the aim of assisting future similar products in terms of problem diagnosis and robust design. Bernard et al. (2007) discuss the range of virtual engineering methods and rapid product development applications that can be integrated within knowledge based design systems. It is within such truly integrated design frameworks that considerable advancements in product lead time and quality can be achieved.

Design approaches that draw from previous experience and analysis provide time and cost effective ways for the identification of better processes. This thesis seeks to enhance the field of knowledge based design in two ways. Firstly, in a similar manner to Shiu 2000, generalized design laws will be extracted from virtual and experimental analysis to allow for the more practically implementable identification of robust processes. The new generalised laws will be developed for clamping sequences, and add to the current knowledge-based design tool-set for sheet metal assembly. Secondly, through the development of advanced quality measurement methods, true quality objectives can be targeted by the range of analysis tools available. These improved analysis results can filter through to knowledge based design frameworks.

2.5 Industry measures of assembly quality

The previous sections have presented a number of key research areas in the field of automotive body assembly. The main goal of research into virtual engineering and knowledge based design can be simplified to the identification of assemblies and processes that are more robust to variation from the outset. In order to identify which processes are the best in terms of dimensional quality, a way of measuring the relative quality of assemblies must be in place. The traditional approach for determining the dimensional quality of a process is to assess the mean and standard deviation of

a set of assumedly statistically independent measurement points on an assembly to measure the deviation and variation of a process. Two major quality assessment tools predominantly used in industry that adopt the assumptions of statistical independence and normally distributed data are the process capability indices, and statistical process control charts. Process Capability (C_p) and the Process Capability Index (C_{pk}) are commonly used for assessing dimensional quality with respect to some specification level determined by both manufacturers and customers (Chen et al., 2001). Process Capability relates the standard deviation or six-sigma spread of an MP to its tolerance specifications

$$C_p = \frac{USL - LSL}{6 \times \sigma} \tag{2.1}$$

The Process Capability Index assesses the standard deviation and mean position of a measurement point in relation to its tolerance specifications

$$C_{pk} = \min \left[\frac{USL - \mu}{3 \times \sigma}, \frac{\mu - LSL}{3 \times \sigma} \right] \tag{2.2}$$

where USL is the upper specification limit, LSL is the lower specification limit, μ is the mean estimate, and σ the standard deviation estimate.

The procedure for controlling process quality in terms of these indices is to firstly reduce the spread of data to within specified tolerance limits, and secondly to shift the mean of the data set towards the nominal design specification. To implement a continuous improvement strategy, manufacturers should seek to continually reduce the spread and mean deviation of measurement points irrespective of whether they are within tolerance specifications or not.

Statistical process control charts also form an important piece of quality control operations (Shewart, 1931). Here, measurements of a set of assumedly statistically independent and normally distributed MP s are tracked over time with respect to a process mean and standard deviation. A set of rules determine whether a process is running with common variation causes that only have a slight affect on the product, or if it is running with assignable variation sources that can have a considerable impact on the process. In the case that common variation causes are identified the process should be left alone, and in the case that assignable variation causes are found the root cause of these issues should be investigated. SPC tools have provided a valuable approach for identifying outlier events such as operator error and assembly mis-location.

2.6 Limitations of univariate measures of variation

Quality assessment tools such as the process capability indices and SPC charts can be labelled as univariate quality tools. This is because they are based upon a model

that assumes statistical independence. The following will discuss a series of key limitations of the univariate measures of assembly quality, which stem from confining model assumptions and the need to interpret newly available high dimensional optical measurement data. The next section will proceed to discuss these limitations in light of the goal of measuring assembly quality.

2.6.1 Model assumptions

When drawing inferences about a population of measurement points or assemblies, it is essential that the underlying representation or model of the data accurately reflects the key behavioral characteristics of that data. If this is not the case, then inferences drawn from an incorrect representation of the data could lead to incorrect conclusions, or perhaps vital diagnostic information will be missed due to the inability of the underlying model to capture such behaviour. The following will discuss two key assumptions of univariate quality measures such as process capability and SPC methods that result in limited representations of assembly process data: statistical independence and normally distributed data.

Statistical independence

A fundamental characteristic of sheet metal assemblies is that they tend to exhibit correlated variation patterns. Traditional measures of assembly quality such as process potential assume statistical independence of measurement points, and therefore omit important information about the nature or geometric manifestations of variation. Previous research has explored multivariate techniques that take into account geometric covariance to provide more powerful analysis and diagnosis tools through the capture of correlation variation patterns. In section 2.3, a number of multivariate methods including principal component analysis (Lian et al., 2002), factor analysis (Apley and Shi, 2001), and partial least square regression (Garcia Guzman et al., 2004) have been adopted for fault diagnosis and variation source detection. Camelio et al. (2004c) extracted linear correlated variation modes from assembly component measurement data using principal component analysis, and using the mechanistic variation simulation model determined the sensitivity of the final assembly to these component variation modes or patterns. Merkeley (1998) investigated the use of Beizer curves to represent free form surfaces and profile tolerances, in order to account for the geometric covariance that arises from constraints on random variation in mating surfaces due to surface continuity conditions . The Beizer curves were used as inputs to a steady state contact solution for simulating non-rigid assembly. As addressed in previous research, statistical representations of sheet metal assembly measurement data must consider the behaviour of geometric covariance in order to provide a more accurate representation

of the physical system, and to provide additional information that can lead to the diagnosis of variation sources. The significance of the multivariate approach presented in this thesis is the development of a mixture model estimate of the multivariate probability density, which previous approaches have not considered. A key motivation for introducing this tool is to provide more accurate density representations so that more valid inferences can be drawn about a process, which in turn can lead to more accurate process control decisions.

Normally distributed data

Process capability indices and SPC methods make the assumption that an underlying data set is normally distributed. This assumption does not always hold, and in some cases it is likely that the underlying data will be highly skewed and/or multi-modal. In such cases, inferences will be drawn from a flawed probabilistic representation of the underlying data set, which is for obvious reasons a questionable approach. The Shapiro-Wilks test (1965) has been applied to check the normality assumption before calculating process capability indices (Han, 2006). The application of capability indices to non-normal data sets has also been explored, which includes methods that seek to transform skewed distributions into normal distributions after which the standard capability formulas can be used (Somerville and Montgomery, 1996), and the calculation of upper and lower percentiles from non-normal distribution estimates (Clements, 1989). While these approaches make inroads into addressing the issue of non-normally distributed data sets, a limitation again emerges in the assumption of statistically independent data: an ability to model both non-normally distributed and highly correlated data sets would provide a key advancement in the statistical representation of assembly process data.

2.6.2 Implications of new measurement technology

The advent of optical measuring devices has allowed for the rapid non-contact measurement of entire free-form surfaces. These new measurement capabilities pose two key issues for univariate measures of assembly variation: the curse of dimensionality, and the description of previously unmeasurable local variation patterns.

The curse of dimensionality

Rather than measuring 10 MP s on an assembly using hard gauges or CMM s, it is now possible to capture 1000 s of points with optical measurement devices. Traditional approaches for process quality monitoring would use process control charts and capability indices for each measurement point. While this approach appears manageable for a relatively small set of MP s, monitoring 1000 process control charts and capability indices

would be quite a cumbersome task. The problem of high dimensional data sets (where each MP can be seen as a dimension) can be even more troublesome when seeking to consider correlated variation patterns and identify useful diagnostic information. The curse of dimensionality was term coined by Bellman (1961) referring to the exponential growth of a hypervolume as a function of dimensionality, and is an issue that must be addressed to allow for feasible interpretation of high sample and dimensional optical measurement data of assemblies. Methods that allow for more manageable interpretation of such high dimensional data sets would increase the attractiveness of optical measurement technology and enable increasingly detailed levels of process inspection.

Local variation patterns

Optical measurement devices are capable of measuring free form surfaces to unprecedented levels of detail. Localised variation patterns such as bumps and ripples that can detract from quality perceptions are now readily measurable. It has already been stated that univariate quality measures do not capture the inherent behaviour of geometric covariance in stampings and assemblies, and therefore cannot really describe variation patterns. The ability to measure local variation patterns now presents the additional need to discriminate between variation patterns of different sizes or scales, in order to enhance the ability of manufacturers to measure local assembly variation that can influence assembly quality. While past research has focused on identifying major (or global) variation patterns in assemblies, new methods that can capture locally occurring variation patterns would provide a valuable improvement in quality discrimination and assessment, and make proper use of optical measurement technology.

2.7 Characterising assembly variation

In terms of automotive body assembly, the measurement of deviation and variation forms the backbone of quality assessment: the lower the deviation/variation of an assembly or population of assemblies, the higher the quality of the product. The most common tools used by industry for assessing and monitoring quality are univariate based approaches such as process capability indices and SPC methods, as discussed in the previous section. Through the use of these techniques it is assumed that the quality of an assembly can be measured solely by the mean and standard deviation of a set of (assumedly) statistically independent and normally distributed measurement points. When a customer looks at the dimensional quality of an auto-body panel, it is not a set of SPC charts or process capability indices they see: it is a three dimensional free-form surface with correlated variation patterns such as bows, twists, buckles, and smaller features such as bumps and ripples. Perhaps instead of looking at the standard deviation or process capability of a series of measurement points, manufacturers should

be looking at whether an assembly has an overall bow or twist, or a buckle on one surface and ripples along another, and most importantly, which correlated variation patterns are more attractive to the end user. If it is correlated variation patterns that a consumer identifies as the determinant of quality, then quality assessment tools must be able to measure and discriminate between such features.

Optical measurement technology has enabled the digital capture of entire surfaces as opposed to a small set of measurement points, therefore allowing the capture of the physical three-dimensional features that customers see on the end product. However, the previous section has identified a number of key limitations of common univariate industry measures of quality that prevent the adequate measure and discrimination of these three-dimensional and highly correlated variation features, which hinders the ability of manufacturers to make decisions that target true quality objectives. For example, the assumptions of statistical independence and normally distributed data make these quality measures incapable of capturing a key characteristic of sheet metal assembly, the correlation between measurement points on a surface, and incapable of representing highly skewed and multi-modal data sets. If model assumptions do not take key behavioural characteristics into account, then judgements based on such models can only be limited. Furthermore, the inability of univariate measures to interpret the additional information provided by optical measurement data, such as dealing with high dimensionality and the characterisation of different scale variation patterns, again limits the ability of manufacturers to assess three-dimensional variation patterns. This inability to adequately measure and assess the physical manifestations of assembly variation that customers see in the end product creates a strong need to develop new quality assessment capabilities. This leads to the key question motivating the work to be presented in this thesis

> *How can correlated variation patterns in sheet metal assemblies be characterised in ways that can enable more advanced levels of dimensional quality assessment and control?*

Once dimensional quality can be more adequately assessed, this can then provide improved quality objectives to target with virtual engineering, process diagnosis, and knowledge-based design tools. This thesis progresses through a number of stages in addressing the key research question. Firstly, the sheet metal assembly process and factors that can influence the quality of assemblies are introduced through an industry case study. Secondly, an aspect of the assembly process that can influence variation propagation and therefore assembly quality, is investigated and refined according to univariate quality measures. This highlights how sheet metal assembly processes can be refined for a particular quality control target. This leads to the need to define more accurate quality targets and the proposal of two shape characterisation approaches:

a multivariate statistical shape model, and new local shape descriptors. Finally, a discussion of how these new shape characterization measures can be implemented in a dimensional quality assessment framework that can lead to the identification of more optimal processes is presented.

2.8 Conclusion

This chapter firstly discussed a range of key research in the area of automotive body assembly simulation, design, and control for maximising dimensional quality. In order to take full advantage of the capabilities of these methods, an accurate measure of assembly quality is required so that true quality objectives can be targeted. While univariate measures of assembly quality such as process capability indices are predominantly used by industry for quality assessment purposes, it can be strongly argued that there are a number of key limitations of these approaches that prevent the accurate measure of assembly quality. Univariate model assumptions of statistical independence and normally distributed data prevent the capture of correlated variation modes and skewed and/or multi-model distributions. In terms of the interpretation of optical measurement data, univariate approaches cannot adequately deal with high dimensional data sets, and in addition to not being able to capture correlated variation modes, they cannot discriminate between different size or scale patterns (such as bumps and ripples) that can also detract from quality. This thesis is therefore aimed at addressing these limitations and proposes new measures that can more adequately measure assembly quality. The next chapter will therefore proceed with an introduction to sheet metal assembly and process factors that can affect assembly quality via an industry case study. This will then be followed by methods for investigating and identifying optimal process factors, and the proposal of new shape characterisation approaches and how they could be implemented within an advanced dimensional quality assessment framework. This leads to the ultimate goal of this research, which is to provide a more advanced quality assessment framework that can lead to new levels of dimensional assessment and control in sheet metal assembly.

Chapter 3

An introduction to sheet metal assembly

3.1 Introduction

This chapter serves as an introduction to variation propagation in sheet metal assembly through the investigation of a production case study. Firstly, the way in which variation propagates through an assembly process is observed, illustrating some of the issues that manufacturers face in attempting to control dimensional variability in automotive body assembly. Secondly, two aspects of the assembly process, namely clamp and weld sequence, are investigated to highlight their influence on the dimensional outcomes of assemblies. This raises the issue of how assembly processes can be employed for dimensional control strategies. The chapter therefore provides a practical context for the research to be presented later in this thesis. The chapter is divided into two key sections: observing assembly variation, and investigating assembly processes.

3.2 Observing assembly variation

Variation in flexible sheet metal assemblies can be quite unpredictable and difficult to control. The purpose of this study was to observe and compare levels of variation in a sheet metal assembly and its input components, in order to develop an understanding of dimensional variation in flexible assemblies. This naturally led to comparison of measured levels of variation and specified tolerance limits. Tolerance limits used by the project partner were assigned according to the six-sigma approach (Placek, 1989), with variation accumulation estimated by the root sum of squares principle, a statistical method that assumes rigidity of components and normally distributed variation. The assembly illustrated in Figure 3.1 was investigated. This assembly positions important front-end features of the final car including headlamps and the hood. While the assem-

bly consists of 11 components, only 6 of these were selected for the study, as they were deemed structurally critical.

Input components and output assemblies were measured at selected characteristics of interest, which consisted of surfaces on welding flanges and the center-point of various locating holes. Initially, nine random samples of each input component were measured. This sample size was chosen due to time and resource constraints. These parts were then built up into corresponding assemblies in a consecutive batch over one shift, and measured at the same features of interest. It should be noted that parts went through four assembly stations to reach the final sub-assembly state, and measurements were only taken at the input component and final sub-assembly stages.

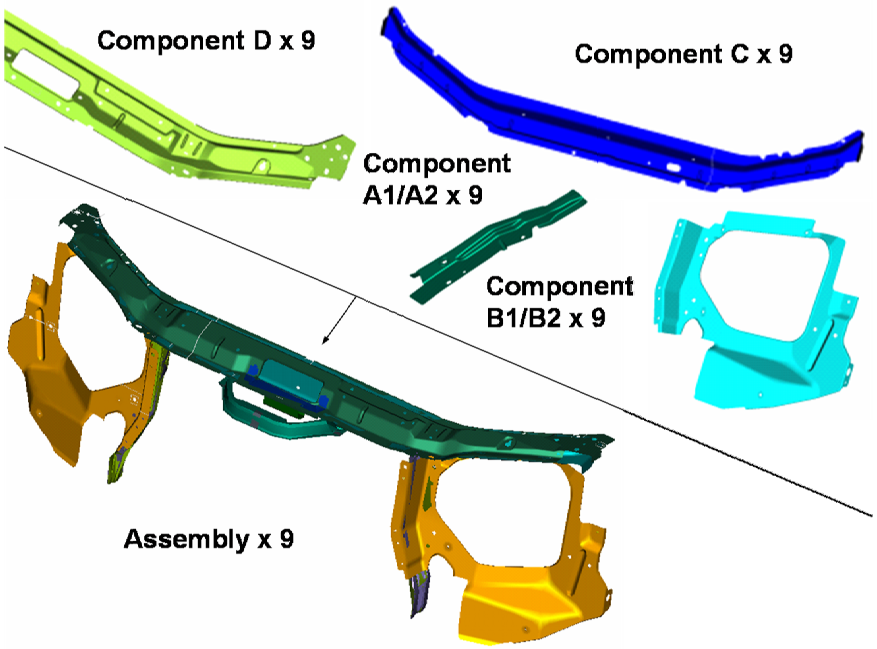

Figure 3.1: Assembly and components.

Coordinate measurement machines (CMM s) were used for dimensional inspection, with assemblies and components located in their respective production measurement gauges. For the purposes of this thesis, Measurement Points (MP s) will refer to measurements of both surface points and the center-point of locating holes. Table 3.1 states the number of features measured for each component and the assembly. Note that parts A1 and A2, and B1 and B2, are corresponding/mirrored left and right components. Key findings of this study are presented in the following sections: Component and assembly variation, Variation stack-up, and Positional shifts.

Table 3.1: Number of holes and points measured for each component and the assembly.

Component	Number of MP s	
/Assembly	Points	Holes
A1	7	2
A2	7	2
B1	8	6
B2	8	6
C	20	0
D	18	9
Assembly	38	22

3.2.1 Component and assembly potential

Components and the assembly were assessed using Process Potential (P_p) to determine how acceptable levels of variation were. This index is defined as the tolerance range for each MP divided by its six-sigma estimate (σ)

$$Pp = \frac{USL - LSL}{6 \times \sigma}, \tag{3.1}$$

where USL is the upper specification limit and LSL the lower specification limit.

Note that the Process Capability C_p was not used as the standard deviation was not calculated from run chart data, but directly from all study samples. Mean position was not considered in this case, as variation alone was the focus of interest. The key finding here was that the assembly displayed consistently higher P_p values than its components. The average assembly P_p value was 24% greater than the average P_p for its components. Therefore according to existing specifications, the assembly is dimensionally better than its components. It should be noted that the assembly has wider tolerance ranges than its components. This may explain the reason for this substantial improvement in P_p readings. However, this difference in P_p values could be highlighting that designers are still learning how to predict tolerance stack-up in flexible assemblies. As mentioned previously, variation in flexible assemblies does not stack-up according to rigid body theory, and is often absorbable (Takezawa, 1980). However, as in the case of this assembly, sheet metal tolerances are often still based upon rigid body assumptions. This could mean that required tolerance increases are overestimated with current prediction methods, resulting in an evident increase in P_p values of the assembly compared to its input components. Figure 3.2 shows a simplified representation of the final assembly, which highlights relative levels of variation in the assembly (according to the P_p values). An interesting observation is the asymmetrical distribution of variation across the assembly, particularly along the top panel. This could be the result of additional parameters that can influence sheet metal assembly

variation stack-up, such as clamp or weld sequence.

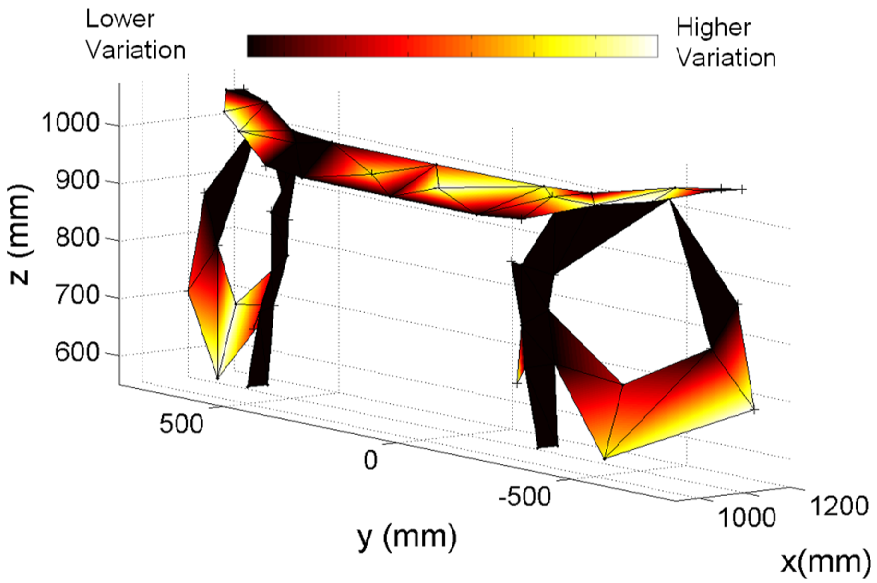

Figure 3.2: Relative levels of acceptable variation according to P_p.

3.2.2 Variation stack-up

To further investigate the behavior of tolerance stack-up in this assembly, variation levels in MP s were compared before and after assembly. A 95% F-test for ratio of variances was used to identify statistically significant changes in variation levels (see Appendix E.1.2). Table 3.2 shows the portion of MP s for each component that were classified as either having a 95% statistical certainty of an increase, or decrease, in variation from components to assemblies. Cases not classified as increasing or decreasing were assumed to have had negligible changes in levels of variation.

Cases of increases in variation noticeably differ between the components. Components A1 and A2 show a substantial portion of MP s displaying an increase in variation, both at 54%. Components C and D show only 5% and 13% of MP s displaying increases in variation respectively. B1 and B2 are at slightly different levels to each other, sitting at 19% and 35%. A key feature of these results is the substantial portion of MP s that show a decrease in variation. This finding is highlighted by the results of component D, where a larger portion of MP s decreased in variation than increased (33% compared to 13%). Component C shows an identical portion of MP s increasing to those decreasing at 5%. The remaining components display significant percentages of MP s

Table 3.2: The percentage of MP s displaying statistically significant increases or decreases in variation levels over the assembly process (95% level of certainty).

Component	Increase	Decrease
A1	54%	38%
A2	54%	31%
B1	19%	12%
B2	35%	8%
C	5%	5%
D	13%	33%

with decreasing variation, but not to the extent of MP s that increased in variation.

Investigation of regions in the final sub-assembly of changes in variation revealed the following trends. Generally, regions where variation increased were flexible and relatively unconstrained in the measurement gauge (ie, little to no clamping or locating surfaces located near these regions). Regions where variation decreased tended to lie in areas that were relatively rigid in the final sub-assembly, and/or positioned in close proximity to locating surfaces and clamps. These findings suggest that increasing the number of constraints on the assembly will better control the measured variation. However, through excessive clamping, important information about the natural shape of an assembly could be lost, and measurement data will therefore not reflect the true quality of an assembly. Investigating the best approaches for clamping in measurement fixtures is therefore an ongoing issue of concern for manufacturers (Majeske and Hammett, 2000).

3.2.3 Positional shifts

Figure 3.3 illustrates some interesting trends about the measured position of holes before and after assembly. A silhouette of component D is overlaid with scaled vectors showing the change in position of each hole, for all nine samples. For each hole, the vectors for each of the nine samples point in a similar direction. It appears that between the components and final assembly, these holes are consistently being shifted in similar directions.

As stated previously, components go through four assembly stations before reaching the final sub-assembly state. There are several locator changes throughout these operations, including both surfaces and holes. In some cases, there are two separate sets of locators on the same part, which are used in different assembly operations. There are also cases where locating methods differ between measurement gauges and assembly stations. As a general design guideline, locator shifts should be minimized as much as possible, as these shifts can introduce an additional variation source. As

in the production case study, this design guideline is not always achievable considering production pressures of cost and time. Locating differences may therefore be the cause of this consistent shift in hole-positions. Another possibility is that the parts may be deformed in a consistent manner due to the specific processes, including clamping and welding sequences. Studies have shown that welding and clamping sequences can have a significant influence on the shape of an assembly (Hu et al., 2001).

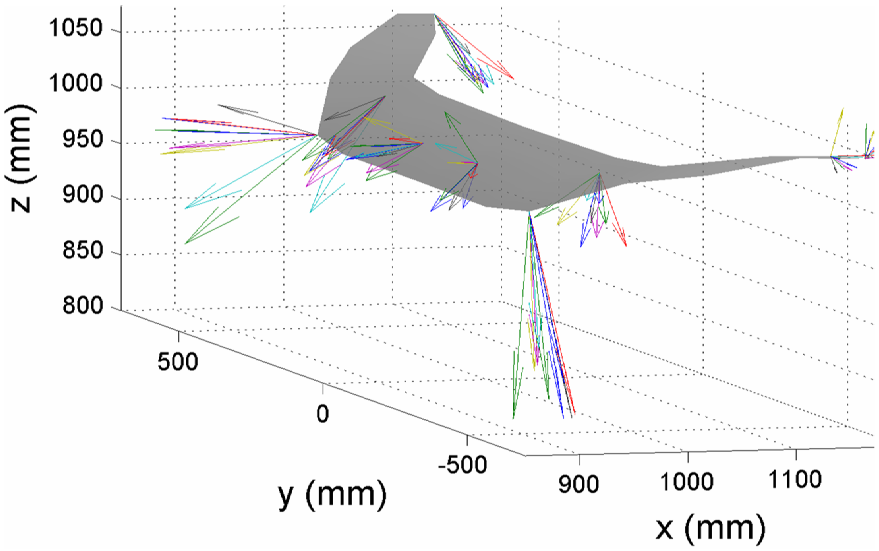

Figure 3.3: Positional shifts of holes from before assembly to after assembly.

3.2.4 Summary of observations

Through the observation of variation stack-up in a production assembly, some of the difficulties facing manufacturers in their attempts to understand and control variation have been revealed, with key findings summarized in the following:

- In terms of process potential, the assembly was dimensionally more acceptable than its components. This raises questions about current tolerance allocation methods, as rigid body theory is used to assign tolerances when it has been shown that flexible assemblies do not follow this law.
- Variation does not necessarily increase over the assembly process, with many cases of reductions in variation levels identified. Inspection of regions in the assembly that displayed these changes in variation over assembly revealed that locating methods might have a significant influence on measured levels of variation.

- Observations of positional shifts of holes from before assembly to after assembly show consistent directional changes. This possibly identifies the effect of locator changes between operations, and/or consistent distortion effects of the particular assembly process.

3.3 Investigating assembly processes

The previous section identified that there are some aspects of the assembly process that make variation propagation difficult to understand and control. This section moves on to investigate some aspects of the assembly process that can influence the dimensional outcomes of assemblies, namely clamp and weld sequence. The same production case study is the focus of investigation, however, only the final assembly operation was the subject of investigation. This operation involves clamping and welding a top plate onto a lower sub-assembly consisting of the lower cross and headlamp surrounds. The upper sub-assembly and lower subassemblies are indicated in Figure 3.4.

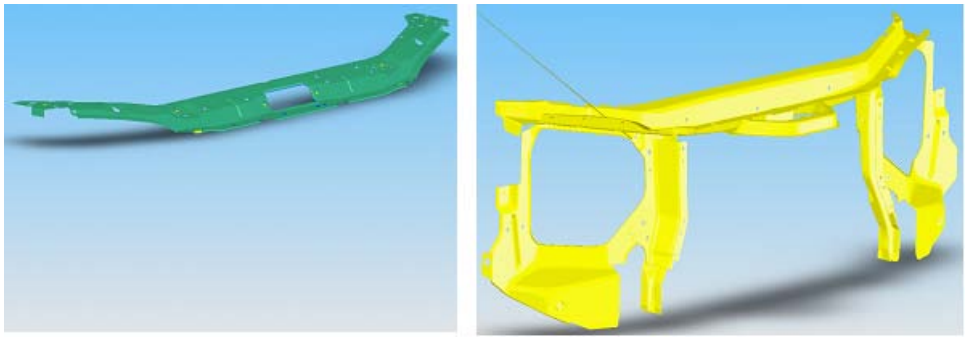

Figure 3.4: Upper and lower subassemblies that are the input components for the final assembly operation.

3.3.1 Clamping sequence

Clamp locations for the last assembly operation are illustrated in Figure 3.5. There are four clamps labelled A through D. Clamps B and C have two clamp contact points (actuated by the same hydraulic cylinder), one on the front flange and the other on the back flange. For the investigation of the effects of clamp sequence on the dimensional outcomes of the final assembly, a dummy build approach was used. This involved applying clamp sequences to the same set of components without actually welding the assembly together, and measuring the dummy build outcomes of each clamp sequence. This allowed direct comparison of clamping sequences as the same set of components would be clamped each time in the assembly fixture. It should be noted that once

two notably different clamp sequences were identified, a new set of panels was clamped and measured with only the two chosen clamp sequences. This was done to minimize any possible plastic deformation effects resulting from repeated clamping forces, which could be misinterpreted as mean shifts between clamp sequences. A combination of the centre-point of holes and surface MP s were measured.

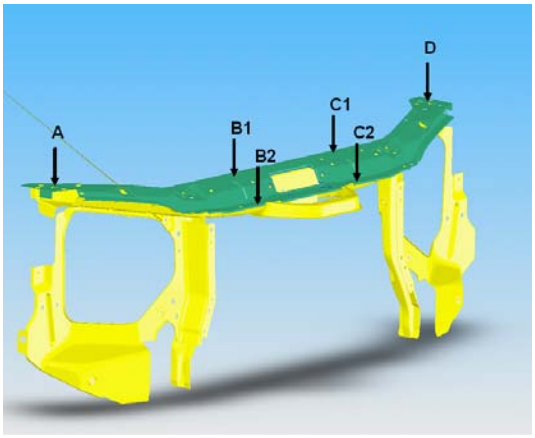

Figure 3.5: Clamp locations.

Two clamp sequences resulting in noticeably different final assembly shapes were clamp sequence ABCD (left to right viewing Figure 3.5), and clamp sequence DCBA (right to left viewing Figure 3.5). The resulting mean shifts between the two clamp sequence are shown in Figure 3.6. It can be seen that there is an apparent side shift when comparing the dimensional outcomes of the assembly, with average and maximum mean shifts of 0.6 mm and 0.9 mm respectively. The observed mean shifts identify clamp sequence as an aspect of the assembly process that can influence the dimensional outcomes of assemblies. This suggests that clamp sequence should be considered during the process design phase.

3.3.2 Weld sequence

To illustrate the effects of different weld sequences on the dimensional outcomes of assemblies, two weld sequences were investigated and compared. There are two weld robots, Robot 9 and Robot 10, which perform welds in the last assembly operation. Robot 10 welds the front edge of the assembly, and Robot 9 the back edge of the assembly (see Figure 3.7). The two weld sequences investigated involved running one robot after the other. For the purposes of this report, the weld sequence that corresponds to welding the front edge of the assembly followed by the back edge will be referred to as R9 , and the weld sequence that corresponds to welding the back edge followed by the front as R10 .

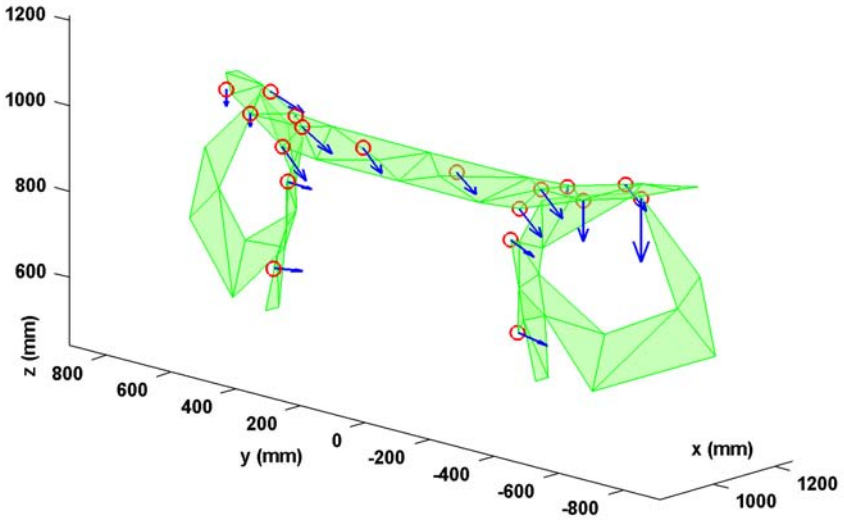

Figure 3.6: Mean shifts resulting from clamp sequence ABCD and DCBA. Vectors show dimensional differences between the two clamp sequences.

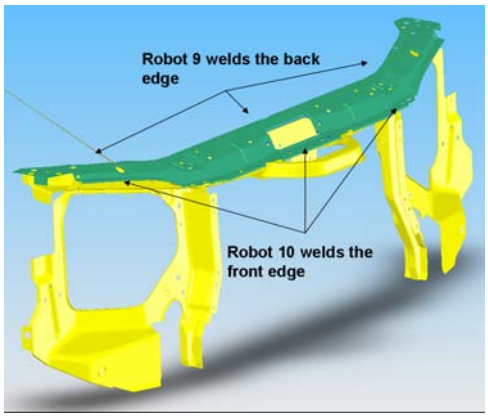

Figure 3.7: Weld locations.

The upper and lower subassemblies were sampled from two 16 piece production runs (32 in total). The experimental assembly details are listed in Table 3.3, where weld sequences R9 and R10 were evenly split over production batches 1 and 2. This was to ensure that any mean shifts between the weld sequences or production batches could also be identified. There are two key sets of results, mean shifts, and variation propagation, which will be presented in the following sections.

Table 3.3: Weld sequence and production batch for each assembly sample.

Sample	Weld Sequence	Batch	Plot notation
1-8	R10	1	+
9-16	R9	1	x
17-24*	R10	2	*
25-32	R9	2	o

Mean shifts

A traditional approach to analysis of this data set in terms of mean shifts would involve the univariate analysis and comparison of each of the four sub groups for each of the 18 MP s (see Appendix E.1.1). Conducting and distilling important information from such an analysis can be a challenging task due to the number of MP s, sub-groups, and paired comparisons that need to be considered. An alternative approach to gaining an overall impression of the data set is to use a dimensional reduction technique known as PCA (Principal Component Analysis), which would allow the 18 MP data set to be represented by a smaller set of factors that describe most of the information in the data. In the following this technique will be introduced and then demonstrated on the weld sequence study data. The technique is also applied in later chapters.

Principal component analysis

Principal Components Analysis (PCA) is a multivariate statistical technique that is often used for dimensional reduction of large data sets. The basic concept is to select a smaller set of variables that can account for most of the information in an original data set of many variables. Applications of PCA in automotive body assembly have often been used as a tool for identifying major fault modes: these methods assume that principal components correspond to a particular fault mode (Ceglarek and Shi, 1996). For the purposes of this thesis, PCA is used only as a data reduction method and makes no assumption about the correlation between fault modes and the components: the following describes the technique.

Suppose the shape data consists of n observations and x_i measurement points:

1. Compute the mean of the variables (or MP s), .

$$\overline{x} = \frac{1}{n}\sum_{i=1}^{n} x_i \tag{3.2}$$

2. Compute the covariance of the data, S.

$$\mathrm{S} = \frac{1}{\mathrm{n}-1}\sum_{i=1}^{n}(x_i - \overline{x})(x_i - \overline{x})^T \tag{3.3}$$

This covariance matrix contains the variations of each measurement point with respect to every other measurement point across the training set.

3. Compute the eigenvectors, and corresponding eigenvalues of the covariance matrix S. Eigenvector/eigenvalue pairs are then sorted in descending order according to their corresponding eigenvalues.

4. Transform the original data set into the reduced dimensional PCA space. For the multivariate shape models to be presented, density estimation is conducted in this reduced dimensional space:

$$b = \Phi^T(x - \overline{x}) \tag{3.4}$$

where , and b represents observation (or sample) scores in the reduced t-dimensional PCA space.

5. Approximate any of the original data set x using the t eigenvectors corresponding to the largest eigenvalues through the following:

$$x \approx \overline{x} + \Phi b \tag{3.5}$$

where b is a weighting vector determining how much of each principal component contributes to the shape x. The more eigenvectors used, the more information of the original data set is retained. However, as the object of this exercise is data reduction, it is more favorable to choose the minimum amount of eigenvectors that represent the data to a desired level of accuracy. The number of eigenvectors t can be chosen so that the model represents a percentage of the total variance of the data (ie, 99%), or so that the model can approximate any training example to a given level of accuracy (ie, a maximum error of 0.1mm). Figure 3.8 below shows an application of PCA to 2D data, where a 1D PCA representation can provide a good approximation of the original data set.

PCA and Mean shifts

In Figure 3.9, the original 18 MP, 32 sample data set, is represented by a 2-Dimensional PCA plot. There are two factors (instead of 18 MP s) describing the data, PC1 and PC2, and each point indicated on the plot represents a measured sample. Referring back to Table 3.3, it can be seen that each of the 4 sub-groups occupy separate and distinct areas within the plot. This indicates that there are mean shifts between each sub-group: the PCA approach therefore provides a compact and informative representation of the overall trends in the data set within a single plot. It should be noted that a common linear classifying technique, Linear Discriminant Analysis (Appendix H.1), was applied to partition the sub-groups.

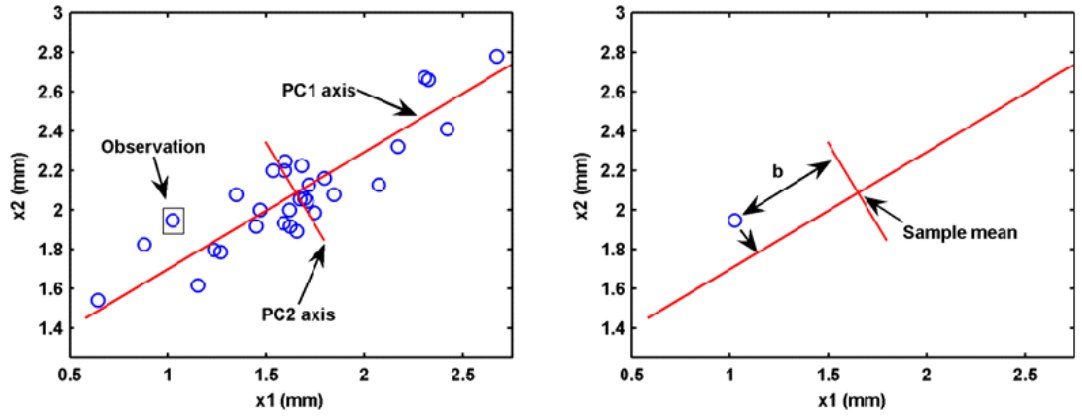

Figure 3.8: A 2D data set with principal component axes (PC1 and PC2) overlaid. An observation can be reasonably approximated by its first principal component score (ie, the point lying on the PC1 axis at a distance b from the sample mean).

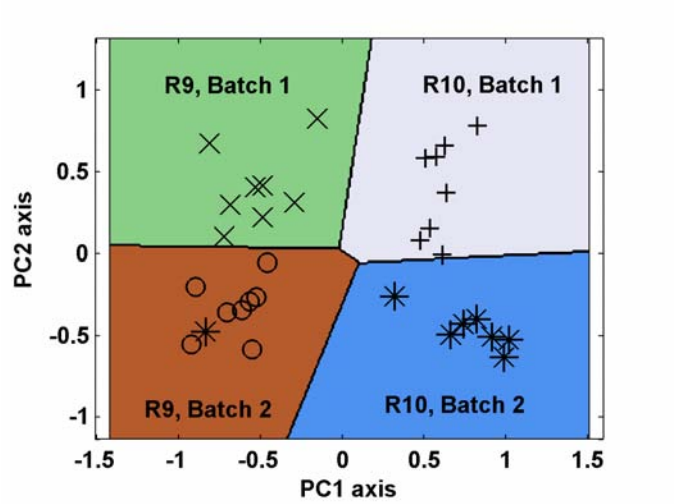

Figure 3.9: A 2D PCA representation of the 32 built assembly samples. It can be seen that there are four distinct clusters. Refer to Table 3.3 for plot notation.

While PCA provides an overall impression of what clusters (or mean shifts) exist in the data set, it is also of interest to see how these mean shifts look in the original body co-ordinate space. Mean shifts between welding sequences in the original body co-ordinate system are highlighted in Figure 3.10. Here, a simplified representation of the assembly is overlaid with vector plots showing the direction and relative magnitude of the mean shifts: the maximum mean shift here was 0.85 mm. The corresponding directional movement between weld sequence means in the 2D PCA plot can be seen

in Appendix G. While not indicated in the Figures, the maximum mean shift resulting from the different production batches was 0.4 mm.

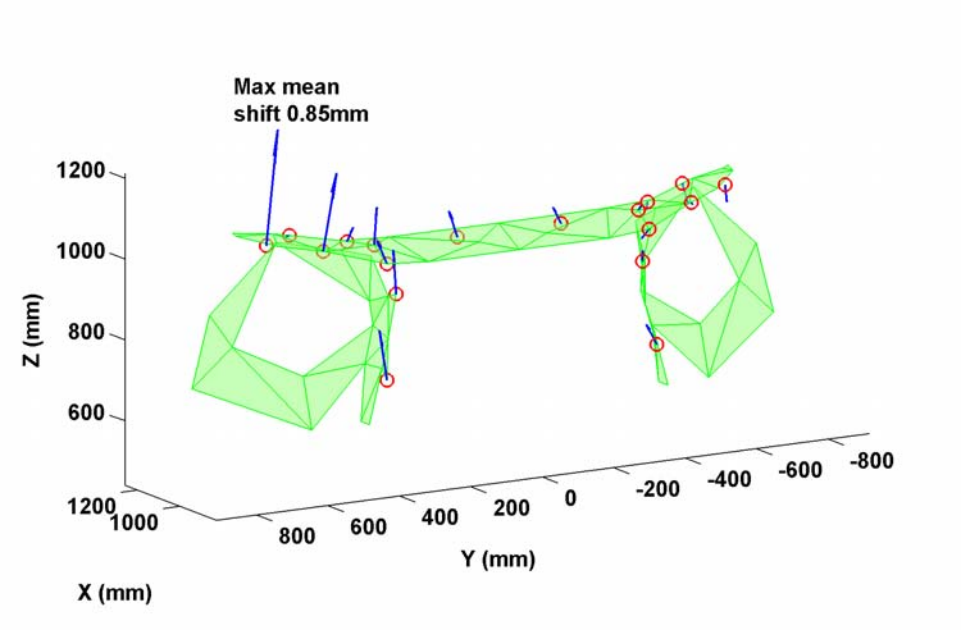

Figure 3.10: Simplified representation of the front cross. Vector plots show the mean shift between weld sequences.

Variation propagation

Variation in rigid component assemblies accumulates according to the additive theorem of variance (ie root sum of squares): for rigid assemblies, variation can therefore be expected to increase throughout the assembly process. It has already been shown that this law does not hold for flexible component assemblies, such as sheet metal assemblies, and that variation can be absorbable (section 1.1.4). To illustrate this behaviour in a production setting, the variance of MP s measured on the sub-assemblies was compared to the variance of the same MP s measured on the final assembly.

Table 3.4 presents the percentages of increases and decreases in variance using an F-test at a 95% certainty (see Appendix E.1.2). It should be noted that variance ratio calculations were made on each of the sub-groups of 8. For example, for group R10, Batch 1 the standard deviations of the MP s of the 8 sample components was compared against the standard deviations of the same MP s from the corresponding 8 sample assemblies. It can be seen that more MP s exhibit a decrease in variance than an increase, which again supports the characteristic of absorbable variation in flexible component assemblies.

Table 3.4: The percentage of MP s displaying statistically significant changes in variance (95% certainty) over the single station assembly process.

Sub-group	Decrease	Increase	No change
R10, Batch 1	17%	1%	82%
R9, Batch 1	17%	2%	81%
R10, Batch 2	15%	1%	84%
R9, Batch 2	17%	1%	82%

3.3.3 Summary of assembly processes

- Clamp and weld sequence were shown to influence the dimensional outcomes of assemblies. Comparison of two clamp sequences revealed mean shifts of up to 0.85 mm, as did comparison of two weld sequences. These observations provide some insight into example factors that can alter assembly variation propagation as a result of the ability of flexible components to bend and distort from process interactions.

- Variation can be absorbed by the assembly process, with approximately 17% of MP s displaying a decrease in variance when comparing subassemblies to the final assembly. This supports the findings of section 3.2, and reinforces the need for sheet metal assemblies to be analyzed and treated in a different manner to rigid assemblies in terms of tolerance and variation stack-up analysis.

3.4 Conclusion

This chapter presents a series of investigative trials performed on a production case study to serve as an introduction to some of the characteristics of sheet metal assembly. Firstly, variation propagation through a multi-stage assembly process was investigated. These observations highlighted some of the difficulties manufacturers face in terms of understanding, predicting, and controlling dimensional variation, as a result of the flexibility of components and their ability to be distorted into conforming (or non-conforming) shapes. Secondly, the influence of clamping and welding sequence on the dimensional outcomes of the assembly was investigated. It was shown that by altering clamp or weld sequence, the dimensional outcomes of assemblies could also be altered in terms of mean shape. These observations provide some insight into two factors that can influence the way in which variation propagates through an assembly process and raises some key issues, including:

- To what extent can these assembly processes change dimensional outcomes and how do they influence assembly variability (and not just mean shape)?

- How can the best assembly processes be identified for dimensional control strategies?

These key issues present key motivational factors for the research to be presented. In particular, the next two chapters will investigate in more detail the effects of assembly processes on final assembly mean shape and variability, and how targeted selection of assembly processes can be used for dimensional control.

Chapter 4

The effects of clamp sequence

4.1 Introduction

Finite element (FE) modelling techniques have become popular tools for exploring welding and clamping sequence dependence in sheet metal assemblies (Hu et al., 2001; Liao, 2003a; Fan et al., 2007). In this chapter, the dimensional variability associated with different assembly clamping sequences is investigated with a FE contact modelling approach implemented in the commercial code Abaqus. The implemented approach allows for a more accurate representation of true contact conditions in comparison to previous approaches. A simplified channel section assembly consisting of a top hat and bottom plate is the case study investigated. Expected variation modes of bow and twist were used to simulate key variability sources in the main structural component under investigation, the top hat of the channel section. The chapter will display how final assembly variability can change considerably depending on clamp sequence selection. It will also demonstrate how different clamp sequences can control particular modes of variation better than others. It will also show that there is not one particular clamping sequence that is the best for containing all variation modes. The chapter serves to illustrate the influence of clamping sequence on variation propagation in sheet metal assembly, and the extent to which assembly variability can change depending on clamp sequence selection. The results therefore suggest the importance of considering clamping sequence during process design if optimal dimensional control strategies are to be reached.

4.2 Simulated assembly

A simplified cross-member structure assembly, consisting of a hat section and flat bottom plate, was chosen as the focus for this experimentation: it is representative of a

larger class of components including chassis rails and structural cross-members. An illustration is presented in Figure 4.1. The component is located by a pin and slot at opposite ends along one flange, and 3 evenly spaced locating clamps down each flange (6 clamps in total). Locator positions remain fixed throughout the study. The channel is 1000mm long, 50mm high, has 25mm flanges, with a sheet metal thickness of 0.8mm.

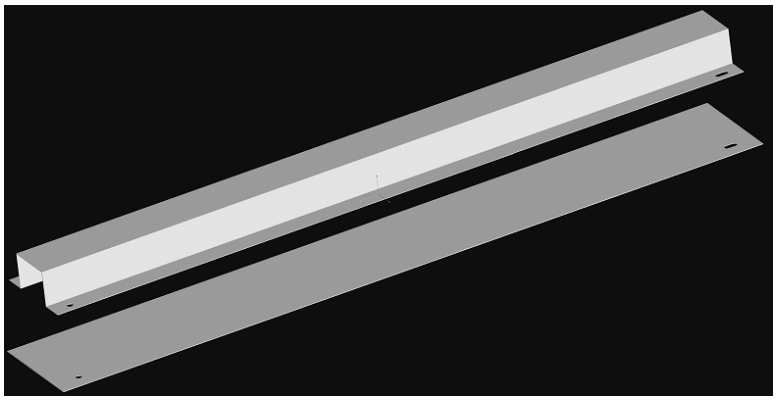

Figure 4.1: Channel section case study, consisting of a top hat and bottom flat plate. The assembly is located by a pin, slot and 3 clamps down each flange.

4.2.1 Finite element approach

This study utilizes a non-linear contact FE simulation model implemented in Abaqus. This model accounts for deformation induced contacts, and contact resulting from the initial placement of parts in assembly fixtures, both of which linear models cannot easily capture. This approach was therefore selected as it is a more accurate representation of the physical assembly process. The FE model used a multi-step framework, consisting of the following stages.

1. Datuming of parts using the locating pins and rest surfaces.
2. Applying clamps
3. Performing welds
4. Releasing the clamps
5. Re-clamping in measurement fixture

These stages have often been referred to as the place, clamp, fasten, and release cycle as presented in section 1.1.2 (Chang and Gossard, 1997). An example FE simulation setup is illustrated in Figure 4.2. The pin P (constraining movement in the x and y directions) and slot S (constraining movement in the y direction) are located at opposite

ends along one flange. Locating clamp locations and their sequence are indicated by numbers 1 through to 6. Each clamp location consists of a rest that lies at $z = 0$ (constraining movement below this point), and a clamp that is applied to the top hat surface. Welding locations are indicated by the letters a through x (note that weld sequence is not altered for this study). Welds are modelled in a similar manner to the clamps, with the addition of a mechanical fastener to tie the components together.

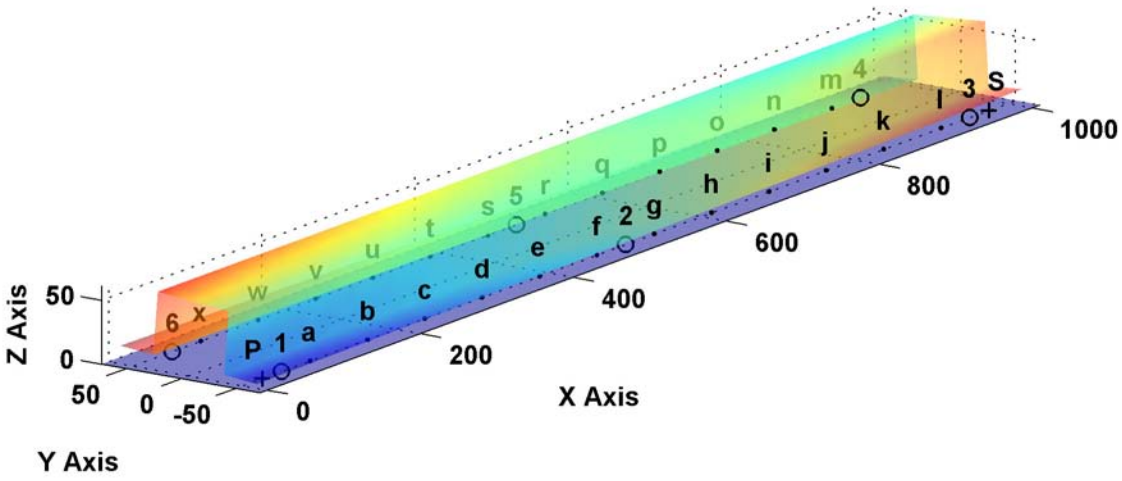

Figure 4.2: Example FE simulation setup. Locating pin and slot locations are indicated by P and S, numbers 1-6 show clamp locations and sequences, and letters a-x are weld locations.

4.2.2 Component variation modes

The key input component variation modes of bow and twist were selected for this study. These variation modes account for surface co-linearity, providing a more realistic representation of part variability. For bow, there is a constant bow radius throughout the length of the part. Twist was created by rotating cross-sections throughout the length of the part. It should be noted that only hat section variation is considered (and not the flat bottom plate). This is because the hat is the primary structural member, and has much greater influence on final assembly variability than the bottom plate. Also, only the hat nodal displacements were considered for data analysis. For the purposes of this paper, twist will be described by the twist angle illustrated in Figures 4.3 and 4.4, and bow will be described by the middle deflection as illustrated in Figures 4.5 and 4.6.

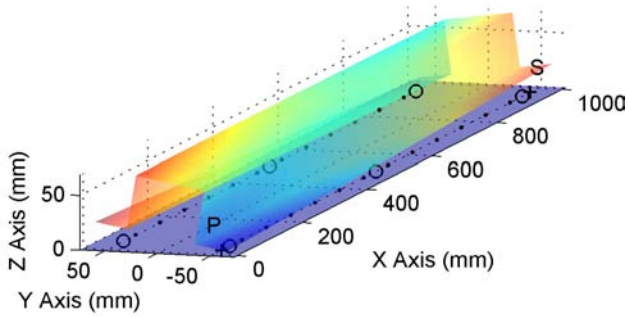

Figure 4.3: Example silhouette of Negative twist.

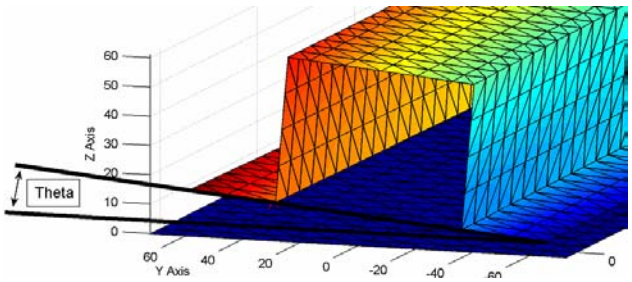

Figure 4.4: Twist angle measure (degrees) for the variation modes Positive twist and Negative twist. Negative twist involves a negative angle (counterclockwise rotation).

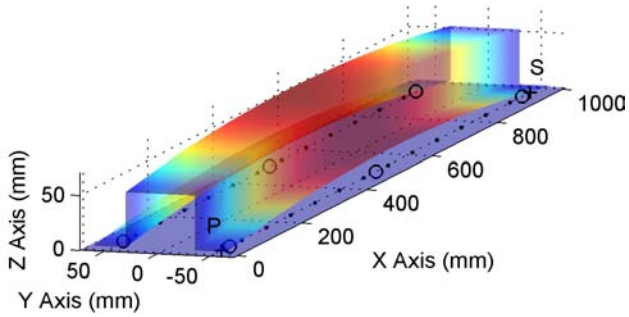

Figure 4.5: Example silhouette of positive bow.

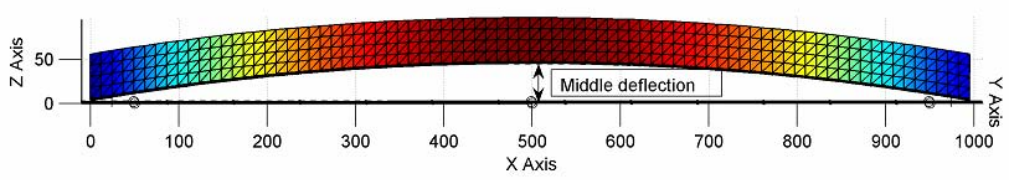

Figure 4.6: Middle deflection measure (mm) for the variation modes Positive and Negative bow. Negative bow has a middle deflection below the zero point of the z axis

4.3 Clamp sequences

There are 720 possible clamp sequences with a 6 clamp configuration. Testing each of these sequences is unrealistic considering the selection of a non-linear FE model for assembly simulation which is computationally intensive. Sixteen clamp sequences were initially chosen from four logical groups of: clamping down one flange and back up the other, clamping from one end to the other, clamping the outer ends and then the middle, and clamping the middle and then the outer edges (see Figures 4.7 and 4.8). FE simulations were run for these 16 clamp sequences to gather basic measures of variability. In consideration of these results, a final subset of 5 clamping sequences from this group of 16 was then chosen for detailed investigation. This selection process is presented in the following section.

4.3.1 Clamp sequence selection

One discrete example from each variation mode was selected: Positive bow of 2.6 mm, Negative bow of -2.6 mm, Positive twist of 3 degrees, and Negative twist of -3 degrees. Simulations were then run for all clamp-sequence/variation-mode combinations. The average displacements from the nominal final assembly shape were calculated for each of these clamp-sequence/variation-mode combinations. These figures provided an indicator of the sensitivity of assembly variability to input variation modes for each of these combinations, allowing for a ranking of the performance of each clamp sequence for each variation mode (see Appendix C for comparison table). Here it was assumed that the closer an assembly shape is to the nominal, the better the shape is. These results were then used to select a subset of 5 clamp sequences to investigate in more detail. Firstly, the clamp sequences that resulted in the minimum average displacement for each variation mode were selected. For example, clamp sequence 621 had the lowest average displacement figure for negative bow at 0.27 mm, and was therefore selected. Secondly, the best and worst overall (across all variation modes) clamp sequences were selected. The overall measure was taken as the sum of the average displacements for all variation modes. For example, clamp sequence 634 had the highest overall value of 1.09 mm and was therefore selected as the worst overall sequence. Coincidentally, clamp sequence 641 was the best for positive bow and overall. The results for the final subset of 5 clamp sequences are presented in Table 4.1. It can also be seen that there is a substantial difference in the average displacement values when comparing the best and worst sequences. For example, for negative bow, the increase from the minimum average displacement to the maximum average displacement is 33%, suggesting that selection of clamp sequence is an important factor for the control of dimensional variability in flexible assemblies. This increase is much higher for the other variation modes.

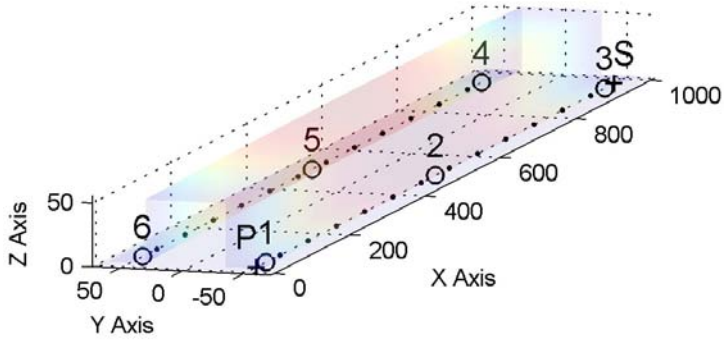

Figure 4.7: Example clamp sequence 611 (down one flange and back starting near the locating pin). Numbers indicate clamp location and sequence, P and S the pin and slot locations.

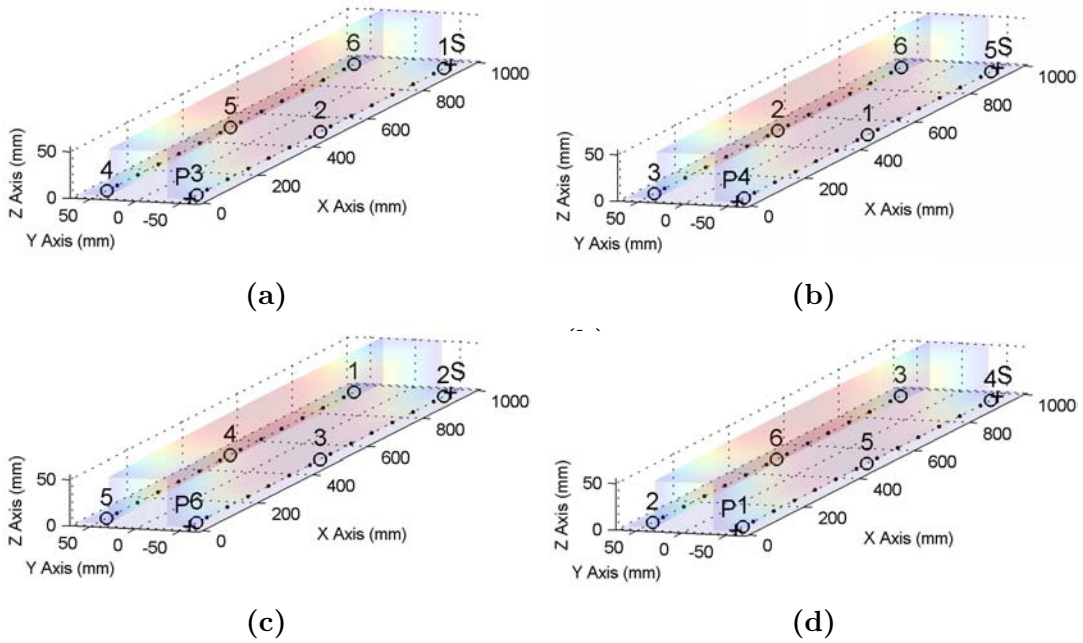

Figure 4.8: Figure (a) displays clamp sequence 612 (Down one flange and back starting at the locating slot). Figure (b) displays clamp sequence 621 (Middle and then the outer ends). Figure (c) displays clamp sequence 634 (One end to the other). Figure (d) displays clamp sequence 641 (Outer ends and then the middle).

4.4 Investigating a population of assemblies

The study presented in the previous section only considered a single example or instance of each variation case (for example, a bow of 2.6mm). To put this study into more practical context, the type of data seen in real-life production situations, such as the

Table 4.1: Final assembly average displacements from nominal for selected clamp sequences. As seen in the table, each clamp sequence was tested against each variation mode.

Clamp sequence number & brief description	Average displacement from nominal (mm)				Overall variation: Row total (mm)
	Negative bow, -2.6mm	Positive bow, 2.6mm	Negative twist, -3°	Positive twist, 3°	
611: Down & back (pin)	0.36	0.35	0.13	0.08	0.91
612: Down & back (slot)	0.32	0.36	0.09	0.11	0.88
621: Middle to out	0.27	0.43	0.10	0.09	0.89
634: One end to other	0.31	0.29	0.21	0.28	1.09
641: Out to middle	0.34	0.22	0.11	0.18	0.84
% Increase Max to Min	33%	95%	133%	250%	30%

measurement of a large set of samples from a production run, was simulated for analysis. Here, the samples would have differing levels of bow and twist resulting from normal process variation. To create such large data sets for detailed inspection, random samples for each of the variation modes at different magnitudes were created using a Gaussian random number generator.

Table 4.2: Parameters used to generate variation modes.

	Positive bow	Negative bow	Positive twist	Negative twist
Standard deviation	1mm	1.6 mm	2°	2°
Mean	0 mm	0 mm	0°	0°
Samples	200	200	200	200
Max. value	2.71 mm	-4.75 mm	4.86°	-4.80°
Max. assembly displacement	2.32 mm	4.03 mm	2.15 mm	1.91 mm

Final assembly shapes were then simulated for each of these samples, for each of the investigated clamping sequences. Appendix B.2 details this simulation procedure, which also involved interpolation techniques designed to reduce the required number of computationally intensive nonlinear contact FE simulations. The input component variation was chosen such that maximum input values corresponded to reasonable final assembly maximum displacements. For example, the maximum positive bow of 2.71 mm corresponded to a final assembly displacement of approximately 2.32 mm for clamp sequence 621 (see Table 4.2). Figure 4.9 displays a histogram of random part variation for positive bow.

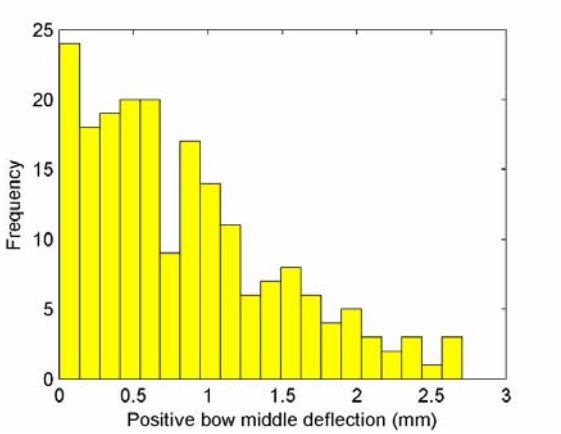

Figure 4.9: Example random distribution of inputs for positive bow. Note that only half of the Gaussian distribution is used for generating the random data set for each variation mode, and the nominal part shape is the most likely shape.

4.5 Assembly population results

The results for the investigation of a population of assembly components described in the last section are presented in three stages. Firstly, the variation associated with each clamping sequence and each of the 4 variation modes (positive/negative bow and twist) is assessed individually (ie, this section is looking to identify the best clamping sequence for each of the individual variation modes). Secondly, the variation associated with each clamp sequence across all variation modes is assessed (ie, this section is looking to identify the best clamp sequence for containing the variation modes overall). Finally, the concept of an adaptable clamping sequence is proposed, where given the shape of each part to be assembled, the optimal clamp sequence can be selected for that assembly case.

4.5.1 Individual variation modes

In this section, the variation associated with each clamp sequence is assessed for each particular variation mode. As the distributions of the assembly variables were highly skewed, a histogram is used to estimate the 90th percentile spread of data. The average of this value across all variables (or nodes) is used as an assessment of the overall population variability. This is illustrated in Figure 4.10. To highlight the differences in variation of the final assembly for the different clamping sequences, Figure 4.11 shows the percentage differences between the maximum and minimum average spread values of each clamp sequence for each variation mode. The results show that different clamp sequences can result in considerably different final assembly variation. For example,

for positive bow the worst clamp sequence results in an average spread value that is 80% more than the best clamp sequence.

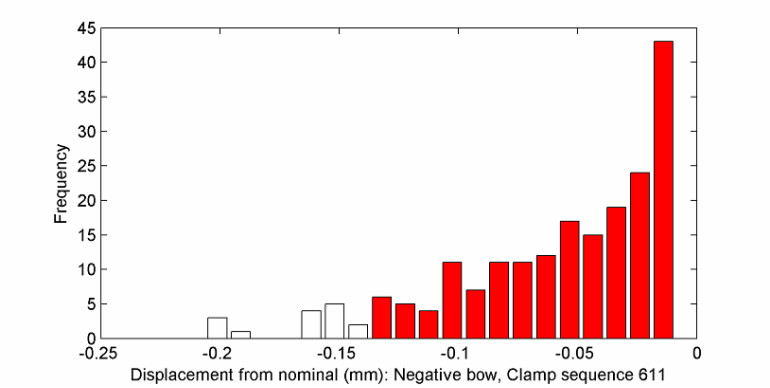

Figure 4.10: Histogram of an example variable from the final assembly, highlighting the 90% spread of data measure, indicated by the filled bars. Note that the measure of spread includes the peak-end of the data and omits the tail-end.

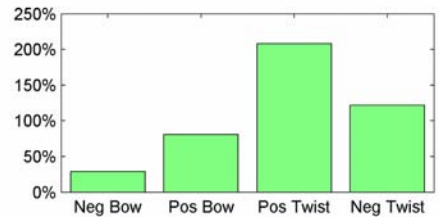

Figure 4.11: The percentage difference between the maximum and minimum average spread values of each clamp sequence.

Table 4.3 shows which clamp sequences were the best and the worst at containing variation in the final assembly. An interesting observation is that each variation mode has a different clamping sequence that results in the lowest assembly variation. Another observation is that the clamping sequence that results in the lowest variation for positive bow results in the highest variation for negative bow (and vice versa). These results show that the best clamp sequence for containing variability depends on which variation mode is present. For further demonstration of the differences between the clamping sequences, a comparison of the maximum differences between final assembly shapes for each clamp sequence given the same input part shape (positive bow of 2.71 mm) was undertaken. It can be seen that by altering the clamp sequence, the final assembly shape can be quite different, with a maximum difference of 2.14 mm between clamp sequences 641 and 621 (see Table 4.4 and Figure 4.12).

Table 4.3: The lowest and highest variation clamp sequences for each variation mode. Note that different variation modes do not share the same lowest variation sequence.

	Positive bow	Negative bow	Positive twist	Negative twist
Lowest variation sequence	621	641	611	612
Highest variation sequence	641	621	634	634

Table 4.4: Maximum difference between final assembly shapes for each clamp sequence, for the example input part shape: Positive bow, 2.71mm middle deflection. For example, the value in row 641, column 621 shows the maximum difference between the final assembly shape of clamp sequences 641 and 621, which is 2.14mm.

Clamp sequence	611	612	621	634
641	2.01 mm	2.12 mm	2.14 mm	1.8 mm
634	1.03 mm	2.10 mm	2.12 mm	
621	1.09 mm	1.01 mm		
612	1.07 mm			

4.5.2 Combination of all variation modes

While the last section presented assessments of the variability associated with individual variation modes, this section looks at which clamp sequences are the best for containing variation across all variation modes. Here it is assumed that part variation consists of all 4 variation modes, with each variation mode having an equal likelihood of occurrence, and the distribution and sample size for each variation mode is as stated earlier (ie, there are 800 samples in total for the combination case). Average standard deviation, maximum standard deviation, and maximum displacement from nominal of all MP s, for each clamp sequence, were used to assess the performance of each clamp sequence in terms of dimensional variability. Table 4.5 presents the maximum and minimum performance values and the respective sequences. When looking at average standard deviation, it can be seen that sequence 612 is the best at controlling variability overall. When looking at maximum standard deviation and maximum displacement sequence 621 appears to be the best at controlling variability in the final assembly. The table also shows considerable differences in the performance of the best and worst clamping sequences across each of the performance measures. For example, the percentage increase in the maximum displacement value from the best to worst clamping sequence is 71%.

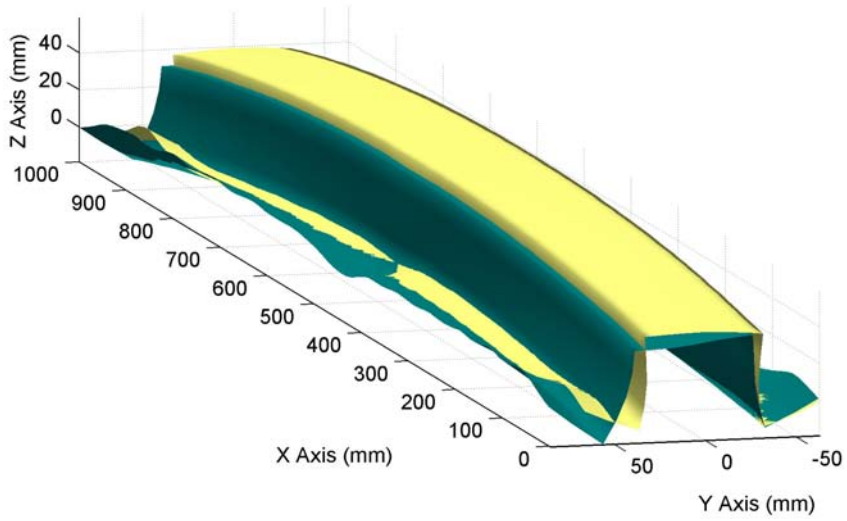

Figure 4.12: Final assembly shapes for clamp sequence 621 (light) and 641(dark) overlaid to highlight differences (10 × magnified displacements from nominal).

Table 4.5: Performance measures for assessing variability of clamping sequences for the case where part variation consists of multiple variation modes.

	Average standard deviation (mm)	Max. standard deviation (mm)	Max. displacement from nominal (mm)
Min	Sequence 612: 0.15	Sequence 621: 0.51	Sequence 621: 2.35
Max	Sequence 634: 0.19	Sequence 634: 1.17	Sequence 634: 4.03
% Increase Min to Max	25%	126%	71%

4.6 Conclusion

In this chapter, the dimensional variability associated with different assembly clamping sequences is investigated with a non-linear contact FE simulation model implemented in a commercial code. Expected input variation to the assembly process was simulated by example correlated variation modes of bow and twist in the main structural component (the top hat). It was found that final assembly variability can change considerably depending on clamp sequence selection. It was also found that different clamp sequences can control particular modes of variation better than others, and that there is not one particular clamping sequence that is the best for containing all variation modes. These observations highlight how an ability to identify the optimal clamping sequence for the particular dominant variation mode in a set of components could notably improve assembly quality. The next chapter will build upon the work presented by experimentally validating the FE modelling approach, and proceeding to develop a set of generalized

clamping laws to allow for a practical approach to robust process design.

Chapter 5

Experimental comparison of clamp sequences

5.1 Introduction

This chapter investigates the influence of assembly clamping sequence on the dimensional outcomes of assemblies through experimentation. The same simplified cross member structure presented in the last chapter is again the subject of investigation, except an 8 clamp configuration is explored. This time a single artificially induced variation mode, negative bow in the top hat, is used to represent an example variation mode that could be present in such a component. The chapter will firstly experimentally validate the finding that different clamp sequences can result in noticeably different geometric outcomes. Secondly, the experimental and simulated approaches will be compared to demonstrate the ability of FEM as a powerful tool for virtual assembly prototyping. The simulated approach will then be applied as in the previous chapter to highlight the influence of clamping sequence on final assembly variability. Finally, through the assessment of further simulated investigations of several logical clamping sequences, a range of generalized clamping design guidelines for minimizing overall assembly variation are proposed. The proposed rules include clamping areas that are closest to nominal first, and clamping from a fixed to free end.

5.2 Experimental clamping study

This section will discuss the experimental setup and approach. The same simplified cross-member structure assembly from chapter 4 is again investigated, however an 8 clamp assembly configuration is explored. A purpose built experimental jig, consisting of locating pins, manual toggle clamps, and a hand held weld gun mounted on linear slides for accurate weld placement, was used for the assembly process. This is illus-

trated in Figure 5.1, where the clamps are also identified A through H for description of clamping sequences. The remaining of this section will present the two clamping sequences investigated for the experimental trials, the key component variation mode that is used to represent typical process variation in stampings, the measurement points that are extracted from the scan data, and finally the approach used to select component samples for the experimental trials.

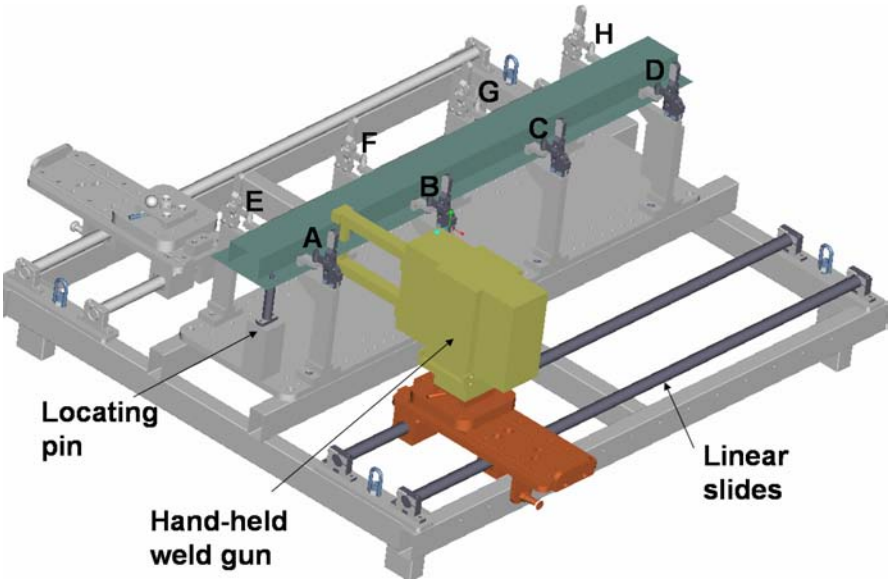

Figure 5.1: Experimental assembly rig.

5.2.1 Experimental and FEM clamp sequences

Preliminary clamp sequence trials on the experimental assembly rig were conducted to determine two clamp sequences to explore in detail. This involved the application of a range of clamp sequences on an example set of components (without welding) to give an indicator of the assembly response to these different clamp sequences. From the range of clamp sequences explored in this preliminary trial, two clamp sequences which exhibited noticeably different assembly shapes were selected for further investigation with both experimental and FEM assembly setups. One sequence applies the outer clamps and then the middle clamps, and the other sequence applies the inner clamps and then the outer clamps. The sequences according to the clamp indicators noted in Figure 5.1 are as follows:

- **Clamp sequence 1:** firstly the middle clamps are applied, followed by the the outer clamps. This corresponds to the following clamp sequence as indicated in Figure 2: F-G-C-B-A-E-H-D.

- **Clamp sequence 2:** firstly the outer clamps are applied, followed by the the middle clamps. This corresponds to the following clamp sequence as indicated in Figure 2: D-H-E-A-B-C-G-F.

5.2.2 Component variation

An artificial variation mode, negative bow in the top hat, was fabricated to simulate the type of variation that could be present in such a component due to variations in the stamping process. The nominal hats (without bow) were fabricated by folding and laser cutting flat pieces of sheet metal. A bow in the hat was then created using a simple hydraulic press setup with tooling made from aluminium plates (see Appendix A.2). All top hats had the same level of bow, a middle deflection of 5 mm. This level of bow is probably more severe than what would be observed in an industrial setting, but it was selected so that any differences in assembly shapes would also be more severe, and therefore more easily discernable to the naked eye: this enabled a greater intuition to be developed about the assembly response to different clamp sequences. It can be expected that any observed trends would also hold at less exaggerated levels of bow. An example top hat with a 5 mm bow is illustrated in Figure 5.2. It should be noted that only hat section variation is considered (and not variation in the flat bottom plate). This is because the hat is the primary structural member, and has a much greater influence on final assembly variability than the bottom plate.

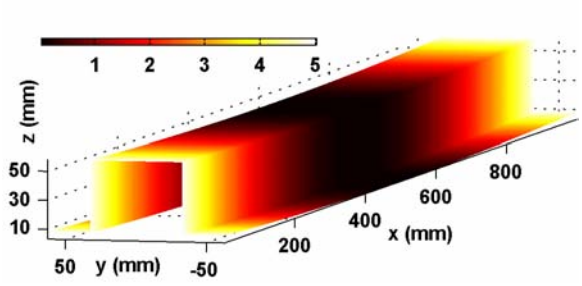

Figure 5.2: Sample top hat highlighting the bow variation mode of 5 mm. Colour map indicates the displacement between the bowed and nominal assembly (mm)

5.2.3 Measurement point extraction

The advancement of optical measurement techniques has allowed for more rapid and accurate dimensional inspection of parts. For this study, a 3D laser scanner was used to capture point cloud measurements of the sheet metal stampings and assemblies. Measurement points (MP s) were extracted from scanned data to give data points similar to that obtained by traditional CMM measurement procedures. Here, a surface

measurement point on a flange or the roof was taken as the z-displacement of a specified co-ordinate in the x-y plane, and a measurement point on a side-wall was taken as the y-displacement of a specified co-ordinate in the x-z plane. Due to the measurement capabilities of the scanner, 1000 s of measurement points were extracted in 5 mm grid formations across the flanges, side-walls, and roof. Figures 5.3 (a) and (b) show 3D scan data, and corresponding MP s sampled at 5mm grid spacings along each surface. It should be noted that while the final assembly consists of the top hat and flat bottom plate, only the top hat is measured for analysis purposes due to measurement access restrictions, and as it was determined to hold the features of most interest.

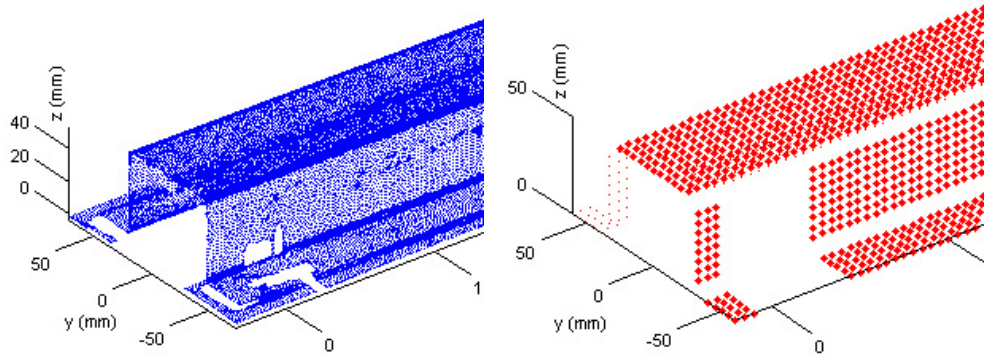

(a) **(b)**

Figure 5.3: Figure 5.3(a) displays example point cloud data from a 3D laser scan. Figure 5.3(b) shows MP s that were extracted from the scanned data. Some areas could not be measured due to physical obstructions (ie, locating pins and clamps).

5.2.4 Component sampling

A population of 30 top hats with a bow of 5mm were fabricated. These samples were then plotted in a multivariate reduced dimensional space, which allows for most of the information in the 6000+ MP data set to be visualised in only 3 dimensions. The steps for performing a Principal Component Analysis decomposition of this 6000+ MP, 30 sample data set can be seen in section 3.3.2. The 30 measured experimental samples were plotted in a 3D PCA space in Figure 5.4. The first purpose of this plot was to identify outliers. The outliers would not be used for assembly as this study was concentrating on the influence of clamping sequence, not initial differences in part shapes. The second purpose of this plot was to split the population into pairs of nearest neighbours: one member from each pair would then be built with clamp sequence 1, and the other member built with clamp sequence 2. This was done to ensure that similar populations were being assembled by each clamp sequence, in order to minimise the influence of differences in initial component populations on any observed shifts

between assembly outcomes. Only 20 samples (or 10 pairs) were actually selected for assembly as these provided more than adequate levels of statistical significance for the assessment of mean shifts.

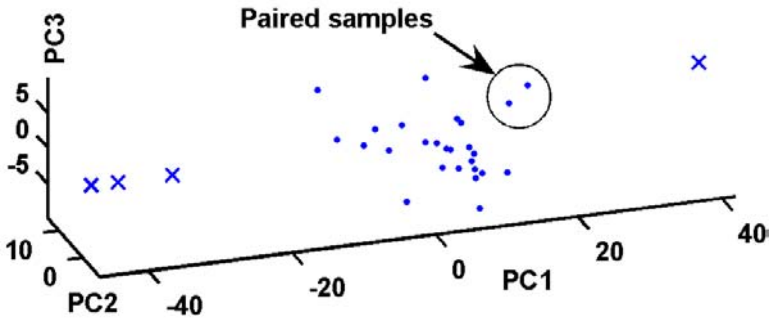

Figure 5.4: Top hat samples plotted in a 3D PCA space. Samples were paired up in groups according to their nearest neighbours. Outliers × were not selected for assembly.

5.3 Experimental results

Ten top hats with bow were assembled with clamp sequence 1, and ten top hats were assembled with clamp sequence 2. The built assemblies were measured using a laser scanner, with corresponding MP s extracted as detailed in section 5.2. The mean assembly shapes of the two populations were compared to reveal any statistically significant differences in the final assembly shapes. Through identifying statistically significant differences in the mean shape, the influence of clamping sequence on variation propagation can be shown. The mean assembly shape of each clamp sequence was then compared to the nominal design to assess the dimensional quality of each clamp sequence. Here, the closer the mean shape to the nominal design, the better quality the assembly, and therefore the better the clamp sequence for dimensional control.

5.3.1 Differences in the mean shape

Figure 5.5 shows an overlaid plot of the final assembly shapes of two example samples: one built with clamp sequence 1, and the other built with clamp sequence 2. The plot is a digital reconstruction of the point could data gathered from the 3D scanner measurements. It can be seen that the two clamp sequences result in noticeably different final assembly shapes. It appears as though clamp sequence 2 tends to force the positive wall (ie, the wall in the region greater than $y = 0$) inwards in relation to clamp sequence 1. This large observed mean shift shows the extent of the influence of clamping sequence on the dimensional outcome of assemblies, and therefore the need to consider clamp

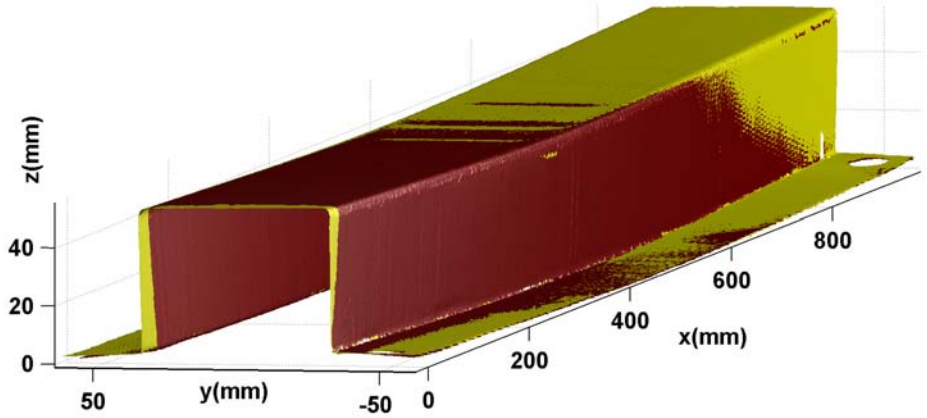

Figure 5.5: Digital recreations of experimental scan measurements for samples built with clamp sequence 1 (light) and clamp sequence 2 (dark).

sequence as part of the assembly design process if optimal dimensional control is to be achieved. Detailed results of the differences in the mean shapes of clamp sequences 1 and 2 will be presented in the following sections.

5.3.2 Comparison cross-sections

Cross sections will firstly be presented to illustrate the extent of the mean shifts between the two sequences. The largest differences in final assembly shapes of the means of clamp sequences 1 and 2 can be seen in the positive wall: a cross section that slices this wall at 12.5mm in the x-y plane is therefore presented in Figure 5.6. It can be seen that clamp sequence 2 dramatically forces the wall inwards (ie, towards $y = 0$ mm), in relation to clamp sequence 1 at $x = 0$ mm: the opposite can be said at $x = 1000$ mm. Differences in final assembly shape can also be seen in the roof: a cross section that slices this roof at $y = 0$ mm in the x-z plane is seen in Figure 5.7. Clamp sequence 1 results in a higher roof at $x = 0$ mm in comparison to clamp sequence 2, and conversely, clamp sequence 2 results in a higher roof height at $x = 1000$ mm. While these cross-sections provide some insight into the dimensional differences between the clamp sequences, manufacturers often use statistical tools to investigate the significance of such mean shifts. The following will therefore proceed to demonstrate the application of univariate and multivariate statistical tools for the investigation of the mean shifts between the two sequences.

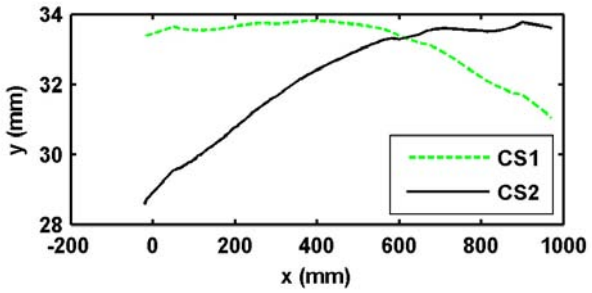

Figure 5.6: Cross section comparison of wall at $z = 12.5$mm in the x-y plane.

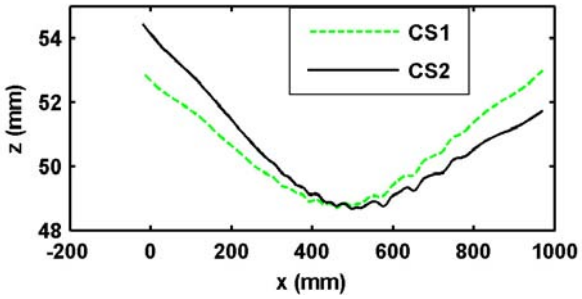

Figure 5.7: Cross section comparison of roof at $y = 0$ mm in the x-z plane.

5.3.3 Mean shifts - univariate approach

A univariate mean shift test (t-test) was undertaken to check the statistical significance of the mean shift of each MP when comparing each clamp sequence (see Appendix E.1.1). Here, the mean of an MP consisting of 10 samples built with clamp sequence 1 was tested against the mean of the same MP consisting of 10 samples built with clamp sequence 2. This test was performed on all 6000+ MP s. The hypothesis that the means are equal was tested against the alternative hypothesis that the means were not equal (to the 95% level). Of the 6000+ MP s, 90% displayed statistically significant differences in the mean. Figure 5.8 shows a histogram of the absolute displacements between corresponding MP s of the means of clamp sequence 1 and 2. It can be seen that there are a large portion of MP s with an absolute difference of 0.5 to 1.5 mm, which highlights the significant differences between the two clamping sequences. The largest difference between the two clamp sequences was 4.95 mm, which occurred in the y-direction on the positive wall at (-10 mm, 7.5 mm) in the x-z plane.

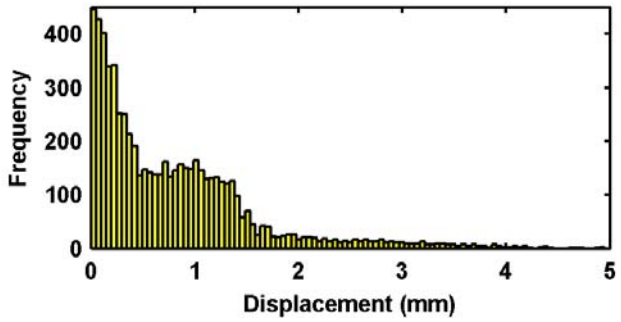

Figure 5.8: The maximum difference between means of the MP s for each clamp sequence was 4.95 mm, and the average difference was 0.78 mm.

5.3.4 Mean shifts - multivariate approach

An alternative approach for assessing differences in the mean is to use multivariate statistical tools, which are perhaps more suitable considering the large amount of MP s considered. Rather than performing univariate mean shift tests on each of the 6000+ MP s, an overall impression of the variability in the data set can be visualized within a single plot. Figure 5.9 shows a 2-dimensional PCA representation of the assembly data set (see section 2 for details on performing PCA). It can be seen that there are two key clusters: cluster A corresponds to clamp sequence 1, and cluster B corresponds to clamp sequence 2. The existence of the two clusters, and the large distance between the clusters, highlights the significant differences between the dimensional outcomes of the two clamp sequences. A technique such as linear discriminant analysis that was applied in section 3.3.2 could be used to provide further discrimination between the two clamp sequences. Such techniques can be combined with machine learning techniques for pattern classification and root cause analysis (Rolfe et al., 2003).

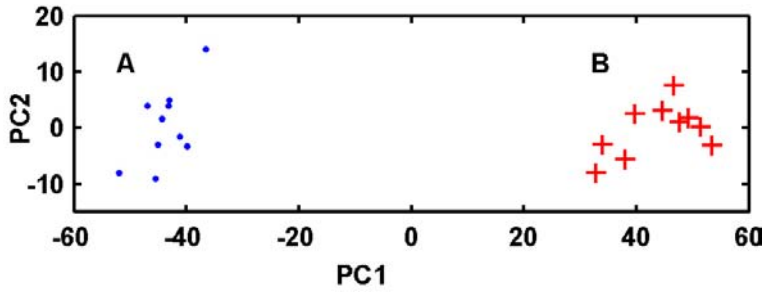

Figure 5.9: 2D PCA representation of the data shows that each clamp sequence forms a distinct cluster, highlighting the differences between the two shapes.

5.3.5 Experimental comparison to nominal

While it has been identified that there are significant differences between the mean shapes of the two clamping sequences, another important aspect to investigate is how close a manufactured assembly is to the nominal design. Figures 5.10 (a) and (b) display surfaces reconstructed from the extracted MP s. Each 2D surface represents a group of MP s at 5 mm grid spacings, and the gaps show areas where it was not possible to measure the surface due to physical obstructions. The color-map represents the difference between the nominal assembly design and the mean manufactured shape for the corresponding clamp sequence. From the color-map, it can be seen that the two clamp sequences differ significantly, with large differences again occurring along the positive wall (the wall in the region above $y = 0$ mm). The average and maximum displacements from nominal were used as a basic measure of shape quality assessment: here, the closer a part is to the nominal design, the higher the dimensional quality. Clamp sequence 1 resulted in an average displacement of 0.78 mm, and a maximum displacement of 2.88 mm. Clamp sequence 1 resulted in an average displacement of 1.12 mm, and a maximum displacement of 6.31 mm. Clamp sequence 1 therefore results in a higher quality assembly than clamp sequence 2 in terms of average and maximum displacement from nominal. This finding indicates that not only can clamp sequence result in different final shapes, but depending on the clamp sequence selected, assembly quality can differ significantly as well.

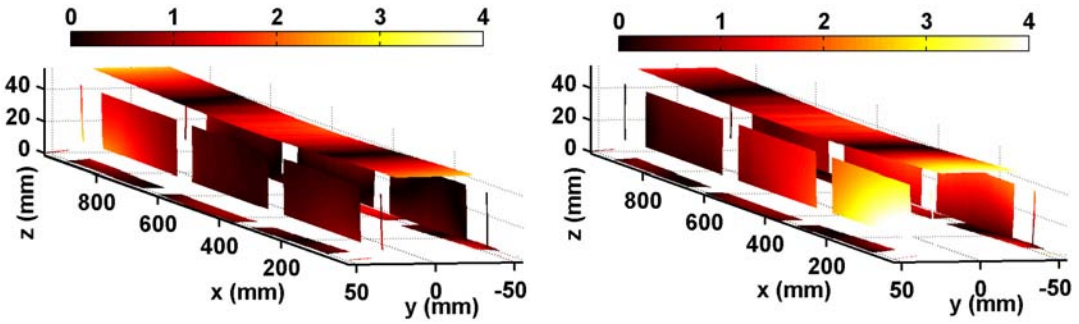

Figure 5.10: Figures 5.3 (a) and (b) show colour-maps of the displacement of the mean of clamp sequence shapes from nominal. It can be seen that the colour-maps are noticeably different.

5.4 Simulated assembly

The previous section investigated the influence of different clamp sequences on the dimensional outcomes of an assembly using an experimental setup. This section seeks to replicate this experiment in a virtual setting using finite element modeling (FEM): if a physical process can be accurately represented by a simulation, then it can be used as a powerful rapid prototyping tool. Later sections will proceed to use the validated FE approach for investigating clamping sequences in more detail. For the FE simulation study, a top hat with an initial bow of 5 mm is assembled with clamp sequence 1, and also with clamp sequence 2. The assembly shapes of the two clamp sequences are then compared. A brief description of the FE assembly approach is initially presented, followed by the simulation outcomes, and then a comparison of the FE results to the experimental.

5.4.1 Finite element approach

The same implicit, multi-step, non-linear contact assembly model as adopted in the previous chapter was used to simulate the assembly process. However, this time an 8 clamp sequence is investigated. The same CMM-MP s extracted in the experimental part were taken from the FEM. This was achieved by using thin plate spline surface interpolation (see Appendix F.3 for a description of the technique) to estimate the surface contact points, as nodal displacements did not match with the required surface measurement co-ordinates.

5.4.2 Simulation results

Figure 5.11 provides an overlaid plot of the FEM simulations outcomes for each of the clamp sequences investigated. It can be seen that the clamp sequences result in noticeably different dimensional outcomes. Clamp sequence 2 appears to force the positive side-wall inwards in comparison to the other clamp sequence: this corresponds with the trends found in the experiential results. However, the maximum displacement between the two clamp sequences is underestimated by the simulations at 2.7 mm, in comparison to the difference of 4.9 mm found with the experimental.

Comparisons to nominal

Table 5.1 lists the average and maximum displacements from nominal for the experimental and FEM, for each of the two clamp sequences investigated. It can be seen that generalised trends appear to hold, with the average and maximum displacements for clamp sequence 2 being noticeably higher than sequence 1, for both experimental and FEM results. The experimental and FEM results look closely comparable for clamp se-

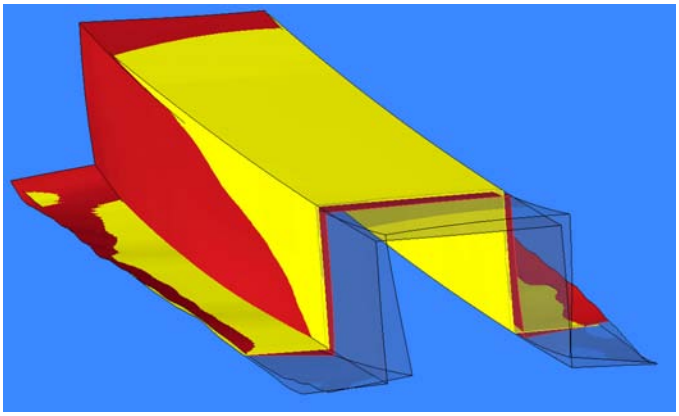

Figure 5.11: FEM simulation, final assemblies clamped. Clamp sequence 2 (dark) and 1 (light) overlaid with magnified displacements and cross section shown.

quence 1, with maximum displacements from nominal at 3.19 mm (FEM) and 2.88 mm (experimental), and average displacements from nominal at 0.79 mm (FEM) and 0.78 mm (experimental). However, it can be seen that the FEM results for clamp sequence 2 appear to underestimate the deformations of the experimental findings, seen in the average displacements from nominal figures of 0.9 mm (FEM) and 1.12 mm (experimental). This is most likely due to the large deformations the assembly undergoes for clamp sequence 2, which causes greater differences between the physical process and simulated model due to modelling idealizations that will be detailed later.

Table 5.1: Maximum and average displacement comparisons. It can be seen that generalised trends hold, but the FEM underestimates the magnitude of displacements.

Clamp	FEM vs Nominal		Experimental vs Nominal	
Sequence	Max	Avg	Max	Avg
1	3.19mm	0.79mm	2.88mm	0.78mm
2	4.34mm	0.90mm	6.31mm	1.12mm

Direct simulation to experimental comparisons

Table 5.2 presents the direct maximum and average displacements between the simulated and experimental results. It can be seen that the average displacements between the FEM and experimental results appear quite low, considering the large deformations that the assemblies underwent. However, the maximum deviations between the experimental and FEM show less correspondence. Again, this can be attributed to the modelling idealizations of the simulation approach. The feature of most interest is the positive wall, which is the source of the largest differences between the two clamping

sequences. Figures 5.12 and 5.13 show comparative experimental to FEM x-z cross sections of the positive wall at $z = 12.5$ mm, for the two clamp sequences. Looking at Figure 5.12, it can be seen that the experimental and FEM results display the same general trend for clamp sequence 2: a fairly severe curve in the side-wall. While this general trend holds, it can be seen that there are discrepancies between the exact measurements. Figure 5.13 compares the experimental and FEM results for clamp sequence 1, displaying slightly less similar trends. It can be seen that the deformation of the side-wall is underestimated by the simulation approach.

Table 5.2: Direct experimental comparisons (average and maximum displacements between corresponding MP s).

Clamp	FEM vs Experimental	
Sequence	Max	Avg
1	1.37mm	0.51mm
2	1.98mm	0.56mm

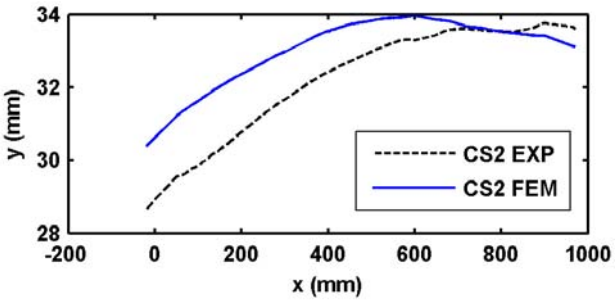

Figure 5.12: Simulated/experimental cross-sectional comparison for clamp sequence 2.

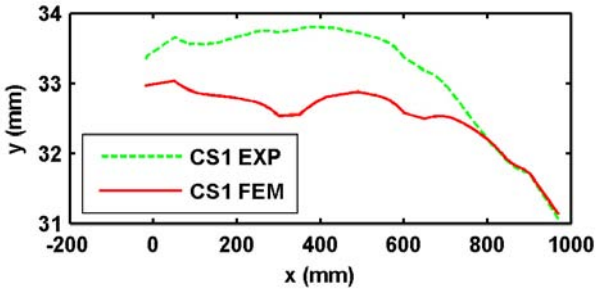

Figure 5.13: Simulated/experimental cross-sectional comparison of wall for clamp sequence 1.

Reasons for discrepancies

There are many reasons for discrepancies between the experimental and FEM results, stemming from differences between the physical process and simulation idealizations. Discrepancies between the experimental and simulated results can be accounted for by the following: slight differences between the simulated and experimental component shapes, a fairly coarse FE mesh, single node contact points, unaccounted frictional forces, the assumption of elastic deformation only, anisotropic material properties of the experimental components, and vertical only clamp forces versus the curved path of the toggle clamps. However, while the experimental and simulation results do not match exactly, the deformations observed are similar, and reveal important general trends, such as the higher average and maximum displacements of clamp sequence 2 in comparison to 1. The simulation approach shows therefore sufficient correspondence with the physical environment to capture generalized design trends, and can be used as a valuable virtual design for the investigation of assembly quality. The next section will therefore proceed to further apply the simulation approach to investigate the 8 clamp configuration.

5.5 Clamp sequence and variability

The previous sections have established that the FEM approach is a sufficient representation of the physical process as observed through the experimental comparisons. For both the experimental and FEM it has been shown that clamp sequence 2 results in a noticeably higher average and maximum displacement from nominal than clamp sequence 1. Also, the overlaid plots of assembly shapes of the experimental and FEM reveal similar deformation characteristics. This section extends the application of the FEM simulation to investigate the influence of different clamping sequences on the dimensional variability of assemblies. While the mean shape of assemblies is a key concern for manufacturers, they tend to focus more on the control of process variability, as this is seen to affect the quality of the assemblies to a greater extent. Therefore, rather than just investigating a single level of bow in the hat (ie, 5 mm), a population of hats with differing levels of bow that represent the type of process variation seen in a physical production situation will be investigated. The same approach used in the last chapter was used to investigate a population of components and assemblies.

5.5.1 Population of input components

In order to make observations on the influence of different clamping sequences on variability, assessments must be made on a population of input component shapes with variability, to see how variability propagates through the system. In this section, an

artificial population of input component shapes with varying magnitudes of bow was generated to simulate the type of variability that could be found in a physical production system. The input component population is represented by Figure 5.14, and for reference an illustration of the bow variation mode can be seen earlier in Figure 5.2. The FE approach was then used to simulate the assembly outcomes of each sample for each clamp sequence. It should be noted that a similar approach to the previous chapter was again used to reduce the computational burden of the simulations (again see Appendix B.2 for more details). The next section will proceed to compare the two populations resulting from the two clamp sequences.

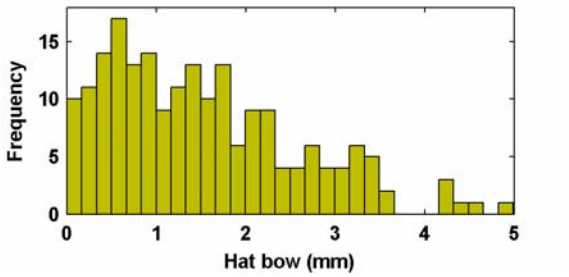

Figure 5.14: Histogram displaying the population of 200 input components (top hats) with various levels of bow.

5.5.2 Assembly and variability comparison

Comparisons of the final assembly variability of the two populations are presented in this section. As the distributions of the assembly variables were highly skewed, a histogram is again used to estimate the 95th percentile spread of data: this is illustrated in Figure 5.15. It can be seen that the measure of spread captures the peak end of the histogram and omits the tail end. The measure of spread values were calculated for every MP, with the average and maximum spread values used as overall indicators assembly quality.

Table 5.3 shows the average and maximum spread values for each clamp sequence. It can be seen that clamp sequence 1 has significantly lower average and maximum standard deviation than clamp sequence 2, with a 28% reduction in average spread and a 17% reduction in the maximum spread measure. In terms of quality of the manufacturing process, clamp sequence 1 is therefore a more attractive option as it results in much lower levels of variation. These results show that the selection of clamp sequence can greatly influence the dimensional variability of assemblies, and that efforts should be made for the optimal design and selection of clamping sequence in assembly.

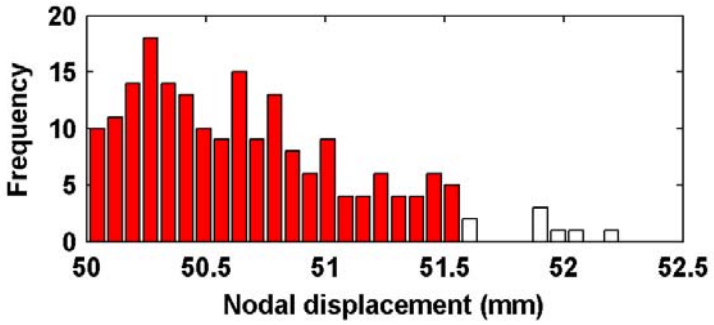

Figure 5.15: 95% spread measure from an example MP. Filled bars indicate the 95% spread region.

Table 5.3: Average and maximum spread performance measures for each clamp sequence.

Clamp Sequence	Average Spread	Maximum Spread
2	0.43mm	2.12mm
1	0.31mm	1.77mm
% reduction	28%	17%

5.6 Clamp sequence design

It has been shown that the selection of clamp sequence can have a substantial influence on the dimensional outcomes of assemblies in terms of both mean shape and variability. For the assembly investigated, it has been shown that assembly variation can be considerably reduced (and therefore assembly quality significantly increased) through the selection of a more optimal clamping sequence. Optimal clamping sequences can be determined by several approaches: a direct approach that would involve investigation of all assembly combinations in order to identify the best sequence, a genetic optimization-based approach (Liao, 2005), or the use of generalized design principles identified from previous experience. While the direct and genetic optimization approaches would be effective, they do require extensive experimentation and/or simulation. The general principle approach would be more practical to implement, however, generalized design guidelines must first be identified and be accurate enough to provide reliable outcomes. In 2000 Shiu et al. proposed design criteria for weld sequence patterns for minimized variability. They showed that there is a positive correlation between welding induced internal stress and dimensional variability. In the design laws proposed, they suggested that welding sequences moving from a fixed to free end minimized internal stress and therefore dimensional variability as well. This stress minimized concept also appears

applicable to the design of clamping sequences for minimized variability, as in a similar manner, the assembly clamping process involves the progressive application of a series of constraints (ie, clamps as opposed to welds). However, there is a glaring difference between the two processes: before clamps are applied, there is no fixed end . A key step to a generalized approach to clamp design is a rule for the selection of the first clamp application. In the following, a series of sequences are compared, from which generalized design guidelines are formed.

5.6.1 Clamp sequence comparison

A series of logical clamp sequence approaches are applied to the FEM case study presented in previous sections. Clamp sequences were assessed according to the average and maximum spread quality indicators presented in section 5.5.2. The clamp sequences were selected to highlight key characteristics that lead to the proposal of a generalized approach to clamp sequence design. These design guidelines are first stated, and then tested on a series of four clamp sequences to illustrate the dimensional quality improvements achievable by applying the guidelines.

Proposed guidelines

The proposed design guidelines were formed from a combination of previous literature, results presented in the previous sections, and intuition developed through exploratory investigation of clamping sequences using the experimental assembly setup. The design guidelines are as follows:

1. Clamp the region that is closest to nominal first: Through clamping regions in an assembly that are the closest to nominal first, it is proposed that there would be less deformation/ displacement of the assembly due to clamping forces (when compared to clamping a region that is farther from nominal). For the example assembly, it should be noted that the hat has a negative bow, so the area closest to nominal before assembly is the middle region of the hat (at $x = 500$ mm), and the ends have the largest displacement from nominal (at $x = 0$ and 1000 mm).

2. Clamp from fixed to free ends: As stated earlier Shiu et al. proposed a stress minimized design criterion for weld patterns which involves welding from a fixed to free end. Once a fixed end has been established (ie, by applying design law 1), then this principle can also be applied to clamp sequence patterns.

Description of clamping sequences

There were four clamping sequences investigated, which are illustrated in Figures 5.16 (a)-(d) using silhouettes of the assemblies and numbers indicating clamp location and

sequence. Clamp sequence A clamps the outer ends first, and then the middle clamps: this corresponds to clamping a region that has a larger displacement from nominal first (ie, it neglects clamp design law 1, and 2). Clamp sequence B runs down one flange and back down the other: this corresponds to clamping from a fixed to free (clamp design law 2). Clamp sequence C applies a pair of middle clamps, followed by the clamps at each end, and finally the remaining pair of middle clamps. It applies clamp design law 1 by clamping an area closest to nominal first (ie, as there is a negative bow, the middle region is closest to nominal), but does not proceed to clamp from a fixed to free end, therefore neglecting clamp design law 2. Clamp sequence D applies the middle clamps first, followed by the outer clamps: this corresponds to clamping the area closest to nominal first and clamping from a fixed to free end (ie, in to out). Clamp sequence D therefore applies both design laws. Outcomes of each of the sequences are presented in the following section.

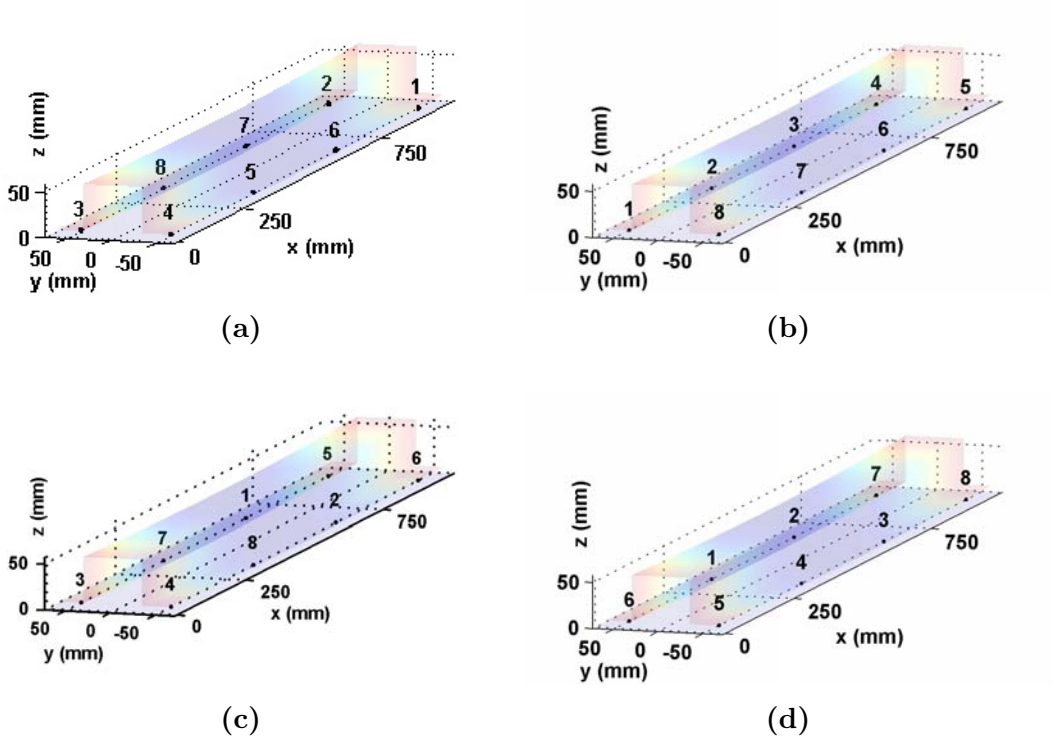

Figure 5.16: The four clamp sequence patterns are illustrated in Figures 5.3(a)-(d). Numbers indicate clamp location and sequence.

5.6.2 Clamp sequence performance

Section 5.6.1 described the proposed clamping laws and the example clamp sequences explored to illustrate the performance of the proposed design laws: Table 5.4 summa-

rizes this study. Each clamp sequence is indicated, along with the design law applied for each clamp sequence, and the resulting average and maximum spread performance measures. It can be seen that clamp sequence A applies none of the proposed design laws, and performs the worst in terms of average and maximum spread. Clamp sequence B applies clamp design law 2 only, and clamp sequence C applies clamp design law 1 only. Both of these sequences show improvements in dimensional quality over clamp sequence A. Finally, clamp sequence D applies both clamp sequence design laws, resulting in the lowest average and maximum spread performance measures of all clamp sequences. These findings suggest that the proposed design guidelines do result in the selection of more optimal clamp sequences for the reduction of overall variability in assemblies. In order to further validate the proposed guidelines, studies should be conducted on a wider range of simulated, experimental and production assemblies, however, the preliminary results from this study are promising.

Table 5.4: Comparisons of proposed general clamping laws.

Clamp Sequence	Description Closest to nominal	General clamping law		Average Spread	Maximum
		Fixed to free end	Spread		
A	Out then middle	No	No	0.43mm	2.12mm
B	Down then back	No	Yes	0.37mm	1.91mm
C	Middle, out, Middle	Yes	No	0.34mm	1.97mm
D	Middle then out	Yes	Yes	0.31mm	1.77mm

5.7 Conclusion

In this chapter, the influence of clamping sequence on the dimensional outcomes of an example sheet metal assembly has been investigated through experimental and simulation. The experiential results confirmed that the selection of assembly clamping sequence can result in considerably different dimensional outcomes in terms of mean shape. The simulation approach showed sufficient correspondence with the experimental, highlighting similar deformation trends in the final assembly for the different clamp sequences: these results highlight the value of simulated assembly as a virtual prototyping tool. Further exploration of the example assembly with the simulation approach revealed that the selection of optimal assembly clamp sequences can result in significant improvements in the dimensional variation of assemblies. A set of generalized design guidelines for assembly clamp sequence are proposed, which are based on previous weld sequence guidelines and the investigation of the experimental assembly. These design guidelines were applied with results showing significant improvements in assembly quality. While previous research has developed extensive analysis approaches

for clamp sequence design, the proposed clamp sequence laws provide a valuable and practically implementable reference tool for quality control efforts. Application of the design laws to other assemblies and refinement of the simulation approach are areas for future work. The chapter essentially shows how aspects of the assembly process, such as clamping sequence, can be refined to produce more optimal outcomes in terms of dimensional quality of assemblies.

Chapter 6

Multivariate statistical shape model

6.1 Introduction

Previous chapters have demonstrated how aspects of the assembly process such as weld and clamp sequence can influence the dimensional outcomes of assemblies: it was shown that assembly quality, defined by average and maximum standard deviation, could be significantly improved by employing more optimal clamping sequences. This measure of quality, as with Statistical Process Control (SPC) and Six-Sigma approaches, uses the assumptions of statistical independence and normally distributed data to create quality process control guidelines. In reality, these assumptions do not hold. For example, surface points on a stamping or an assembly tend to vary in a correlated fashion, which contradicts the assumption of statistical independence. Inferences or decisions based upon univariate representations of manufacturing variation are therefore questionable as the underlying model is a poor representation of the physical system. Key limitations of univariate approaches include their inability to characterise correlated variation modes, deal with high dimensional data sets, and accurately estimate the overall shape distribution. In this chapter, a combination of the Point Distribution Model, which is based on Principal Components Analysis, and Kernel Density Estimation, is used to develop a multivariate statistical shape model (the KDE-PDM) that addresses the limitations of previous statistical models. Several case study examples are presented to highlight the advantages of the KDE-PDM over two other statistical approaches: the univariate shape model, and the original PDM. The KDE-PDM s capabilities make it particularly suited to variation monitoring and diagnosis of high dimensional measurement data sets made available by optical measurement devices, and some suggestions for its implementation are also presented. In summary, this chapter seeks to find a better statistical representation of manufacturing variation, to allow manufacturers to

make more accurate decisions about the true variability of their processes.

6.2 Multivariate process monitoring

Multivariate process monitoring has become more commonplace in automotive industry as a means of taking into account the characteristic of correlated variation patterns (Apley and Shi, 1998). This chapter seeks to extend the application of multivariate methods to automotive body assembly by considering multivariate density estimation, enabling a more accurate depiction of the underlying variability of a process. Multivariate density estimation has been successfully applied to the areas of computer vision and industrial chemical process monitoring, which will be presented in the following. Later sections will then proceed to develop the theory behind the proposed approach.

6.2.1 Computer vision

Computer vision is a widely developed field with applications including image compression, shape classification, and image tracking. The Point Distribution Model (PDM) is a statistical deformable shape model that was developed by Cootes et al. (1995) for pattern recognition in computer vision. It is based around Principal Component Analysis and assumptions of unimodal, normally distributed data, and can effectively represent correlated variation modes in shapes. Applications of this model have included describing variation modes in medical images in 2D (Cootes et al., 1992) and 3D (Hill et al., 1993), and face tracking (Sirovich and Kirby, 1987). Extensions of this technique outside of computer vision have included shape error analysis of turbine blades by Daniel et al. (1997) and sheet metal forming spring-back by Rolfe et al. (2003). Previously mentioned classification methods for diagnosis of sheet metal assembly faults mentioned in section 2.3 are also closely aligned with the PDM.

The original PDM is limited in its assumption of unimodal normally distributed data: for some shape distributions this might not hold. Various non-linear extensions to this model have been proposed. Sozou et al. developed nonlinear PDM s based on polynomial regression (1994) and artificial neural networks (1995) to identify non-linear principal components. Kernel PCA is another method proposed for capturing non-linearity (Rathi et al., 2006). Effective implementation of these methods is highly dependent on user judgment and knowledge of the underlying shape patterns. An extension of the PDM which uses a Kernel Density Estimate (KDE) provides another approach for characterizing nonlinear shape distributions (Cootes and Taylor, 1999). Through minimizing assumptions on underlying shape distributions, this method can effectively model highly skewed, multi-modal data. This paper proposes the KDE-PDM as a method for more effectively characterizing shape variation in sheet metal stampings and assemblies.

6.2.2 Chemical process control

Multivariate process monitoring techniques have been widely applied to industrial chemical processes, and many approaches are very similar to multivariate statistical shape models: the main difference is simply the field of application. Chen et al. (1999a) combine PCA and kernel density estimation to provide more accurate representations of highly correlated and nonlinear data sets to enhance process monitoring capabilities. Choi et al. (2004) combine PCA, discriminant analysis, and Gaussian mixture models to create another process monitoring framework with fault identification. These approaches which were developed for chemical processes are largely transferable to the field of dimensional control in automotive body assembly.

6.3 Methods

The key motivation behind this chapter is to provide a more accurate model of the underlying shape distribution of manufactured parts, so that more valid inferences can be drawn about the underlying shape distributions. This section develops key steps and theory that form the basis of the shape models to be presented in subsequent sections. The key areas include measurement of stampings and assemblies, the Gaussian distribution, dimensional reduction through PCA, and kernel density estimation. The application of these methods in creating the proposed KDE-PDM, along with the comparison with the univariate shape model, and original PDM, will be detailed in later sections.

6.3.1 Measurement of free-form manufactured parts

A set of measurement points must be selected to capture variation information about a manufactured part. The measurement process involves two key steps, datuming or registration of measurement points, and of course performing the measurements. As stampings and assemblies are datumed by gauges before measurement, the data set is assumed to be already aligned. In previous applications of shape models, this is not the case, where registration techniques are required to firstly align the data set. Inspection of stampings and assemblies in their free-state may require such techniques (Rolfe et al., 2003), but this is not explored in this chapter.

Manufacturers tend to measure a set of features that they deem are most critical for the dimensional quality of the final product. In the past this set of features has been limited by the available measurement techniques such as hard gauges and co-ordinate measuring machines (CMM s). The advancement of optical measurement techniques has allowed for more rapid and accurate dimensional inspection of parts, and an emerging issue is how to interpret and/or limit the amount of measurement

points required for effective diagnosis (Camelio et al., 2005). For the purposes of this chapter, the amount of measurements points (MP s) measured does not really matter, but generally speaking the more MP s measured the more effectively shape variability can be characterized.

6.3.2 Gaussian distribution

All of the statistical shape models presented in this chapter are in some way based around the Gaussian distribution: The univariate shape model uses univariate Gaussians, the PDM a single multivariate Gaussian, and the KDE-PDM a mixture of multivariate Gaussians. The multivariate form of the Gaussian distribution is presented in the following

$$f(x_1 ..., x_n) = \frac{1}{(2\pi)\,|\sum|} e^{\left[-\frac{1}{2}(x-\mu)^T \sum^{-1}(x-\mu)\right]} \tag{6.1}$$

where μ is the mean value, $\sum$ the covariance matrix, and $|\sum|$ the determinant of the covariance matrix.

6.3.3 Dimensional reduction using PCA

Principal Components Analysis is a multivariate statistical technique that is often used for dimensional reduction of large data sets. The basic concept is to select a smaller set of variables that can account for most of the information in an original data set of many variables. PCA in automotive body assembly has often been used as a tool for identifying major fault modes, as first illustrated by Hu and Wu (1992). These methods often assume that principal components correspond to a particular fault mode (Ceglarek and Shi, 1996). For the purposes of this chapter, PCA is used only as a data reduction method and makes no assumption about the correlation between fault modes and the components: section 3.3.2 details the steps of a PCA decomposition.

6.3.4 Kernel density estimation

A single multivariate Gaussian distribution can be used to model the distribution of multidimensional data sets. Such models can take into account correlation of variables when generating random shapes, but the assumption of normality does not always hold. For example, these estimation methods cannot take into account multimodal and highly skewed data. A method which relaxes assumptions on the underlying distribution and can model any distribution to higher levels of accuracy is kernel density estimation, which will be applied in this chapter. The kernel method of density estimation (Scott, 1992) gives an estimate of the probability density function from which n samples, have been taken:

$$f(x) = \frac{1}{Nh^d} \sum_{i=1}^{n} K(\frac{x - x_i}{h}) \tag{6.2}$$

where K is some kernel (often the Gaussian), h is the bandwidth or smoothing parameter, and d is the dimension of the data. In the case of assembly process measurement data, each measurement point is seen as a dimension. Studies have shown that the selection of a kernel is not as important as the choice of the smoothing parameter (Marron, 1988). For the purposes of this paper, maximum likelihood cross-validation is used: this method chooses a smoothing parameter h that maximizes the log likelihood

$$\log L = \sum_{i=1}^{n} \log f_{-i}(x_i) \tag{6.3}$$

where the leave one out cross validation density estimator of the underlying distribution f is:

$$f_{-i}(x_i) = \frac{1}{(n-1)h} \sum_{j \neq i}^{n} K(\frac{x_i - x_j}{h}) \tag{6.4}$$

In summary, the cross validation estimator involves removing one data point and using the remaining n-1 points to construct a density estimator, and evaluating the estimate of the nth data point. This step is repeated n times for each data point, and the results averaged. Maximum likelihood cross-validation effectively identifies an h that minimizes the Kullback-Liebler distance, I, a measure of the difference between two probability distributions (Hall, 1987). In this case, h is selected to minimize the distance between the estimated distribution and the true underlying distribution

$$I(f, f) = \int f(x) \log \left(\frac{f(x)}{f(x)} \right) dx \tag{6.5}$$

Density estimation in this paper will be limited to the kernel density estimate with a Gaussian kernel with a symmetrical covariance matrix. It should be noted that other approaches for smoothing parameter selection exist, including Plug-in methods (Marron, 1988), and Least-squares cross-validation (Sain et al., 1994). More flexible implementations of the kernel density estimate, where the smoothing parameter and orientation of each kernel can differ from point to point, have also been explored (Sain, 2002). A range of other multivariate density estimate approaches have also been proposed, with Gaussian mixture models that use a smaller subset of Gaussians to model distributions proving to be another popular tool for multivariate density estimation (Choi et al., 2004). Examples of computationally efficient multivariate density estimation methods include the Reduced Set Density Estimator (Girolami and He, 2003), and the Improved Fast Gaussian Transform (Greegard and Strain, 1991). All of these

methods can be explored in future research of statistical shape modelling of stampings and assemblies.

6.3.5 Statistical shape models

The previous section highlighted a number of methods that are used as building blocks for the statistical shape models presented in this paper. This section explains how each of these methods is combined to form the univariate shape model, the PDM, and KDE-PDM. Illustrated case study examples of these models will be presented in later sections.

Univariate shape model

The univariate shape model involves representing underlying shape distributions with a single univariate Gaussian for each MP (ie, MP s are assumed to be statistically independent). Therefore, for a population of n manufactured shapes and x_i MP s, the univariate shape model would consist of the standard deviation and mean of each of the x_i MP s.

Point Distribution Model

The PDM overcomes the limitation of a univariate model s inability to capture co-linearity between MP s. It uses a PCA decomposition to represent most of the variation information in a data set by a smaller set of variables. The distribution of observations (or shapes) within this reduced dimensional space is then estimated by a single multivariate Gaussian. For a sample of n shapes, and x_i measurement points, the model would be created as follows:

1. Represent the original i-dimensional data set in a reduced t-dimensional space using PCA as outlined in section 3.3.2.

2. Estimate the distribution of observations (shapes) in this reduced dimensional space by a multivariate Gaussian as described in section 6.3.2.

Kernel Density Estimate/Point Distribution Model

For the purpose of this chapter, we are interested in creating a statistical shape model of manufactured stampings or assemblies that can accurately represent the underlying shape distribution. Kernel density estimation makes minimal assumptions about an underlying data set, apart from that it can be approximated by a Gaussian mixture. It can provide more accurate estimations of skewed and nonlinear data sets than by fitting a single multivariate Gaussian to the data. Combining the Point Distribution Model

and Kernel Density Estimation provides an approach that can capture correlated shape modes and estimate more complex shape distributions: this approach will be referred to as the KDE-PDM. For a sample of n shapes, and x_i measurement points, the KDE-PDM would be created as follows:

1. Represent the original i-dimensional data set in a reduced t-dimensional space using PCA as outlined in section 3.3.2.

2. Estimate the distribution of observations (shapes) in this reduced dimensional space by the Kernel Density Estimate (KDE) method as described in section 6.3.4.

Figure 6.1 illustrates this process on a fictional data set of a headlamp surround. Firstly, 50 samples of the manufactured shape are measured at 8 MP s. Each of the MP s are measured in the x, y and z co-ordinates so in total it is a 24 dimensional data set. Secondly, the 50 observation, 24 dimension data set is transformed into a 2D PCA space which accounts for most of the variability in the data. Finally, Kernel Density Estimation of the observations in the 2D PC space is performed to represent the underlying shape distribution of the data set.

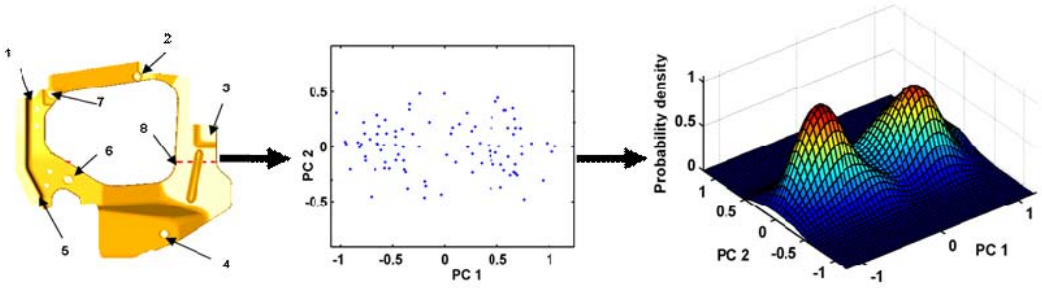

Figure 6.1: Pictorial representation of the key stages in the KDE-PDM: measurement, dimensional reduction, and kernel density estimation.

6.4 Results

There are several sets of results presented to highlight a range of capabilities of the proposed multivariate statistical shape model. Firstly, an overview of a simulated case study assembly is presented. Three shape models based on the simulated case study data are then presented: the Univariate shape model, the Point Distribution model (PDM), and the Kernel Density Estimate/Point Distribution Model (KDE-PDM). Comparisons between the shape models are made to highlight the advantages of using the proposed KDE-PDM over existing methods for statistical modelling of stampings and assemblies. In-line data from a production assembly is then used to demonstrate

the ability of the multivariate shape model to characterize multi-modal distributions, with a view to clustering and process diagnosis for dimensional control.

6.4.1 Simulated case study

The same simple assembly and nonlinear contact finite element simulation model used in earlier chapters was used to create an example assembly data set. The FE simulation setup is again illustrated in Figure 6.2. The pin P and slot S are located at opposite ends along one flange. Locating clamp locations and their sequence are indicated by numbers 1 through to 6. Welding locations are indicated by the letters a through x. Nodal displacements in the x, y and z are considered as measurement points or variables for the purposes of this chapter, and the top hat consists of approximately 1400 nodes.

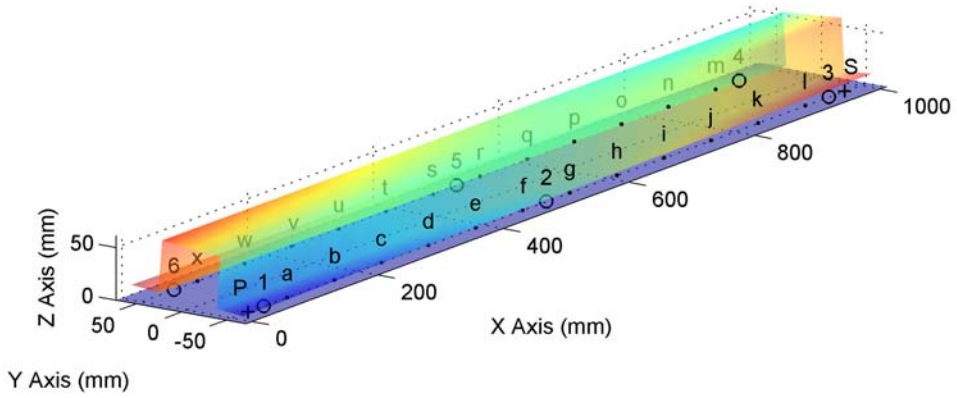

Figure 6.2: Example FE assembly model setup.

As in chapter 4, anticipated correlated part variation modes of bow and twist were used as inputs to the FE assembly model. For the purposes of this study, only the top hat section was considered to have dimensional variability, as it is the dominant component in the two piece assembly. Furthermore, only the top hat shape is considered for illustrating the concepts in this chapter. The following shapes show key examples of part variation modes: initial hat twist is described by theta in Figure 6.3, and initial hat bow is described by middle deflection in Figure 6.4. Corresponding example assembly shapes for input component variation modes of bow and twist are shown in Figure 6.5. Large data sets were created to simulate the type of data seen in actual production situations. The statistical shape models were then trained using this data and comparisons made. The simulated case study assembly therefore consisted of input part variation modes of bow and twist. There were 800 samples in total: 400 samples of input part bow with a Middle deflection ranging from -4.75 mm to +2.71 mm, and 400

samples of input part twist with a theta ranging from -4.80 degrees to +4.86 degrees. There are 1500+ measurement points in the FE mesh.

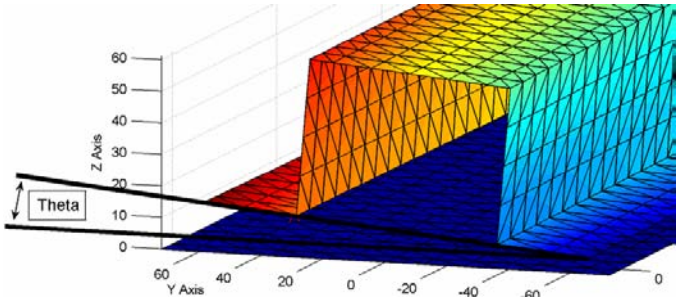

Figure 6.3: Example FE assembly model setup.

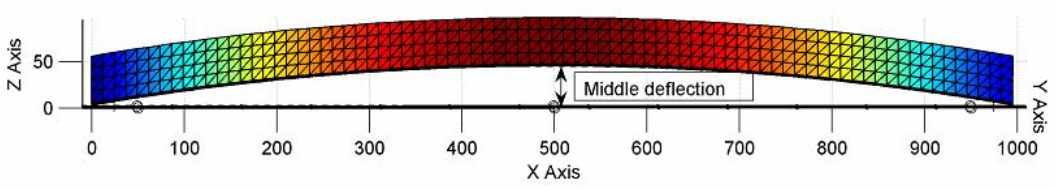

Figure 6.4: Bow input part variation mode.

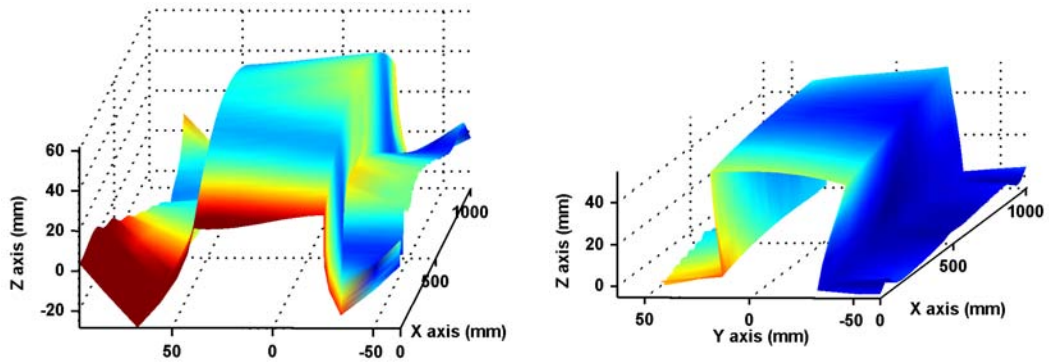

(a) **(b)**

Figure 6.5: Corresponding assembly shapes for input part variation modes of twist (a) and bow (b). Note that the assembly also includes a flat bottom plate, but for the purposes of this paper only the top hat is investigated.

6.4.2 Univariate shape model

This approach models the shape distribution of a manufactured part by assuming that each measurement point is statistically independent. The model therefore involves simply calculating the mean and standard deviation of each measurement point. The application of this model to the 800 observation, 1500+ dimensional, case study data can be summarized by Figure 6.6. One difficulty facing the univariate shape model for high dimensional data sets is the interpretation of the equally large model outputs (ie, each measurement point has a corresponding mean and standard deviation). Distilling important information from such a large set of descriptive statistics and developing an intuitive understanding of dimensional variation in the manufactured assembly is a non trivial task. A more vital limitation of this approach is the assumption of statistical independence. Surface continuity conditions generally dictate that points on a surface in close proximity will move in a correlated fashion (Merkley, 1998). The univariate model therefore does not capture this key characteristic of manufactured sheet metal parts and assemblies. To illustrate this obvious limitation, Figure 6.7 shows an example random shape generated from the univariate shape model. It can be seen that the surface is highly erratic and not a very plausible representation of a physical shape occurrence. An example ramification of this shape misrepresentation can be seen with the use of univariate shape models as inputs for stochastic modelling for variation propagation analysis (Liu and Hu, 1997a). In this case, by feeding highly implausible shapes into the stochastic model, much of the analysis is effectively redundant as implausible assembly combinations are being investigated.

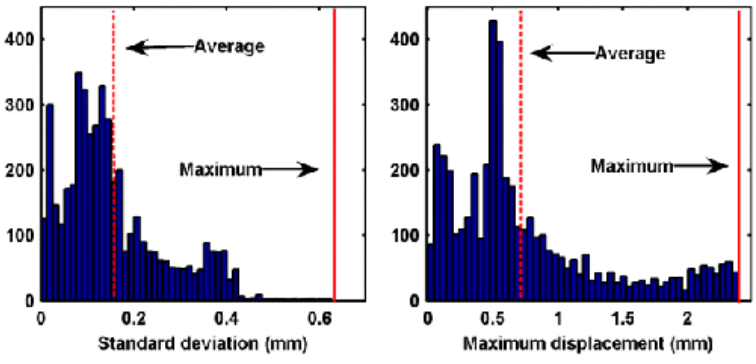

Figure 6.6: Histograms showing the spread of Standard deviation and Maximum absolute displacement from nominal for each MP.

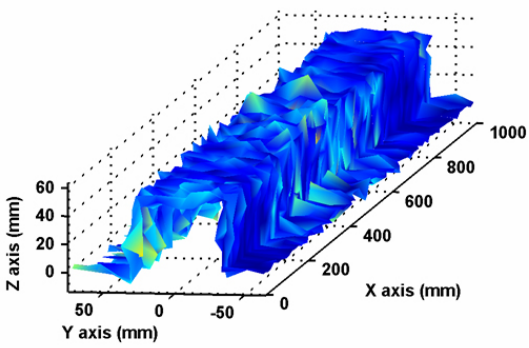

Figure 6.7: Example random assembly shape generated from a univariate statistical shape model.

6.4.3 Point Distribution Model

Two main limitations of the univariate model have been identified: difficulties with interpreting large amounts of measurement data, and poor overall shape representation stemming from an inability to capture surface co-linearity. The Point Distribution Model (PDM) addresses both of these issues: firstly by using a dimensional reduction technique to reduce the amount of variables required to represent the data, and secondly by representing correlated variation through a multidimensional interpretation of the data set. As described in section 6.3.5, the PDM involves using PCA to transform the original data set (800 observations and 1500+ MP s) into a lower dimensional representation.

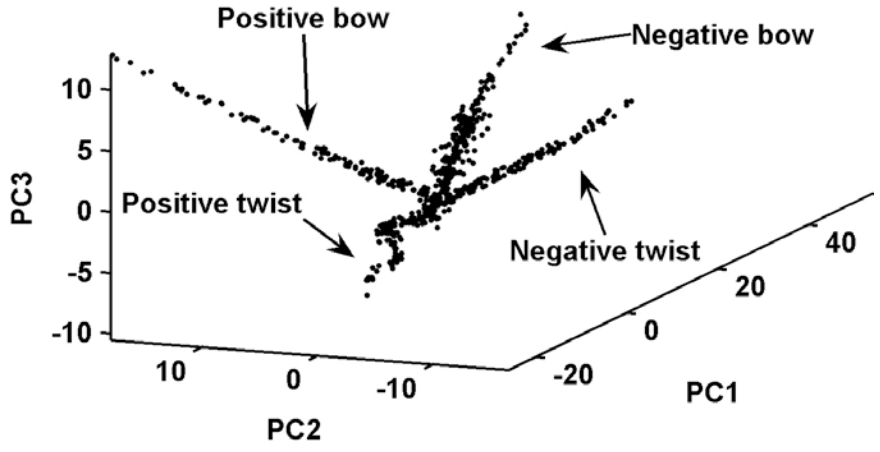

Figure 6.8: 3D PCA representation of the original case study data (800 sample, 1500+ dimension). Variation modes corresponding to particular input part shapes clearly identifiable.

A three dimensional PCA representation of the case study, with the addition of noise to represent a more realistic data set, can be seen in Figure 6.8. From this reduced dimensional representation, the underlying relationships are quite evident, with each extending line representing a particular variation mode. These assembly variation modes correspond to the input part variation modes of negative and positive twist and bow. This plot highlights how dimensional reduction techniques can distill important information from large data sets.

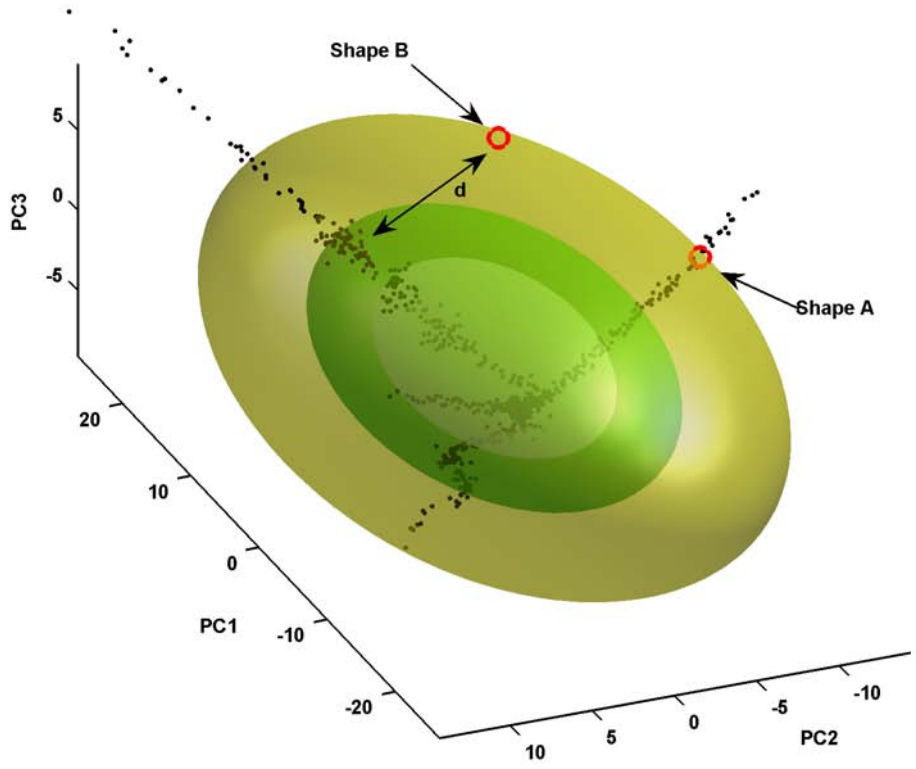

Figure 6.9: A three level probability density contour shell plot of the PDM. Shapes A and B have a similar probability of occurrence according to the PDM, but it can be seen that Shape A lies close to the samples, whereas Shape B is some distance from its nearest sample.

The PDM estimates the distribution of the reduced dimensional PCA space with a single multivariate Gaussian (see section 6.3.2). Figure 6.9 illustrates a three-level probability contour shell plot of the single multivariate Gaussian estimate in a 3D PCA space. Any regions that fall within the shell are statistically valid shape occurrences according to this model. It can be seen that a single multivariate Gaussian does not provide a good estimate of the underlying shape distribution. While correlated variation modes will be represented, not all of the statistically valid shapes are physically

plausible shape occurrences. Two points or shapes are highlighted in the plot of the PDM, and both are equally probable shapes according to the model. Shape A is also a plausible shape occurrence, but Shape B is not a plausible shape occurrence. This can be seen by the distance of Shape B to the nearest case study sample. The representation of Shape A and Shape B in the original body co-ordinate system is shown in Figure 6.10.

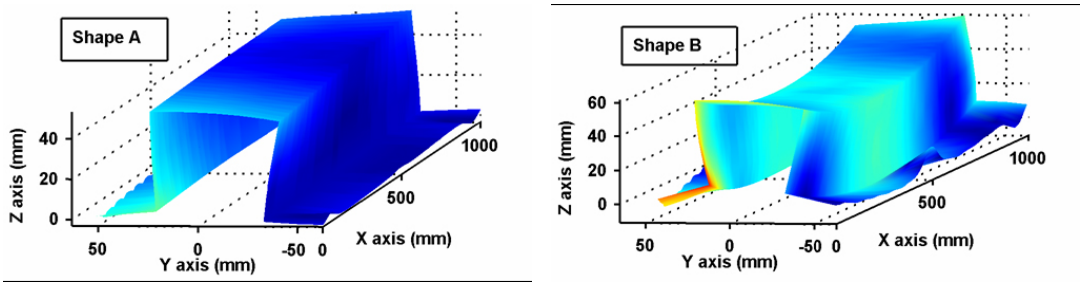

(a) **(b)**

Figure 6.10: Shapes A and B show surface correlation and are equally probable according to the PDM. However, while Shape A closely resembles the assembly response to an input part variation mode of twist, Shape B is quite different from any sample in the case study.

6.4.4 Kernel Density Estimate/Point Distribution Model

It has been established that the PDM holds two main improvements over the univariate shape model: an ability to represent correlated variation modes, and dimensional reduction. However, a limitation of the PDM is its inability to provide accurate estimates of nonlinear shape distributions. This can be overcome by using Kernel Density Estimation instead of a single multivariate Gaussian to estimate the underlying shape distribution: therein lies the motivation for the Kernel Density Estimation/Point Distribution Model (KDE-PDM) as described in section 6.3.5. Figure 6.11 illustrates a three level probability density contour shell plot of the KDE-PDM for the case study data. It can be seen that the KDE-PDM probability contour wraps nicely around the case study samples, providing a much better estimate of the underlying shape distribution than the single Gaussian fit. It can also be seen that the KDE-PDM does not class Shape B as a probable shape occurrence (whereas the single Gaussian fit of the PDM did).

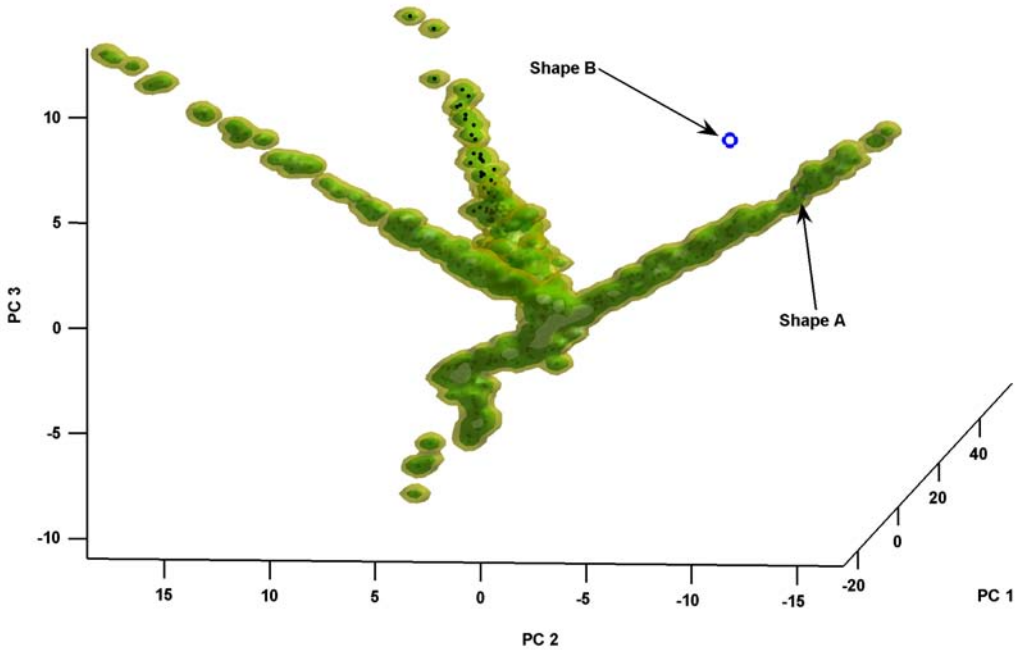

Figure 6.11: A three level contour probability density plot of the KDE-PDM. It can be seen that Shape B is not a highly probable shape according to the model.

6.4.5 Industry case study

This section presents the ability of the KDE-PDM to represent skewed and or multi-modal distributions, with a view to clustering applications. Production assembly data is used in this section, with the case study assembly from chapter 3 again illustrated in Figure 6.12. The assembly is a front cross member, which positions key front-end features such as headlamps, fenders, grills and the hood. Excessive variation in this sub-assembly can therefore have a large impact on customer quality perceptions. There are 16 critical points measured as part of regular production quality monitoring procedures, and the data taken for this study consisted of 60 samples taken over a three month period.

Simple multi-modal illustration

In order to demonstrate the capability of a kernel density estimate to characterize multi-modal distributions, a single measurement point is first investigated. Figure 6.13 shows a histogram plot of one of the measurement points from the case study assembly. A kernel density probability estimate and a normal distribution probability estimate are also overlaid. It can be seen that the kernel estimate is able to capture two key modes that are clear to see in the histogram plot, whereas the normal distribution estimate

cannot. These two modes might have a physical reason for their occurrence, and an ability to identify such features in data can provide engineers with a target for quality control investigations. The kernel density estimate therefore can provide a useful tool for identifying interesting features in the underlying data set.

Figure 6.12: Production case study assembly.

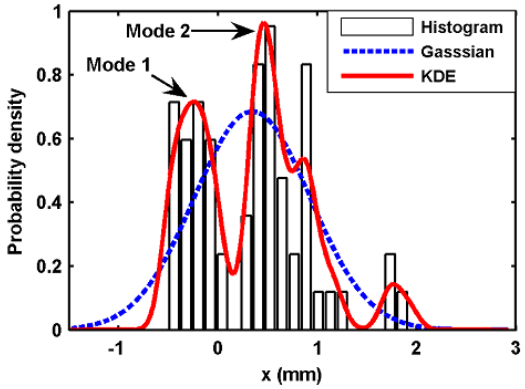

Figure 6.13: Kernel Density Estimate vs Single Gaussian fit.

KDE-PDM data clustering

The previous example showed how a kernel density estimate can represent multi-modal data in a single dimension. The example in this section shows how the KDE-PDM can represent multi-modal data in a multidimensional PCA space. Figure 6.14 illustrates a three-level contour shell plot of the probability of the KDE-PDM for the original 60 sample, 16 dimension data set. It can be seen from the data that there are two dominant clusters or modes within the data set. This means that there are two identifiable shape

groups that have a high likelihood of occurrence. Through identifying clusters in data, quality engineers can concentrate their efforts around this knowledge. For this case study data, it was revealed that the two clusters were explained by mean shifts of the assembly fixtures. While in this example the clusters were identified through a visual representation of the data, this process of identifying clusters can be automated: example methods could use local optimization techniques to find each of the modes in the data, and probabilistic thresholds to partition the data set into meaningful clusters. An advantage of using such approached over other clustering methods such as k-means (Duda et al., 2001) is that the user would not need to specify the amount of clusters to search for.

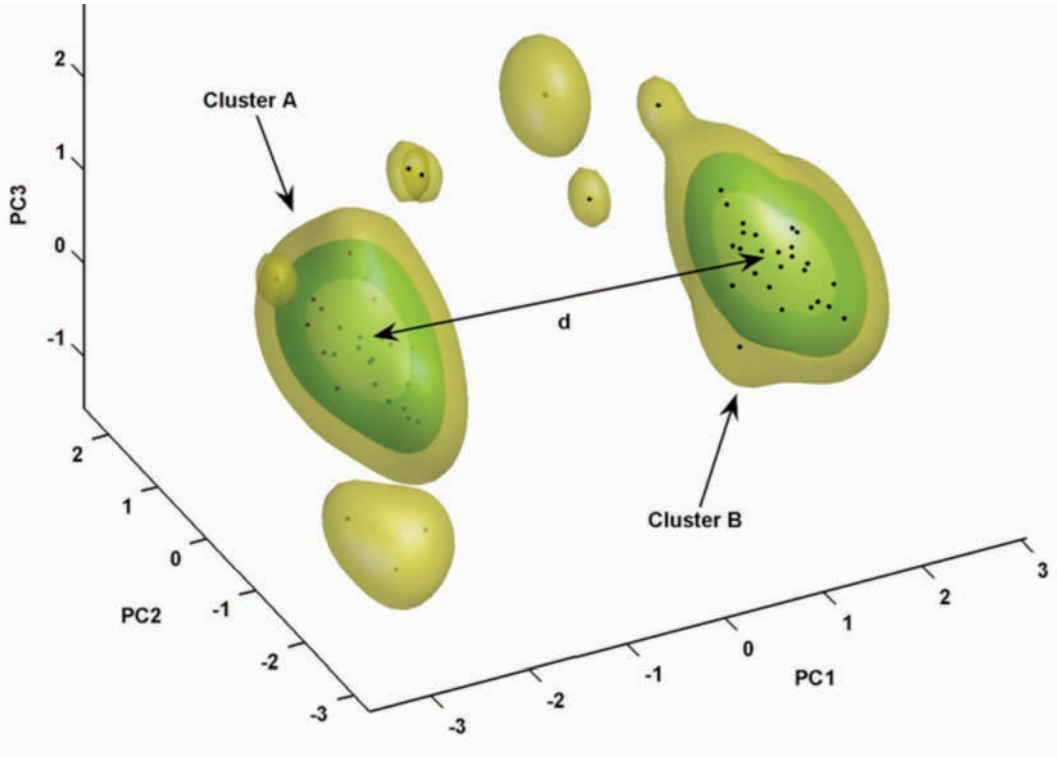

Figure 6.14: A three level contour probability density plot of the KDE-PDM of the industry case study data. Note the two major clusters are some distance d apart: this was identified as a mean shift in the assembly fixture.

6.5 Discussion

The two case study examples have highlighted the capabilities of the KDE-PDM. This section discusses how the KDE-PDM can be used in a dimensional inspection framework for automotive stampings and assemblies. There are three key stages of this frame-

work: Creating the KDE-PDM, Data mining using the KDE-PDM, and a tolerancing approach for the KDE-PDM. Finally, some suggestions for refining the KDE-PDM in terms of computational efficiency are presented.

6.5.1 Creating the KDE-PDM

There are a number of aspects to consider when creating a KDE-PDM of a population of part shapes, some examples being data sampling, noise, and modeling accuracy. The use of optical measurement devices to capture high sample, high dimensional data sets should be encouraged as it would take advantage of the model s capabilities, and allow for new levels of variation inspection and diagnosis. As in most cases, measurement and process noise is highly undesirable, as this can severely affect the dimensional reduction abilities of the model. If the number of dimensions required to adequately represent the original data set is too high (see section 3.3.2), or if the number of training samples is too low, then the quality of the density estimate of the KDE-PDM will suffer. Guidelines on how to deal with these problems in a systematic manner need to be identified.

6.5.2 Data mining with the KDE-PDM

Once a KDE-PDM has been created for a population of manufactured shapes, data mining techniques can be used in efforts to identify interesting features in the data set and segment the data set into logical groupings. As seen back in section 6.4.3, variation modes in the shape data of the simulated case study were visually discernable. Similarly, as seen with the industry case study, mean shifts in the data were also visually discernable. An ability to firstly identify these features (ie, variation modes and clusters), and then relate them back to meaningful variation sources would provide a valuable diagnostic tool for manufacturers. The probabilistic based clustering proposed in section 6.4.5 is one example approach for automating feature identification using the KDE-PDM. This concept will be revisited in section 8.2.

6.5.3 A tolerancing approach for the KDE-PDM

Tolerances are a key feature of traditional univariate process monitoring techniques such as SPC. These methods involve the individual assessment of a series of MP s on an assembly. This approach would be quite cumbersome with potentially large data sets obtained from optical measurement devices. The KDE-PDM provides new possibilities in terms of dimensional assessment. For one, the KDE-PDM reduces the number of dimensions required to describe the data, which can make data interpretation more manageable. Furthermore, the KDE-PDM can provide accurate estimates of the probability of occurrence of a particular shape: this opens the possibility for probabilistic

tolerancing zones within the model. Monitoring a process with an existing KDE-PDM of a manufactured part would involve the following steps:

1. Transforming the process samples into the reduced dimensional space of the KDE-PDM.

2. Calculating the probability of this sample with the density estimate of the KDE-PDM, and then:

   (a) if the sample probability is above a pre-determined probability threshold, the sample is within tolerance.

   (b) if the sample probability is below the pre-determined probability threshold, the sample is out of tolerance.

An important point to note is that when assessing parts using this technique, traditional plus/minus tolerancing approaches cannot be adopted, as tolerance zones in the body co-ordinate system will change. This is because an individual MP is assessed as being in or out of tolerance depending on the entire shape of the manufactured shape, not just the MP s individual value. The concept of tolerancing with the KDE-PDM will also be revisited in section 8.2.

6.5.4 Computational issues

The KDE-PDM provides a general framework for the statistical modeling of automotive stampings and assemblies. However, the techniques proposed are not as computationally efficient as desired for commercial applications, particularly if optical measurement devices are used to capture high dimensional data sets. Performing PCA can become a demanding task as it requires the calculation of eigenvalues and eigenvectors: approaches for estimating principal components using Artificial Neural Networks have been proposed to speed up the process (Kung et al., 1994). Kernel density estimation can also be quite demanding: other density estimation techniques mentioned in section 6.3.5 can improve computational efficiency.

6.6 Conclusion

This chapter combines the Point Distribution Model and Kernel Density Estimation to provide a statistical shape modelling approach for the manufacture of stampings and assemblies, referred to as the KDE-PDM. The KDE-PDM can deal with high dimensional data sets, represent correlated variation modes, and provide accurate estimates of the underlying shape distribution. Simulated and production case study examples are presented to highlight the advantages of the KDE-PDM over previous methods

including the univariate statistical model, and the original Point Distribution Model. The KDE-PDM s capabilities make it particularly suited to variation monitoring and diagnosis applications of high dimensional measurement data sets made available by optical measurement devices. A guideline for implementing the KDE-PDM in a variation monitoring diagnosis system is also suggested, which includes: issues to consider when constructing a KDE-PDM, how the KDE-PDM can be used for data mining applications, and importantly how the KDE-PDM could be adapted for an advanced tolerancing framework specifically suited for deformable stampings and assemblies. Essentially, this chapter presents a more accurate statistical representation of manufacturing variation, enabling manufacturers to make more accurate decisions about the underlying process and how to control it. The next chapter will proceed to make further use of the high dimensional data made available to propose methods for numerically describing local correlated variation modes in the form of bumps and ripples. section 8.2 will then illustrate how all of the methods can be integrated in to a forward thinking quality assessment tool for optimal process selection.

Chapter 7

Local shape characterization

7.1 Introduction

In order to select the assembly process that results in the best assembly outcomes, there must be a well defined measure of product quality. Traditionally, univariate methods have formed the basis of quality control measures within frameworks such as statistical process control and six sigma approaches. Here, the mean and standard deviation of a set of assumedly statistically independent measurement points have been the sole determinants of the quality of manufactured parts. The emergence of optical measurement devices has enabled the capture of entire free form surfaces, allowing for more detailed approaches to process monitoring. A limitation of univariate process monitoring methods is that they cannot adequately describe localized correlated variation patterns on a surface that can be obvious to the eye, such as ripples and bumps, which can also have adverse effects on customer perceptions of quality. An inability to adequately describe such local features has meant they have not been included as criteria for the quality assessment of manufactured items. This chapter seeks to expand upon traditional approaches to quality assessment by taking advantage of the data made available by optical measurement devices, and providing a set of numerical descriptors for localized correlated variation modes such as bumps and ripples. These local shape descriptors provide a rich set of features with which to discriminate between differing manifestations of surface deviation, with a view to shape classification, quality assessment, and ultimately optimal process selection. Specific techniques for the proposed local shape characterization approach include: surface curvature energy, multi-scale surface analysis, and curvature-based automatic local feature detection.

7.2 Surface classification

An ability to classify the world that surrounds us into logical groupings is an essential part of the decision making process. Pattern classification can be seen to consist of two key steps. The first is to find a set of measures that are capable of describing or discriminating between particular features of interest. The second step is to partition the data set into a set of meaningful sub-groups with these measures. This chapter deals with the first key step of pattern classification. Here, a set of numerical measures or descriptors that are capable of distinguishing between differing manifestations of localized surface variation are proposed. The local shape characterization measures to be proposed are based around surface curvature and the continuous wavelet transform, which will be discussed in the following.

The emergence of optical measurement devices has enabled the inspection of entire free-form surfaces. Curvature based methods have often been used to describe surfaces, and an extension to the description of scanned surfaces is a logical step. Two curvature based methods to be applied in this chapter are curvature energy and curvature segmentation. Bending energy which is closely linked to curvature energy has been used as a tool for fitting splines (Wahba, 1990). Here, it is desirable to find the smoothest interpolant of an underlying data set by minimising the energy of the second derivatives across a surface (see Appendix F.3). In section 7.5, the average curvature energy of a surface is used to measure the relative smoothness of a surface, with the aim of discriminating between surfaces with differing levels of local features.

Curvature segmentation of surfaces emerged out of the need to classify surfaces into similar groupings for applications in computer and robot vision, computer graphics, geometric modelling, and industrial and biomedical engineering. Through curvature segmentation, a surface or object can be broken down into discrete areas of similar curvature or shape, and matched with other shapes of similar feature compositions. Ferrari et al. (2006) combine curvature segmentation with graph structures for free-form feature representation and comparison. Curvature tensor analysis has been applied to surface segmentation to create cleaner boundaries (Lavoue et al., 2005). Segmentation and smooth surface extraction of noisy surfaces through region growing is another approach (Vieira and Shimada, 2005). In section 7.7, a simple form of curvature segmentation based on thresholds is employed to identify local features of interest on sheet metal surfaces.

Wavelets have emerged as a popular signal and image processing technique due to their ability to characterize a signal in the frequency and spatial domains. The decomposition of manufacturing surfaces into different scale (or frequency) components has formed a key area of research, with a focus on surface roughness evaluation (Chen et al., 1999b). The lifting wavelet has been proposed to assess the functional performance of

a three dimensional surface (Jiang et al., 2001). Chang and Ravathur presented a non-contact, area-based roughness assessment system, through wavelet transforms of digital images of surfaces (2005). Wavelets analysis has also been combined with discrimination processes for surface roughness characterization (Josso and Burton, 2001). The complex wavelet transform has also been proposed to overcome the shift variance and poor directional sensitivity of discrete wavelet transform approaches for surface metrology (Ma, 2005). Amaratunga proposed a surface variation error measure using a geometry adapted wavelet transform (Amaratunga, 1999).

A wavelets based approach has also been used by Liao et al. to represent surface geometry of non-rigid assemblies (2005b). Here, sampled part variation is treated as a signal, and a wavelets transformation was applied to decompose this signal into different scale components. Shape data generated from these scales was then used as inputs to FE assembly models, and the influence of these different scales on final assembly variation was identified. Fractal geometry was also proposed to represent detailed surface micro-geometry of non-rigid assemblies (Liao and Wang, 2005a), however, the wavelet approach is more suitable as it can represent all non-stationary part variation, and is not limited to just fractal variation. In section 7.6, the continuous wavelet transform is applied to characterise local features of interest such as bumps and ripples on a sheet metal component. This type of feature is larger and less erratic than the surface roughness features of interest in the previously mentioned literature, and therefore a smoother wavelet at larger scales is selected for the purposes of this chapter.

The remainder of this chapter will be arranged as follows. Firstly, two example manufactured components used to demonstrate the local shape characterization measures will be introduced. This will be followed by a description of the registration and normalization process, an essential data preparation step for the application of the proposed approaches. Qualitative descriptions of surfaces from the two example manufactured components will then be presented for later comparison with the local shape characterization descriptors. Finally, the local shape characterization approach will be described, demonstrated, and discussed.

7.3 Example manufactured components

The local shape characterization approach will be demonstrated on 3D scanned data of two manufactured shapes with different variation modes. Again, the top hat channel section is the panel of interest. One hat has a positive bow, and the other a negative bow. The hats were fabricated through a process of CNC folding, laser cutting, and the bow was induced by the same press tool used in chapter 5. The hat is 1000 mm long, 50 mm high, flanges are 30 mm, and the roof is 65 mm wide. It should be noted that the press tool is reconfigurable, enabling both positive and negative bow to be

induced in the part (see Appendix A.2). The tooling results in approximately a 5 mm middle deflection of the channel. A scanned channel with positive bow that will be investigated is illustrated in Figure 7.1. A scanned channel with negative bow can be seen in Appendix D.

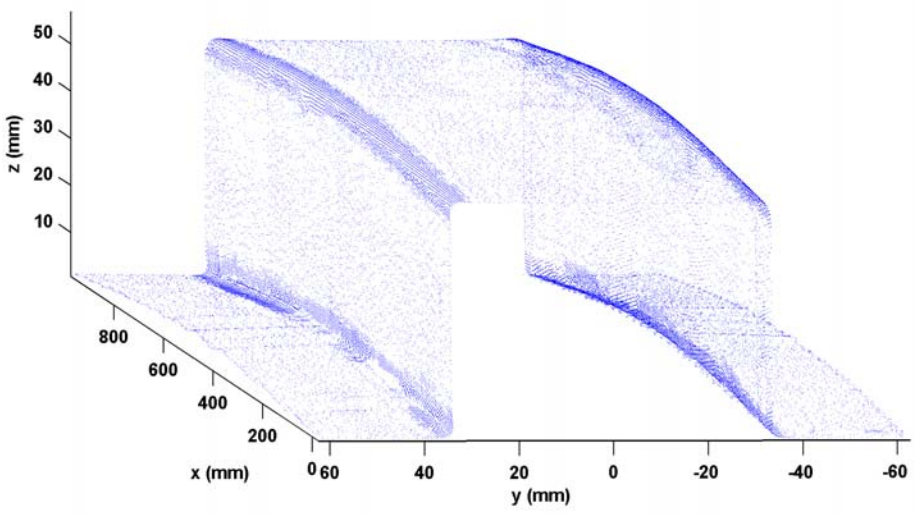

Figure 7.1: Channel with positive bow (point cloud from 3D scan).

7.3.1 Registration and Normalization

For the application of the local shape characterization tools, a common frame of reference describing the deviation of a sample from the nominal design needs to be established. This process can be referred to as registration and normalization.

Registration

Registration involves the extraction of corresponding sets of measurement points on all samples. In terms of automotive body process monitoring, registration is traditionally achieved by measuring the position of a surface point at a particular co-ordinate in a plane on each manufactured sample (for example, the z-displacement of a surface at a particular point in the x-y plane). This traditional approach to registration is also employed for this thesis. However, due to the scanning capabilities 1000 s of MP s are extracted, which is in contrast to the limited number that can be measured using hard gauges or CMM s. Here, rectangular grids with 2 mm spacings are taken along the roof, positive side wall, and positive flange. Figure 7.2 illustrates the scanned data and extracted MP s once again.

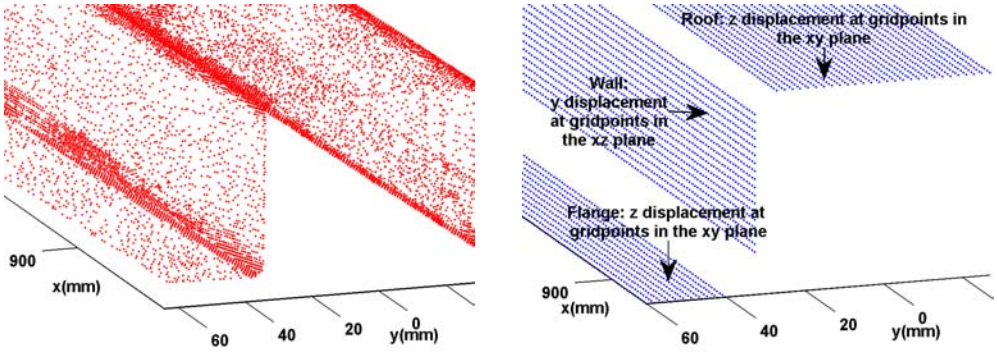

(a) **(b)**

Figure 7.2: Figure7.2(a) shows a closeup of the scanned data. Figure7.2(b) shows a closeup of the nominal grid used to extract corresponding MP s.

Normalization

Normalization is the process of creating a 2.5D representation of the distance between a sample and its nominal design, allowing for the application of established image processing techniques (Smith and Hancock, 2006). Due to the chosen registration approach, and the flat nominal surfaces of the example manufactured part, this process is quite straightforward in this case. Here, the nominal rectangular grid already defines a 2D plane, and the difference between the registered and nominal grids defines the distance measure at each measurement point. This process is illustrated in Figure 7.3. It should be noted that the 2.5D representations for each surface (the positive flange, positive wall, and roof), are processed independently by the local shape characterisation methods. Approaches for generalizing the registration and normalization process to capture entire surfaces and nominally curved surfaces will be discussed later.

7.3.2 Qualitative surface descriptions

This section illustrates and qualitatively describes each of the six example surfaces: one flange, one wall, and the roof for each of the two scanned channels. The six surfaces provide a good example set of differing manifestations of local shape variation. The illustrations are surface reconstructions of the registered and normalized grids as described in section 7.3.1. It should be noted that the axes are scaled to best show the local features present on each surface. These surfaces will be referred to in later sections when applying the local shape characterisation techniques.

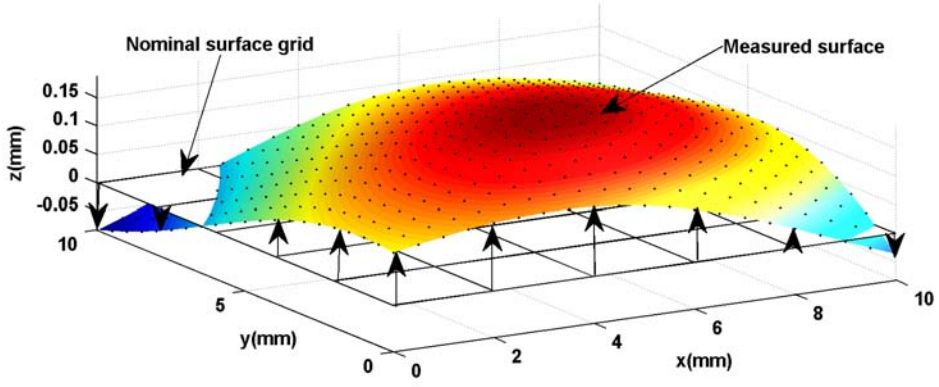

Figure 7.3: The normalization process: The nominal surface grid defines a 2D plane. Arrows indicate the distance between nominal and measured surface at each grid-point, which is simply the z-displacement. This can also be seen as the distance between the nominal and measured surface in the direction of the nominal surface normal at each grid-point.

Roof

The roof for the channels with positive and negative bow are show in Figures 7.4 and 7.5 respectively, and will be referred to as the positive roof and negative roof. It can be seen that the positive roof has a fairly gentle and uniform curvature along its length. In contrast, the negative roof appears to have fairly severe ripples along its length. In terms of aesthetic appeal, the roof from the channel with positive bow is far more attractive than the roof with negative bow, due to the unsightly localised features (ripples).

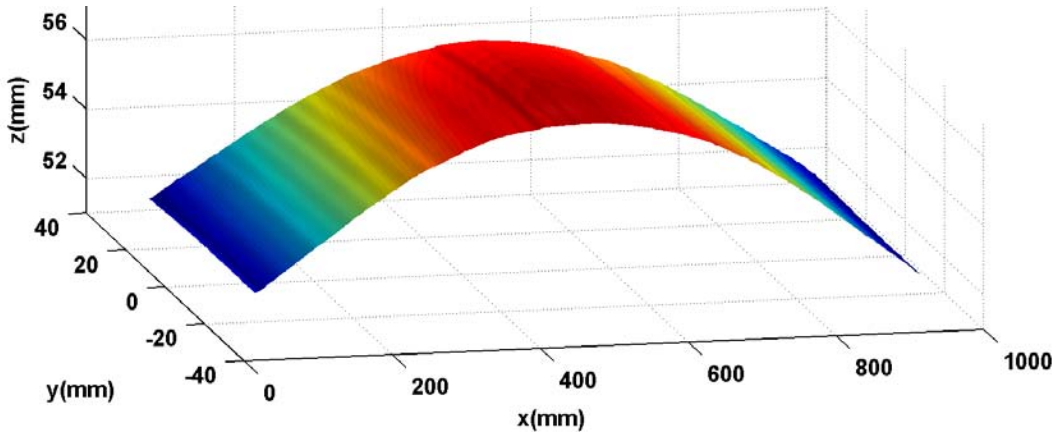

Figure 7.4: Positive bow roof surface

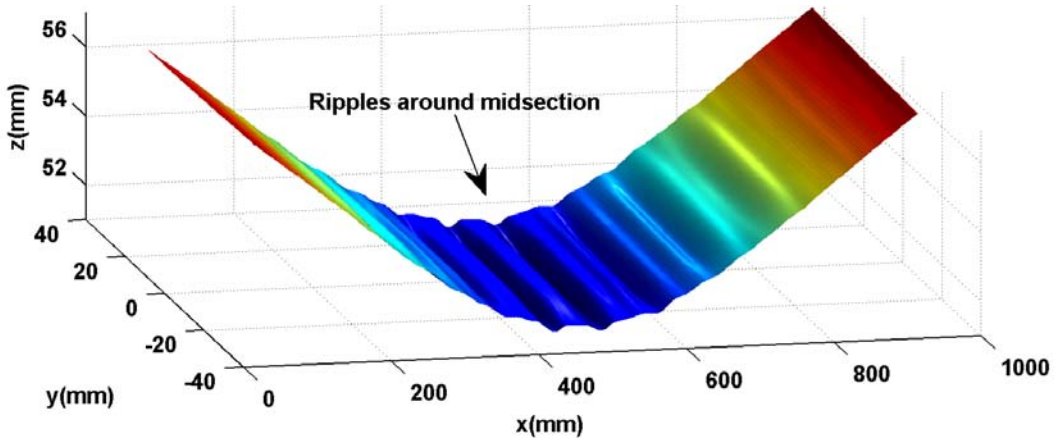

Figure 7.5: Negative bow roof surface

Walls

The wall surfaces that lie above $y = 0$ for the channels with positive and negative bow are presented in Figures 7.6 and 7.7, and will be referred to as the negative wall and positive wall. It should be noted that the axes have been changed to make the walls lie flat in the Figures. The positive wall appears to have quite a severe buckle at its midsection, particularly at the lower end (near $z = 10$), whereas the negative wall has more slight ripples that mostly occur along the top end (along $z = 40$)

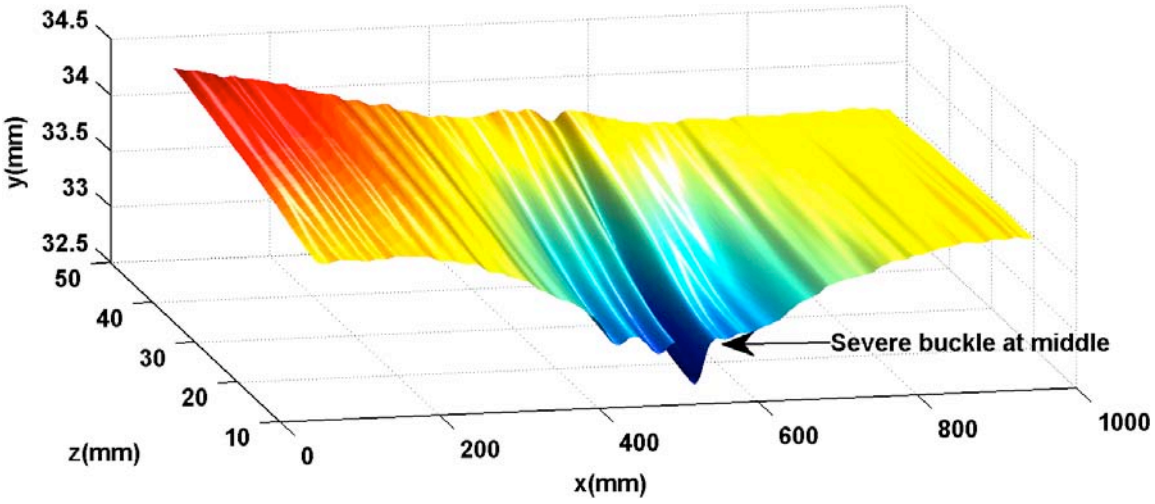

Figure 7.6: Positive bow wall surface.

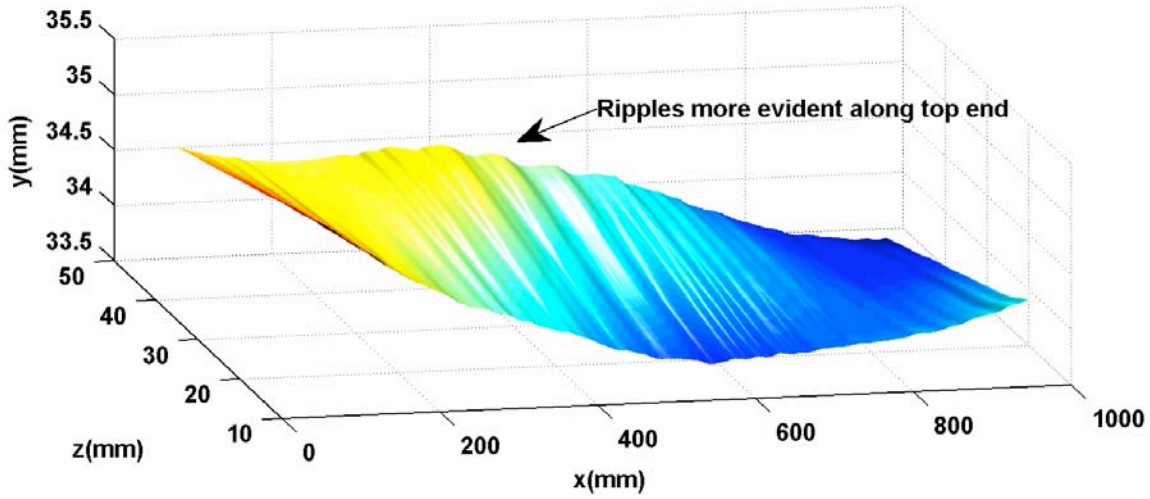

Figure 7.7: Negative bow wall surface.

Flanges

The flanges for the channels with positive and negative bow are shown in Figures 7.8 and 7.9, and will be referred to as the positive flange and negative flange. In this case, the positive flange has severe rippling near its midsection, whereas the negative flange has quite a nice and smooth bow. This is a similar finding to the roofs, except the negative roof (in contrast to the positive flange) was subject to wrinkling. The occurrence of wrinkling can be attributed to the compressive forces along the flanges when inducing a positive bow, with a smoother bow shape formed along the roof where tensile forces act. The opposite can be said when inducing a negative bow.

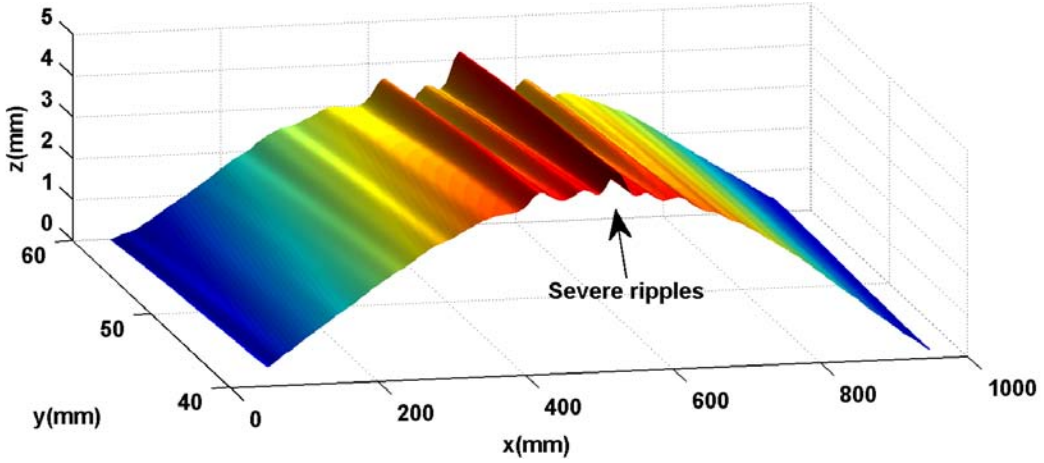

Figure 7.8: Positive bow flange surface.

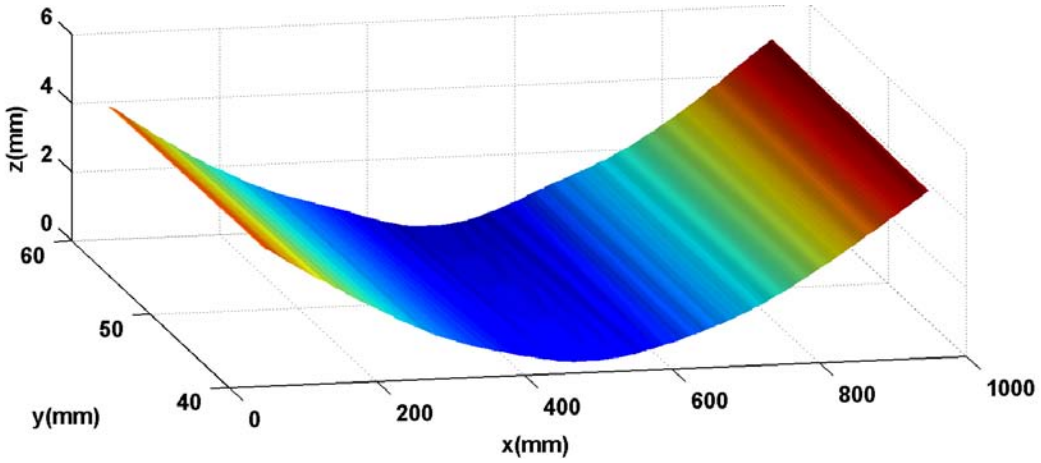

Figure 7.9: Negative bow flange surface.

7.4 Approach to local shape characterization

In previous chapters, univariate measures of shape quality such as average and maximum displacement from nominal have been used to assess assemblies. A limitation of such measures is that while a set of manufactured parts might have similar average and maximum displacements from nominal, they could have significantly different local variation patterns. For example, in Figures 7.8 and 7.9, the two surfaces have similar average displacements from nominal, however, it is clearly evident through visual inspection that the type of variation present on the surface is markedly different. Furthermore, it can be seen that the rippling along the surface shown in Figure 7.8 is quite undesirable in comparison to the surface in Figure 7.9 which is quite smooth. The univariate measures presented thus far are therefore incapable of adequately distinguishing between these surfaces, one of which is more desirable than the other in terms of assembly quality. This gives rise to the motivation of the local shape characterization approach presented in this chapter, which is to proposed a number of techniques that are capable of providing discrimination between different types of local surface variation present on a sheet metal panel or assembly.

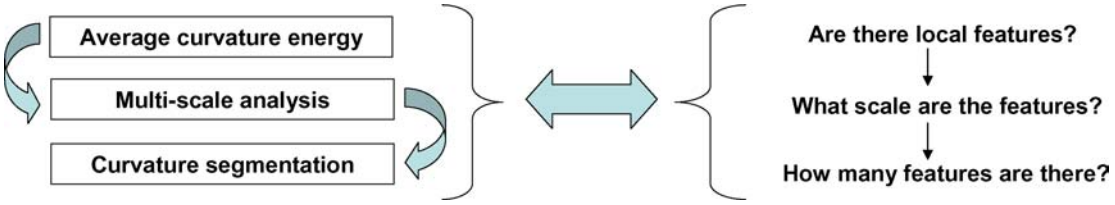

Figure 7.10: Local shape characterization approach.

The local shape characterization method proposed can be seen to take a cascading approach for the description of local surface features, as illustrated in Figure 7.10. Firstly, curvature energy of a surface provides an overall indicator of the presence of notable curved features on a surface. A continuous wavelet transform approach is then used to determine the scale or size of features present on a surface. Finally, a curvature segmentation approach provides further insight by identifying particular curvature-defined local features. Each of the mentioned methods will be described and applied in the following sections to highlight how they can provide discrimination between different types and combinations of local features on a surface.

7.5 Average curvature energy

Average mean curvature energy is the first proposed measure of local surface features on stamping and assembly surfaces. In this section, the method for the calculation of surface curvature will be presented, followed by a definition of average curvature energy, and finally the application of this measure to the six example surfaces, and for comparison between the two example channels as a whole.

7.5.1 Surface curvature

If p is a point on a surface S, consider all curves Ci passing though the point p. Each curve has an associated curvature at the given p. Of all the curves passing through p, there exists at least one curve with the maximal curvature κ_1, and another curve with the minimal curvature κ_2. These two curvatures are known as the principal curvatures of S. There are many approaches for the estimation of the principal curvatures of scanned surfaces. In this thesis, a biquadratic is fitted to a local area (14 mm radius) around each measurement point, where the local co-ordinate system is positioned with the point of interest at the origin, and the z-axis is aligned with the surface normal at that point. The biquadratic surface is given as follows:

$$z = ax^2 + bxy + cy^2 \tag{7.1}$$

The two principal curvatures κ_1 and κ_2 are then given as the real roots of the following equation:

$$k^2 - (a + b)\, k - c^2 = 0 \tag{7.2}$$

Mean curvature can then be calculated from the principal curvatures:

$$K = \frac{\kappa_1 + \kappa_2}{2} = a + c \tag{7.3}$$

Mean curvature can distinguish between locally concave or convex regions on a surface, and was chosen as the measure of surface curvature for the local shape characterization approach as it can adequately capture local features of interest. Other measures of curvature, such as Gaussian curvature, could be applied in the future for a more detailed curvature-based surface decomposition. A key issue to address when estimating curvature from scan data is the sensitivity to noise, which was identified by Trucco and Fisher in their 1995 study which aimed to partition range data into patches using Gaussian and mean curvature. Smoothing is therefore a key requirement for accurate curvature estimation, and it should be noted that the 2D Discrete Cosine Transform was used to denoise surfaces before curvature calculations were performed (see Appendix H.2). Figure 7.11 presents the positive flange surface with mean curvature K indicated by the colour-map.

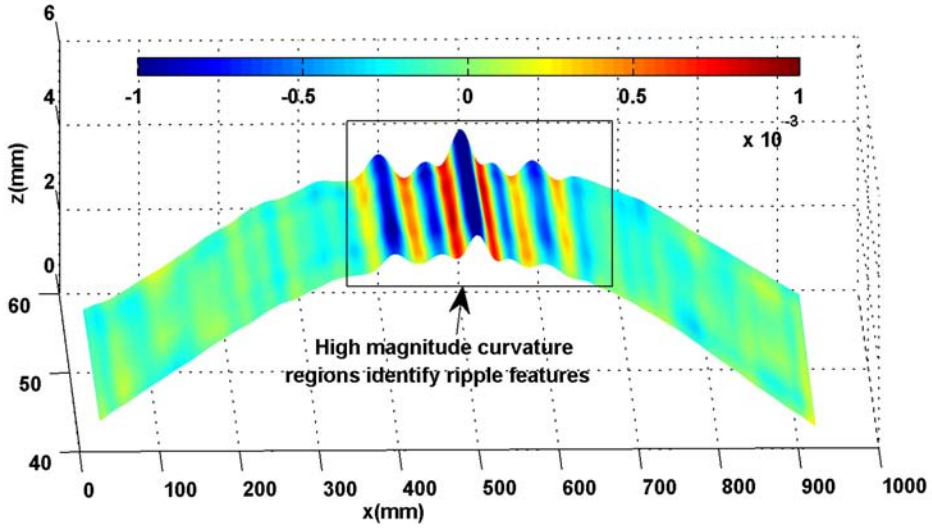

Figure 7.11: Plot of the positive flange with a mean curvature colourmap.

7.5.2 Curvature energy

Surface curvature energy, E, can be defined as the integral of the curvature squared across a surface. It provides a descriptor for the global curvature energy of free-form surfaces:

$$E = \int \int K^2 dA \tag{7.4}$$

where K is mean curvature. For the purposes of this thesis, a similar measure is employed to get an overall indicator of the amount of curvature present in a surface, and therefore an indicator of the amount of local features present. The average curvature energy measure is defined as follows:

$$E_{avg} = \frac{\sum_{i=1}^{n} K_i^2}{n} \tag{7.5}$$

Where n is the number of measurement points on a surface, and K_i is the Mean curvature at each point. Note that measurement points are evenly spaced over a rectangular grid as defined in section 7.3.1.

7.5.3 Surface assessment

To illustrate the application of the average curvature energy as a way of numerically describing local deviations on a surface, the surfaces presented in section 7.3.2 will be analyzed and compared. Table 7.1 presents the average curvature energy values for each of the surfaces, and total average curvature energy for the positive and negative channels (a weighted average of the three surfaces on each channel).

Table 7.1: Average curvature energy of the different surfaces and the two parts as a whole.

Component	Average Curvature Energy	
	Negative bow	Positive bow
Roof	11.31×10^{-8}	0.88×10^{-8}
Wall	2.64×10^{-8}	3.71×10^{-8}
Flange	0.60×10^{-8}	10.24×10^{-8}
Channel	6.70×10^{-8}	3.42×10^{-8}

It can be seen that the two surfaces with the largest presence of local features, the negative roof and positive flange, exhibit the greatest average curvature values. Two surfaces with a large overall bow, but little in terms of local features, exhibit the smallest average curvature values of all surfaces: the positive roof and negative flange. The positive and negative walls display moderate average curvature values, with the presence of more slight local features on these surfaces. It should also be noted that the overall surface range, defined by the maximum and minimum surface z-displacements, is much smaller for the walls than it is for the flanges and roof (a range of 2 mm in comparison to 5 mm). When considering all surfaces, the channel with negative bow has a greater average curvature energy than the positive channel. It should be noted that only one wall, one flange, and the roof from each channel is considered in the overall channel calculations.

7.6 Multi-scale surface assessment

The continuous wavelet transform approach proposed in this chapter allows for the description of local features of a particular scale or size. In the following sections, the continuous wavelet transform will be introduced, followed by a demonstration of the method on one of the six example surfaces. The process of selecting appropriate scales for the description of features of interest will then be presented, followed by an application of the local shape assessment approach to the six example surfaces, and for comparison between the two example channels as a whole.

7.6.1 The continuous wavelet transform

The continuous wavelet transform (CWT) has an ability to examine a signal simultaneously in both the time/space and frequency domains, which addresses a key limitation of the Fourier Transform (Daubechies, 1992). This ability has made it a popular approach for pattern recognition applications where it is required to identify features that are highly localized in spatial positions. In this chapter, the CWT is employed to identify local features along a set of manufactured surfaces. The wavelet decomposition for a function is expressed as:

$$T(a,b) = \int_{-\infty}^{\infty} f(x)\psi_{a,b}(x)dx \tag{7.6}$$

where the normalized wavelet function at the scale a, and shift location b, is given by:

$$\psi_{a,b} = \frac{1}{\sqrt{a}}\psi\left(\frac{x-b}{a}\right) \tag{7.7}$$

The Mexican hat wavelet given in Equation 7.8 was chosen for the purposes of this chapter, as it appears well suited for detecting features in the form of bumps and ripples. It is proportional to the second derivative of the Gaussian probability distribution function.

$$\psi(x) = \left(\frac{2}{\sqrt{3}}\pi^{-1/4}\right)\left(1-x^2\right)e^{\frac{-x^2}{2}} \tag{7.8}$$

Average energies of the continuous wavelet transforms of lengthwise surface cross-sections at a set of specified scales will be calculated. This will provide a measure of the amount of features present in a surface according to these scales. The Mexican hat wavelet at two different scales is presented in the following Figure 7.12, and the translated wavelet is shown in Figure 7.13.

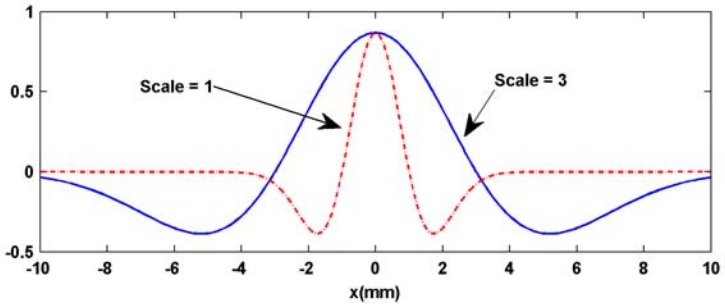

Figure 7.12: Mexican hat wavelet at two different scales.

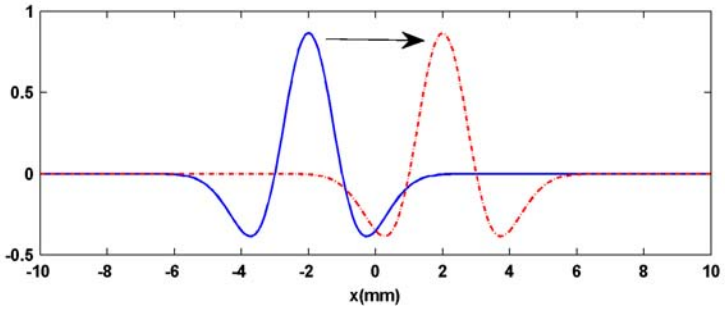

Figure 7.13: Translated Mexican hat wavelet.

7.6.2 Surface example

To illustrate the application of the CWT as a way of numerically describing local deviations on a surface, the wall surface of the hat with negative bow shown in Figure 7.7 will be analyzed with the proposed approach. The continuous wavelet transform will be applied to a series of lengthwise cross sections to capture the local feature present across an entire surface. Figure 7.14 shows an example lengthwise cross section of the negative wall, and Figure 7.15 shows the corresponding continuous wavelet transform with the scale ranging from 0.1 to 150.

An explanation of the continuous wavelet transform plot is as follows. The x-axis indicates the length along a signal, and the y-axis indicates the scale of the wavelet that is fitted at each sample point along the length of the signal. The better the fit of the wavelet at a particular scale to the underlying signal at a specific point, the higher the magnitude of the wavelet transform (indicated by the z-axis). For example, if a local area is of a similar shape to the Mexican hat wavelet, such as a ripple, the wavelet transform at that point will be of a relatively large magnitude in comparison to a local area that does not match the wavelet (such as a flat surface). Indicated on Figure 7.15 are two different scales, 17 and 150, which appear to capture different scale features

of interest. These scales will be investigated in more detail in the following section. It should be noted that the cross-section was extended using a local linear fit at each end in order to eliminate the effects of high magnitude regions that occur at either end of a signal. Such high magnitude regions can dwarf the presence of local features and are therefore undesirable. Here, signals were artificially extended, the wavelet transform performed on the extended signal, and then only the component of the wavelet transform corresponding to the original signal was used for power calculations. This allows for high power regions at the end of the extended signal to be avoided. For more details on this method, see Appendix D.

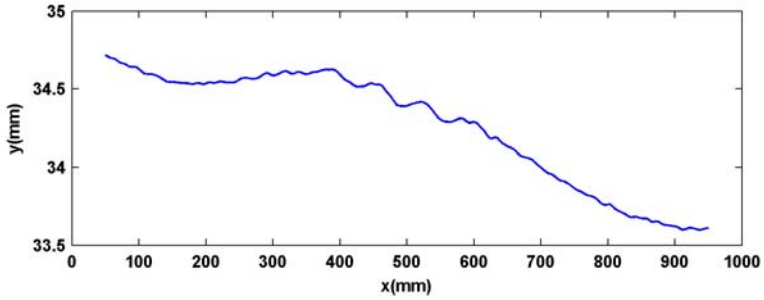

Figure 7.14: Example lengthwise wall cross section at $z = 44.5$ mm.

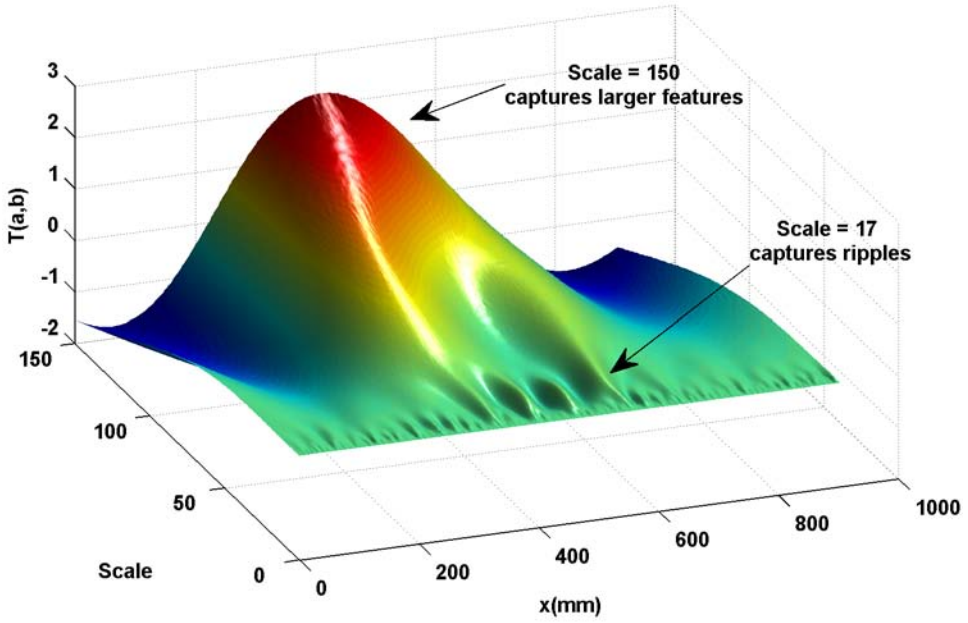

Figure 7.15: Corresponding continuous wavelet transform of a lengthwise cross section of the wall at $z = 44.5$ mm, with scale ranging from 0.1 to 150.

7.6.3 Selecting scales

As stated earlier, the average energy of the continuous wavelet transform at a set of pre-defied scales will be used to identify the presence of local features on a surface. Two example scales are presented in the following to illustrate how different types of features can be captured by appropriately selected scales. Firstly, in Figure 7.16 the example cross section and the wavelet transform at a scale of 17 is presented. It can be seen that there are ripples along the mid-section of the signal, which could possibly have adverse effects on quality perceptions. It can also be seen that these ripples are captured by the continuous wavelet transform at a scale of 17. At a scale of 17, the Mexican hat wavelet is of a similar size and shape to the ripple features of interest, which results in high power regions corresponding to the ripple locations.

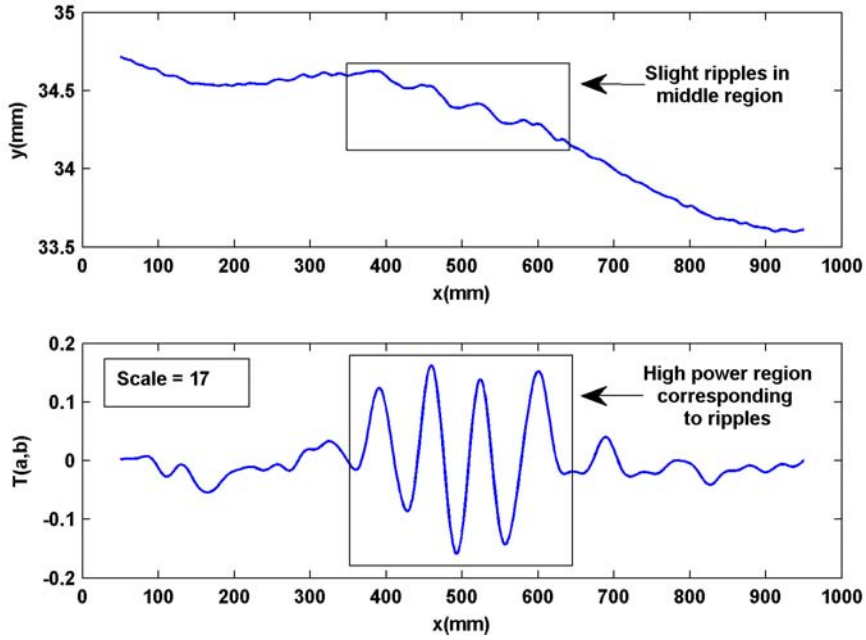

Figure 7.16: The cross section and corresponding continuous wavelet transform at a scale of 17.

In Figure 7.17 the example cross section and the wavelet transform at a scale of 150 is presented. It can be seen that there are larger features in the cross section: a peak in the middle of the signal, and two troughs at either side. These larger surface features are captured by the continuous wavelet transform at a scale of 150. Again, at a scale of 150, the Mexican hat wavelet is of a similar size and shape to the features of interest, resulting in high power regions corresponding to the feature locations. Therefore, if the size of a set of particular features is known, the continuous wavelet transform at a scale that corresponds the feature size can be used to identify such features on any

surface. The continuous wavelet transform can therefore be employed as a powerful tool for describing and discriminating surfaces with local features.

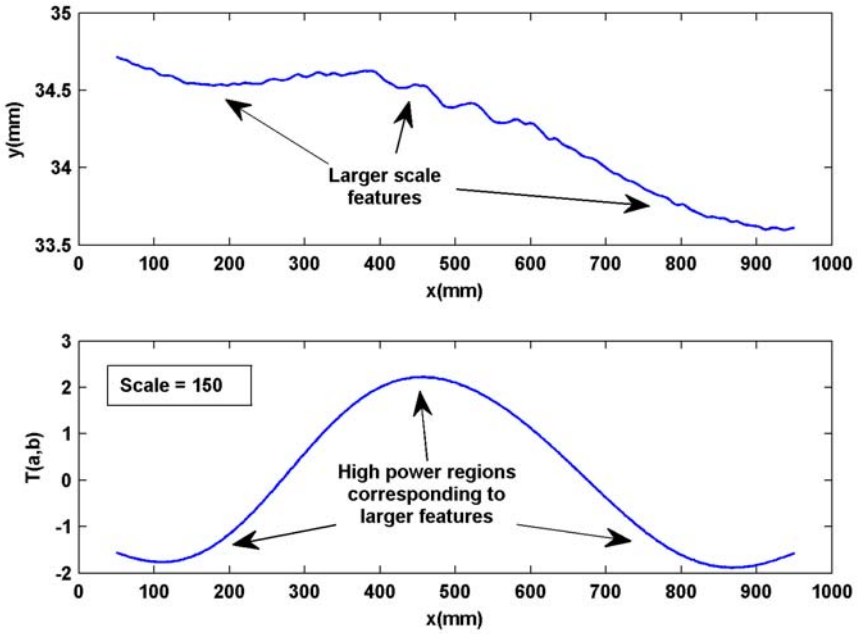

Figure 7.17: The cross section and corresponding continuous wavelet transform at a scale of 150.

7.6.4 Average power

This section defines the wavelet transform average power measure used to assess surfaces at different scales. The average power is defined as the sum of the wavelet transform of n samples taken from all surface cross sections. It should be noted that when calculating the average energy values, a threshold of 0.125 was used to eliminate noise from smaller scale features.

$$P_{scale=a} = \frac{\sum_{i=1}^{n} P_i}{n} \tag{7.9}$$

where

$$P_i = \left\{ \begin{array}{ccc} |T(a,b)| & \text{for} & |T(a,b)| \geq 0.125 \\ 0 & \text{for} & |T(a,b)| < 0.125 \end{array} \right\} \tag{7.10}$$

7.6.5 Surface assessment

Again, to illustrate the application of the wavelets based surface description as a way of numerically describing local deviations on a surface, the surfaces presented in section 7.3.2 will be analyzed and compared. Table 7.2 presents the average power values for each of the surfaces at a scale of 17, and total power for the positive and negative channels (a weighted average of the three surfaces on each channel). Table 7.3 presents the average power values for each of the surfaces at a scale of 150, and total power for the positive and negative channels (a weighted average of the three surfaces on each channel).

Table 7.2: Average power of the different surfaces at a scale of 17.

Component	Average Power (Scale = 17)	
	Negative bow	Positive bow
Roof	0.2314	0.0025
Wall	0.024	0.0325
Flange	0.0192	0.1762
Channel	0.1250	0.0455

As seen with the average curvature values, the average power levels at a scale of 17 appear to distinguish between the different levels of local surface features, with the positive flange and negative roof exhibiting the highest values, followed by the walls, and finally the positive roof and negative flange (the smoothest surfaces). Again, overall the channel with negative bow has a higher average power value.

Table 7.3: Average power of the different surfaces at a scale of 150.

Component	Average Power (Scale = 150)	
	Negative bow	Positive bow
Roof	14.6440	13.4680
Wall	1.8287	1.8338
Flange	16.8238	10.2322
Channel	11.0177	9.1696

At a scale of 150, larger scale features can be captured. At this scale, the difference between the walls and other surfaces is clearly evident, where the surface deviation range of the walls is much less that for the other surfaces. Overall, the positive and negative channels display similar average power levels at this scale, showing how they have similar larger scale features, namely a bow of approximately 5 mm.

7.7 Curvature segmentation

The final local shape characterization measure, curvature segmentation, is designed to extract more detailed information about the size and number of features present in a surface. Here, regions on a surface that are above or below a certain curvature threshold are deemed to be a notable feature. For this process, points above a certain curvature threshold are determined to lie on a feature of notable interest. A clustering approach involving a nearest-neighbors method is then employed to group a set of points into single features. A simple example of this approach is presented in Figure 7.18. Here, a test data point is assigned to a group by the following criteria:

- If another point lies within a particular distance of the test point, it is determined to be a member of the same class.
- The test point is also tied to the same class as points that lie within a particular distance of its direct neighbours, and points that are neighbours of this new set of points, and so on.

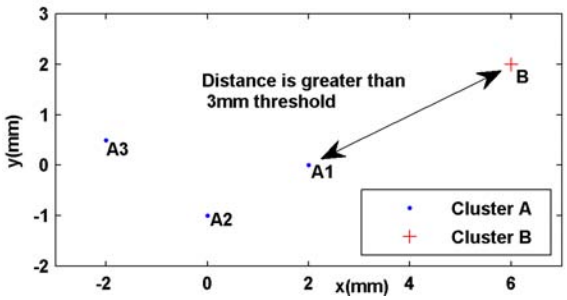

Figure 7.18: Nearest neighbours clusters at a 3mm threshold. The distance between points A1 and B is greater than 3mm, so they are deemed to be in different clusters. Points A1 and A2 are within 3 mm of each other and are therefore deemed to be in the same cluster. Points A1 and A3 are more then 3 mm apart, however, as point A2 is within 3 mm of both points, they are deemed to fall within the same cluster.

Figure 7.11 from section 7.5.1 presented the flange surface from the channel with positive bow with a colour-map indicating mean curvature. It could be seen that near the middle of the surface, there were high magnitude curvature regions. Figure 7.11 indicates the regions identified by the curvature segmentation process, which correspond to notable high-magnitude curvature features of interest. These features extracted by the curvature segmentation process are then described by the following (Note that MP s are arranged in 2 mm grid spacings):

- C_L = Number of large features (features consisting of more than 15 gridpoints/MP s)

- C_S = Number of small features (features consisting of less than 15 gridpoints/MP s)
- $C_{\%}$ = Total % of surface covered by high curvature features.

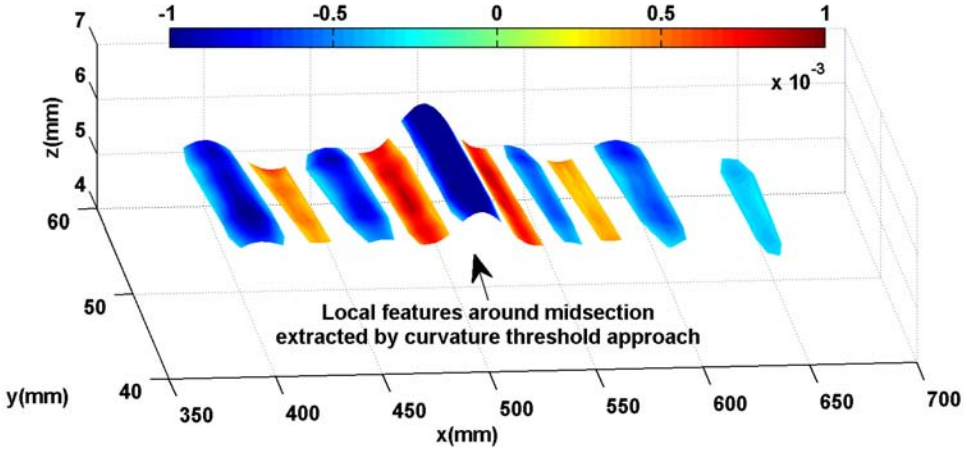

Figure 7.19: Example extracted features from the curvature threshold approach. It should be noted that there are also features with much smaller surface area present on different regions of the surface which are not shown.

7.7.1 Surface assessment

Finally, to illustrate the application of the curvature segmentation descriptors as a way of numerically describing local deviations on a surface, the surfaces presented in section 7.3.2 will be analyzed and compared. Tables 7.4 and 7.5 present the number of large features, number of small features, and percentage surface area covered by features, for each of the surfaces, and overall for the positive and negative channels (a weighted average of the three surfaces on each channel). The selected threshold cutoff was 3×10^{-4} as it appeared to isolate/identify the desired features of interest.

Table 7.4: Curvature segmentation local surface descriptors. Channel with positive bow.

Component	C_L	C_S	$C_{\%}$
Roof	0	3	0.2%
Wall	4	5	8.0%
Flange	10	9	16.3%
Channel	14	17	5.7%

Again, it can be seen that the positive flange and negative roof have a much greater presence of local features in comparison to the other surface, with the % surface area

Table 7.5: Curvature segmentation local surface descriptors. Channel with negative bow.

Component	C_L	C_S	$C_{\%}$
Roof	23	6	25.3%
Wall	3	7	8.4%
Flange	0	0	0.0%
Channel	26	13	15.1%

with local features at 16.3% and 25.3% respectively. The negative flange has absolutely no local features according to the curvature segmentation approach. Overall, the channel with negative bow is identified to have the largest presence of local features, and is therefore the more unattractive component in terms of localized variation. Again, it should be noted that only one wall and one flange is measured for the overall channel indicator measures.

7.8 Local shape characterization vector

This chapter has proposed three key approaches that are all capable of discriminating between different levels of local shape variation on manufactured surfaces: average curvature energy E_{avg}, wavelet transform average power levels P, and curvature segmentation based descriptors C. These measures can be formalized into the following local shape characterization vector:

$$LSC = [E_{avg}, P_{scale=a_1}, ..., P_{scale=a_N}, C_{L,}C_{S,}C_{\%}] \tag{7.11}$$

It should be noted that the curvature segmentation values for a number of large and small features (C_L and C_S) should be standardized to the number of features per standard area (for example, number of features per metre squared).

Each of these measures takes a slighting different approach to the description of local features of a manufactured surface, and together they provide a rich array of measures for the discrimination of surfaces, with a view to surface classification, assessment, and ultimately optimal process selection.

7.9 Future developments

This section will discuss important future developments of the registration and normalization process, the local shape characterization measures, and how the measures could be implemented within a dimensional assessment framework.

7.9.1 Registration and Normalization

Future generalization of the registration and normalization process to capture variation across an entire surface (rather than rectangular grids which only capture part of the surface within a specified area), and surfaces that are not nominally flat, will require different treatment to that proposed in this thesis. In applications such as computer vision, a different approach to the registration of deformable objects such as sheet metal assemblies known as non-rigid point set registration is often used (Zitova and Flusser, 2003). These approaches involve a combination of spatial feature detection (such as edges and corners), and constrained point set mapping, and could allow for registration of entire surfaces. These techniques were not applied in this thesis as there are several issues that need to be addressed before they can be effectively implemented for this approach, such as questions over accuracy of the method (due to the small deformations that need to be captured), required quality of scan data, and processing time, which were deemed beyond the scope of this thesis. The normalization process for surfaces that are not nominally flat also presents many issues, such as the need to map the nominally curved surface into a 2.5D representation. This could be achieved using established methods (Sheffer and de Sturler, 2001), however, it is again beyond the scope of this thesis.

7.9.2 Curvature-based methods

Once the registration and normalization issues have been addressed, the curvature energy and thresholds approaches are easily adaptable to any surface, as the approaches are scale, translation, and rotation invariant. This means that irrespective of the orientation of the surfaces or local features, the same curvature based assessment will result. Key areas of refinement required for the future use of these methods however is surface denoising, the curvature calculation method, and computational speed. Curvature calculations are very sensitive to noise, so effective denoising is an important step for the accurate implementation of such methods. The curvature calculation method used in this chapter where a biquadratic is fit to a local area is one of the more popular approaches, however, there are other methods that could be explored to check for suitability for this application. Magid et al. (2007) provide an overview of a range of approaches for curvature calculation. Perhaps the biggest issue to address is that of computational speed. In order for the approach to be more practically implementable, particularly in a fast paced manufacturing environment, the curvature measures must be quickly accessible. The advent of less expensive and more powerful multi-core computers could be a solution, as surface curvature calculations lend themselves well to multi-threading approaches.

7.9.3 Multi-scale surface analysis

In this chapter, the average power of the continuous wavelet transform of a series of lengthwise cross-sections at specified scales was used to identify the presence of local features of interest on a surface. One advantage of this approach is that as only a few select scales are required, the computational burden is relatively low. Usually when applying the CWT for signal analysis, calculation of the transform across a large range of scales is required which can be computationally expensive; the discrete wavelet transform has therefore often been chosen in favour of the CWT due to computational advantages. The discrete wavelet transform however can only compute at particular scales (2^n) due to a down-sampling process. This makes it difficult to match the appropriate scale to the size of the local features of interest using the DWT, which is why it was not selected for this application. The CWT approach presented in this chapter also holds a few benefits over the curvature-based methods. For one, the CWT approach is well suited to dealing with noise, whereas the curvature-based methods can suffer considerably in the presence of noise. Furthermore, the CWT approach is more computationally forgiving than the curvature-based approaches.

For future use, the CWT approach can be readily developed to allow for a more general local characterisation of free form surfaces. For one, cross-sections in other directions could be used, such as in the width-wise and diagonal directions as done with the discrete wavelet transform. This would enable scale features in other directions to be captured as well. As the CWT approach is not rotation invariant (ie, the scale of features found on a surface is largely dependant on the orientation of the cross section), taking the cross sections at a number of angles could be an important method for reducing the sensitivity of the approach to orientation. Another key extension to the method is to ensure that the same effective size of features is being investigated. This can be achieved by adjusting the wavelet scale according to the length of the signal. This is especially suited to dealing with non-rectangular surfaces, where cross-sectional lengths could change. Other user defined wavelets could also be proposed to more closely match the exact type of local features of interest. Overall, the CWT method proposed for local shape characterization provides a powerful and potentially very practical approach for describing localized features in manufactured shapes.

7.9.4 A view to surface classification

This chapter has proposed a shape characterization vector that can provide discrimination between differing manifestations of local shape varication. Now that a way of describing local variation has been developed, the next key stage in a quality assessment framework is to develop a relationship between the local shape vector and customer perceptions of quality, which is far from a trivial task. A common approach in pattern

recognition is to use a labelled training data set with which to train a classifier. This could involve a customer defining or ranking a set of manufactured shapes based on some criteria, and then testing to see if a classifier built around the local shape characterization measures can replicate the customer definitions of quality. This process will be disused in more detail in the following chapter.

7.10 Conclusion

This chapter presents a novel approach for the description of the nature in which a manufactured surface locally deviates from its nominal design. A multi-tiered approach is suggested:

- Surface curvature energy, which is the integral of the curvature squared across a surface, provides an overall measure of the curvature of a surface, and can therefore distinguish between translated and highly distorted parts.
- The continuous wavelet transform is used to decompose the surface into scale components. Average energy values are then used to rank surfaces in terms of different scale components present in surfaces.
- Curvature based thresholds are then used to extract curvature defined features of interest.

Each shape characterization tier addresses a limitation of the previous measure, and in combination with each other, the measures provide a diverse mix of features with which to discriminate between different types of local deviations of a manufactured surface from its nominal design. Now that a numerical local shape characterization approach has been developed, the next key step is to develop a mapping between these features and customer quality perceptions of an end product. The next chapter will therefore firstly proceed to discuss how the local shape characterization approach can be integrated within a shape quality framework for the classification, assessment, and section of optimal processes for dimensional control. The next chapter will then summarise the key contributions of this thesis along with avenues of future research.

Chapter 8

Conclusion

8.1 Introduction

This chapter initially provides a conceptual framework for the implementation and integration of the various tools and techniques presented throughout this thesis for the purpose of dimensional control of sheet metal assembly variation. It will then proceed to review the major contributions of this thesis, and finally discuss future avenues of research that would extend the application of the work proposed by this thesis.

8.2 A framework for quality assessment

Chapter 2 provided an overview of three key research areas that have provided significant advancements into the dimensional control of automotive body assemblies: Virtual assembly, Process diagnosis, and Knowledge based design. In order to take full advantage of these advanced simulation, monitoring and design tools, a well defined measure of assembly quality must be in place so the right objectives can be targeted. Chapter 2 also discussed univariate quality measures such as process capability indices and SPC, and some key limitations preventing the adequate description of assembly quality. The key limitations were an inability to capture correlated variation patterns, monitor non-normally distributed data, interpret high dimensional data, and measure local variation patterns of different sizes or scales. While some previous research has partially addressed some of these limitations, this thesis presents two major tools that are specifically aimed at overcoming each of the mentioned limitations: the multivariate statistical shape model (KDE-PDM), and the local shape descriptors. The next sections will discuss firstly how these approaches address the limitations of univariate measures of assembly quality, and secondly how they can be applied to enhance current capabilities to identify more optimal processes for dimensional control.

8.2.1 Multivariate statistical shape model

In Chapter 6, a multivariate model that combines Kernel Density Estimation and the Point Distribution Model (the KDE-PDM) was introduced to provide a more accurate statistical representation of the entire shape of sheet metal stamping and assemblies. Major advancements of this approach over univariate approaches are that the model is capable of representing correlated variation modes, dealing with high dimensional data sets, and capturing non-normal distributions. The ability of this multivariate approach to capture correlated variation modes is important as geometric covariance is an inherent characteristic of sheet metal assembly variation. Through capturing correlated variation patterns more information can be extracted about the type or nature of variation present, allowing for more detailed assessments about the quality of the assembly. High dimensional data sets are made to be more manageable through the dimensional reduction technique PCA, which allows for the representation of a large set of MP s with a smaller set of factors. Non-normally distributed data is accounted for through the kernel density estimation technique which is capable of estimating any type of distribution, allowing for a more accurate inferences to be drawn from a more accurate statistical representation of the underlying data set. Areas for possible implementation of the multivariate shape model (or KDE-PDM) include data mining and diagnosis, interpreting quality, and tolerance zones.

Data mining and diagnosis

Multivariate tools have been applied for the purposes of fault diagnosis from process monitoring data. Rather than just highlighting a sample as being out-of-control as in SPC, multivariate techniques can uncover the type of variation pattern present which can often be matched with a root cause. The majority of methods involve a supervised approach to process diagnosis, where fault vectors are pre-determined from theoretical assembly functions, process data is decomposed using a method such as PCA to identify physical fault patterns (Yang, 1996), and the theoretical and physically occurring patterns compared to identify the particular fault mode present (Ceglarek and Shi, 1996). It is not always possible or practical to identify all possible theoretical fault modes. Apley et al. aim to use unsupervised approaches to reveal unknown fault patterns in process data (2001; 2007). The statistical shape model proposed adds another dimension to multivariate analysis which enables further avenues for unsupervised pattern identification: the kernel (or mixture model) density estimate. Probabilistic representations can be used to reveal underlying structures in a data set. For example, probabilistic thresholds could be applied to identify clusters within a data set. In many cases it is possible that the formation of such shape clusters will be a result of process factors. Probabilistic thresholding could therefore provide targets for quality engineers

in their quality control efforts. Furthermore, corresponding physical shapes for each cluster could be used to aid in process diagnosis through an ability to visualise the three dimensional correlated variation patterns. Figure 8.1 looks at an artificial data set presented in the form of the KDE-PDM to illustrate the data mining concepts. It can be seen that the probabilistic representation highlights an underlying structure in the data.

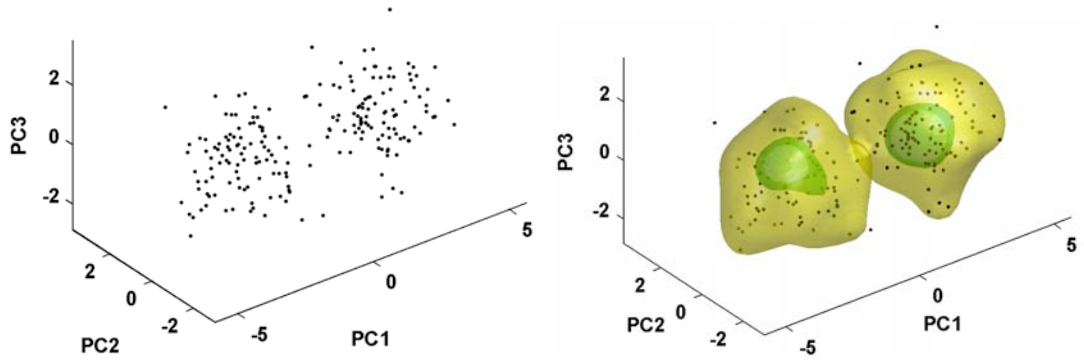

Figure 8.1: Figure (a) shows an example measurement data set in the reduced 3D PCA space. Figure (b) shows a three level density contour plot at the 7.5%, 15% and 75% levels within the same plot space (ie, 7.5% of samples will fall within the 7.5% contour level and so on). Note how the underlying data structure consisting of two main clusters is highlighted by the density estimate.

Interpreting quality

The multivariate statistical shape model has the potential to provide a more intuitive interpretation of assembly quality through the ability to visualise the probabilistic representation of the data set in parallel with corresponding physical shapes. This improved interpretation of assembly variation could assist the investigation of both virtual and physical process data, and for the selection of processes for dimensional control. There are three key approaches that could be taken for improving the dimensional quality of processes within the context of the multivariate statistical shape model: reducing the spread of data, and shifting the process towards the nominal and/or away from less desirable variation patterns.

1. ***Reducing variation or spread of the data set by pushing the process in towards the mean:*** An example procedural approach to achieving this goal could be to firstly reduce the number of clusters in the data set (ideally down to one cluster), and secondly to reduce the spread of each remaining cluster.

- As seen in section 6.4.5, it is likely that the formation of clusters in a data set is an indicator of mean shifts such as operator error or process setup differences. Through targeting these clusters, it is likely that a great deal of the problematic variation in a process will be eliminated. Figures 8.2 (a) and (b) show a graphical representation of the process of eliminating separate clusters using the probabilistic representation of the multivariate shape model.
- Finally, once the number of clusters have been reduced, the remaining avenue of dimensional improvement is to reduce the spread of the remaining clusters, which could for example be achieved by identifying a more optimal clamping sequence for dimensional control. Figures 8.2 (c) and (d) graphically demonstrate this example procedural approach.

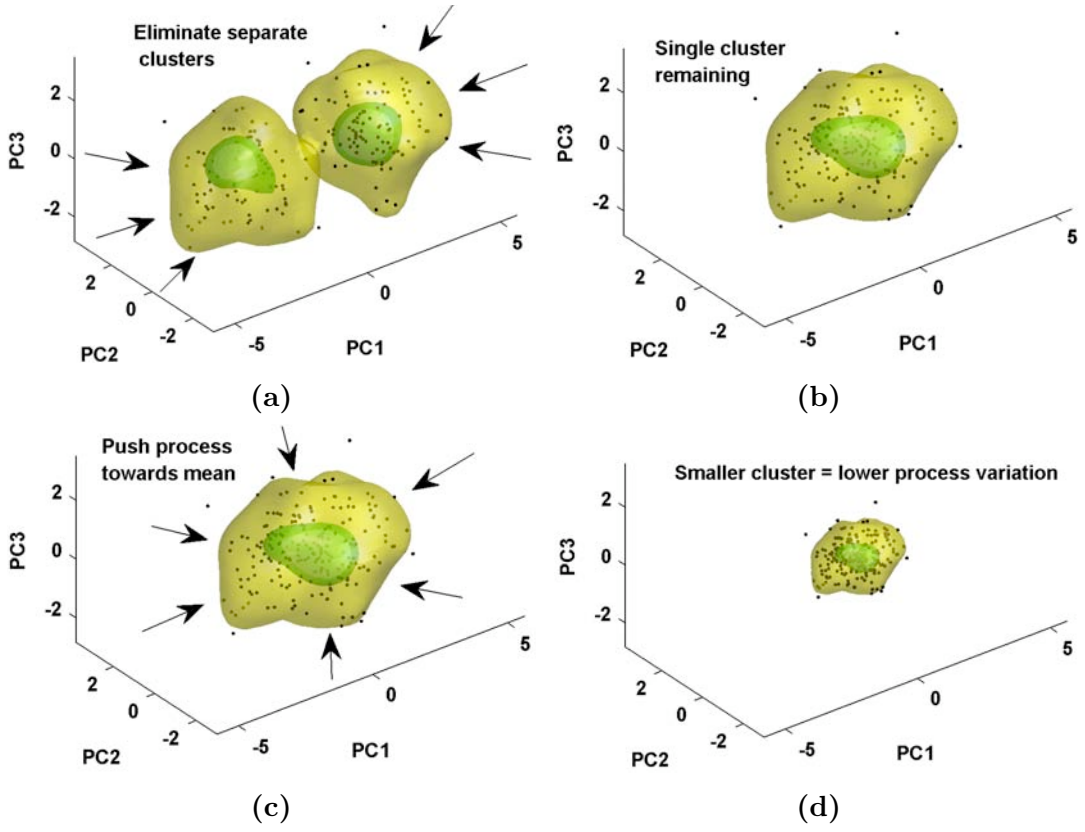

Figure 8.2: Figures (a) and (b) show how the elimination of major variation sources such as process setup errors could reduce the amount of clusters. Figures (c) and (d) show how the process could be pushed towards a mean by a method such as identifying a more robust clamping sequence. A three level density contour plot is shown at the 7.5%, 15% and 75% levels in all plots.

2. ***Moving the mean shape closer to the nominal specification:*** Once the spread of the data has been controlled the next stage could be to shift the mean of the data set towards the nominal design specification as indicated in Figure 8.3.

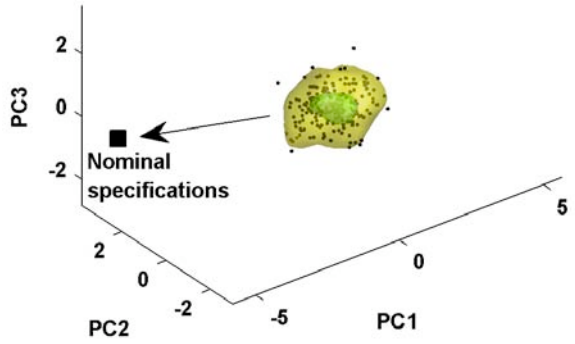

Figure 8.3: Moving the process towards its nominal specifications could for example be achieved by clamp shimming (Yi et al., 2005). A three level density contour plot is shown at the 7.5%, 15% and 75% levels.

3. ***Moving the process from undesirable variation patterns to desirable variation patterns:*** Some manufactured shapes will be more or less desirable according to the amount and type of variation present. The desirability of a manufactured shape will often be a subjective issue that manufacturers will need to decide upon, however, the probabilistic and physical representations made available by the multivariate shape model should provide much needed assistance for this purpose. Section 8.2.2 will proceed to discuss the local shape descriptors that delve into the concept of the desirability of correlated variation patterns in relation to quality perceptions.

Dimensional quality of a population of assemblies or stampings according to the global statistical shape model can be seen to depend on the spread of data including the number of clusters, distance between the population mean and nominal specification, and the type of global variation patterns present. The process for dimensional control utilising the global shape model differs from a univariate approach in that correlated variation patterns, rather than just individual MP s, can be targeted with process control measures. Coupling the multivariate global shape model with shape visualisation capabilities would further enhance the diagnostic toolset by allowing process engineering to see what variation patterns are present, which could lead to a more intuitive understanding of the process and how to manipulate it for dimensional control.

New tolerancing approach

The multivariate statistical shape model provides an advanced probabilistic representation of auto-body assembly processes. In practice tolerances are often based on a univariate probabilistic representation where 99.7% or more of process data should fall within the specified tolerance zone. This concept could be extended to the multivariate shape model. Here, probabilistic thresholds could be set such that all regions above this threshold account for 99.7% or more of the training process data. Test process samples that fall above the set probability threshold would be within the tolerance region, and test samples that fall below the threshold will be outside the tolerance region. This concept is illustrated in Figure 8.4 using the same example data set as in section 8.2.1. This tolerancing approach would allow for the monitoring of a single probabilistic model, rather than a series of independent models as is currently the practice, which would be very advantageous given high dimensional data sets made available by OCMM s. In general, it provides a more informative and implementable approach for statistical modelling and tolerancing of flexible assemblies given high dimensional measurement data. Again, when coupled with the visualisation of corresponding physical shape variation patterns the approach has the potential to enable a more intuitive diagnosis of out-of-control process cases.

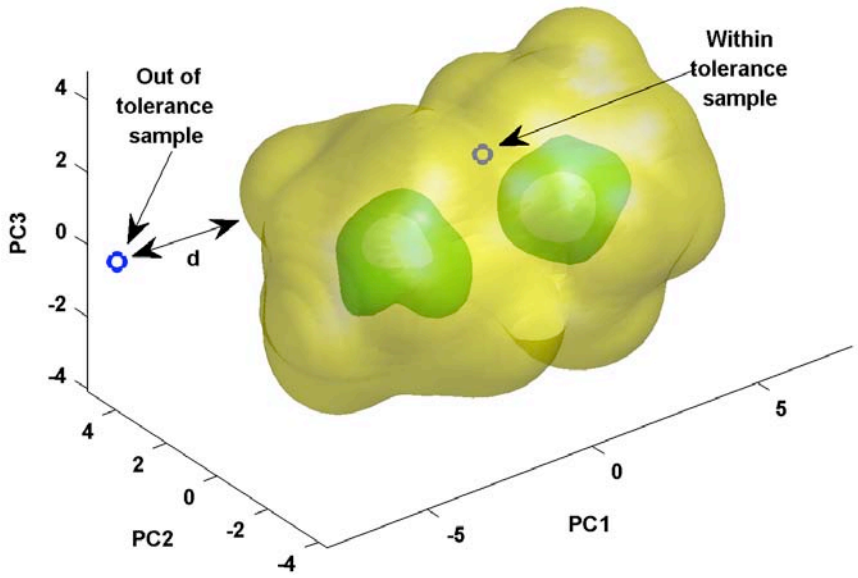

Figure 8.4: Example tolerance zone within a multivariate statistical shape model. A three level probability contour at the 10%, 40%, and 99.7% levels is indicated. Here, 99.7% of process samples should fall within the indicated contours. For a new tolerancing approach, samples falling within the 99.7% contour could be deemed within-tolerance, and samples falling outside this zone out-of-tolerance.

8.2.2 Local shape descriptors

In chapter 7, a set of numerical descriptors for local variation patterns such as bumps, ripples and buckles was presented. The descriptors overcome limitations of univariate measures through their ability to represent correlated variation patterns of different sizes and scales. The simplest goal of these descriptors is to identify which components or assemblies are more favourable than others in terms of local variation patterns, and to move the process to the more favourable regions in a similar manner to that described in section 8.2.1. These descriptors could be applied for the assessment of both virtual and physical assemblies. An advantage of the local shape descriptors is that they could be used to compare different components and assemblies, whereas the multivariate shape model can only be used to assess a particular component or assembly and its process variants (ie, different clamp sequences). An important development that needs to be made is to establish the relationship between the numerical local shape descriptors and customer quality perceptions. While the local descriptors provide some level of discrimination between differing levels of local variation patterns, they do not specific how acceptable each of the variation levels are. Possible approaches for establishing this relationship will be discussed in the following section.

Establishing local shape aversion

The local shape descriptors facilitate the quantitative description of correlated local features such as bumps and ripples, which can detract from assembly quality. The descriptors therefore allow the systematic discrimination of differing levels and types of local variation patterns present on an assembly. As stated in the last chapter, pattern classification can be seen to consist of two key steps. The first is to find a set of measures that are capable of describing or discriminating between particular features of interest: the proposed local shape descriptors serve to address this step. The second step is to partition the data set into a set of meaningful sub-groups with these measures. In terms of local variation patterns in sheet metal assembly, the goal is to separate favourable and unfavourable types and combinations of patterns. Pattern recognition has emerged as a rich field for separating classes or groupings of data, with successful applications in areas such as computer vision (Theodoridis and Koutroumbas, 2006), and sheet metal forming (Rolfe et al., 2003). For developing a local shape quality assessment model using pattern recognition techniques, a supervised learning approach could be adopted. The would involve the following steps:

1. ***Label training data:*** This step involves ranking the relative quality of a population of manufactured shapes with differing levels of local variation patterns. Example rankings could be good versus bad, or a more detailed score of 1 to 10. The easiest approach for this data labelling process would be to get a single ex-

pert or a panel of experts (such as senior quality engineers) to define the sample rankings. A more detailed and perhaps more beneficial approach could be to get a broader population of customers to assess and rank the samples and develop a quality ranking, as it is the end customer that ultimately decides upon the quality of a purchased product.

2. ***Train a classifier:*** Using the local shape descriptors, train a classifier to replicate the quality rankings defined by the previous step. There are many methods available ranging from simple linear classifiers such as linear discriminant analysis which was introduced in chapter 4, through to more advanced nonlinear classifiers such as radial basis networks which are closely related to the kernel density estimation (Bishop, 2007). Techniques such as cross-validation could be used to ensure model generalization.

3. ***Automated local quality assessment:*** Now that an automatic local shape assessment classifier has been determined, it can be used to rank the quality of new process samples in a systematic manner. The goal of manufacturers accordingly would then be to move process toward more favourable local variation patterns, however, manufacturers must also consider other aspects of assembly quality when making decisions for process control. For example, optimizing for local variation might not be the best move for optimising variation levels according to the multivariate statistical model. Figure 8.5 shows what the decision boundaries could look like on a trained local shape model, and it is also indicated how the goal would be to move the process towards lower levels of local variation (and therefore higher quality levels).

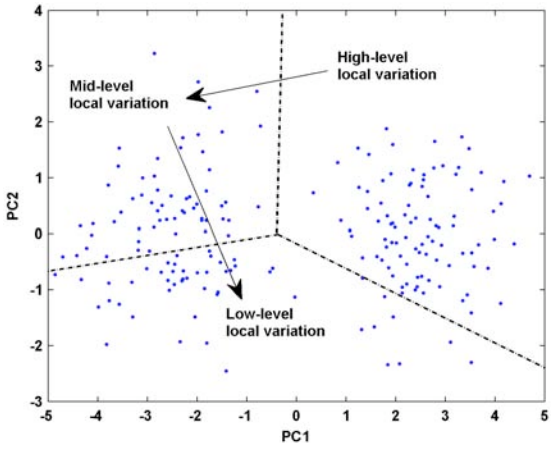

Figure 8.5: An example of the decision boundaries of a trained local shape assessment classifier with three levels: low, medium and high.

8.2.3 Summary of quality assessment framework

This section has discussed the integration and application of the newly proposed shape characterisation tools. This provides a dimensional quality assessment framework that can potentially allow manufacturers to more accurately define and assess assembly quality, which can lead to the ultimate goal of optimal process design for dimensional control. The next sections will now present the key contributions of this thesis along with areas for future research.

8.3 Contributions

Sheet metal assembly is a complex process involving component-to-component and component-to-tooling interactions. A key characteristic of sheet metal assemblies, the flexibility of components, means that variation does not stack-up according to the additive theorem of variance that applies to rigid bodies. Instead, components can be bent and distorted into conforming or non-conforming shapes by assembly interactions. This characteristic of flexibility also means that in comparison to rigid body assembly, additional aspects of the assembly process, such as clamp sequence and weld sequence, can influence the way in which variation propagates. In order to accurately investigate and model variation stack-up in sheet metal assemblies, the mechanistic behaviour of the assemblies must be taken into account. In this thesis, variation propagation in sheet metal assemblies is firstly investigated through a combination of finite element simulation and experimentation. It was shown how different clamping sequences can change the dimensional outcomes in terms of mean shape and variability, and therefore dimensional quality. It was also shown how clamping sequences could be adjusted to target particular quality assessment criteria. However, it has been discussed how existing univariate measures of assembly quality such as mean, standard deviation, process capability, and SPC methods, are perhaps not the best measure of assembly quality. This is primarily due to their inability to adequately capture a key characteristic of assemblies: correlated variation patterns. This thesis proposes that assembly quality cannot be simply assessed by the mean and variance of a set of assumedly statistically independent measurement points, and that correlated variation patterns in the form of bows, buckles, twists and ripples also form a large part of assembly quality perceptions. In order to truly optimise a process for dimensional quality, correlated variation patterns must therefore be taken into account. This leads to the research question posed at the beginnig of this thesis:

> *How can correlated variation patterns in sheet metal assemblies be characterised in ways that can lead to more advanced levels of dimensional quality assessment and control?*

In addressing this question, two key shape characterization methods were proposed: the multivariate statistical shape model, and the local shape descriptors. These shape charaterisation measures were designed to overcome key limitations of existing univariate quality measures including an inability to capture correlated variation patterns, monitor non-normally distributed data, interpret high dimensional data, and measure local variation patterns of different sizes or scales. Through addressing these limitations a more accurate description of assembly variation is achieved, allowing for improved quality assessment practices. Investigation of the sheet metal assembly process and development of the new shape characterization measures resulted in several main contributions: the clamp sequence simulation approach, clamp sequence design, the multivariate statistical shape model, the local shape descriptors, and a quality assessment framework.

8.3.1 Clamp sequence simulation

In this thesis a non-linear finite element contact model implemented in a commercial code was adopted to provide a detailed representation of the physical sheet metal assembly clamping process. An advantage of this approach over commonly used linearized approaches is that it can capture contact resulting from the initial placement of components in assembly fixtures, and for deformation induced contact. Linearized approaches require contact points to be pre-specified, which often means that only weld points and clamp locations are assigned to come into contact: other surface locations can therefore effectively pass through each other as they have not been specified as contact locations. Efforts have been made to estimate possible deformation induced contact points, however, non-linear contact models still provides a more detailed representation of the process. A key disadvantage of nonlinear contact models is that they are computationally intensive, and therefore are not easily combined with Monte Carlo simulation for variation propagation analysis.

8.3.2 Clamp sequence design

This thesis highlights the possible extent of the influence of clamping sequence on both mean shape and variability, and how clamp sequence can be altered for the dimensional control of different variation patterns. Furthermore, a set of generalised clamp sequence design laws is developed to provide a practical guideline for future process design, which could be readily integrated within increasingly popular knowledge based design systems.

8.3.3 Multivariate statistical shape model

The multivariate statistical shape model (KDE-PDM) was developed to provide a more advanced statistical representation of assembly process measurement data, enabling

more valid inferences to be drawn from the improved representation. Major benefits of this model over univariate models that are commonly used by industry are its ability to characterise correlated variation modes, deal with high dimensional data sets, and accurately estimate the overall shape distribution. While some previous approaches for the analysis of sheet metal assembly data have adopted multivariate techniques, to the author s knowledge none have developed the application of mixture models for multivariate density estimation.

8.3.4 Local shape descriptors

Local shape descriptors were developed to take advantage of optical measurement data and provide quantitative descriptions of local variation patterns of different sizes and scales, such as bumps and ripples, that can detract from product quality. These local descriptors provide a systematic approach for the discrimination of differing types and combinations of variation patterns in sheet metal surfaces.

8.3.5 Dimensional assessment framework

This thesis has demonstrated a number of key approaches, including simulation and experimental trails of assembly processes, quality improvement through smarter process design and the formulation of generalised process design laws, multivariate process modelling, and localised shape description. This thesis has also discussed how these key approaches can be combined and applied to provide an integrated tool for dimensional assessment and control of sheet metal assemblies.

8.4 Suggestions for further work

While the previous section has illustrated key contributions of this thesis, there are also important avenues for future research. Suggestions for future work will be addressed under the sections of mechanistic simulation, Virtual assembly and metal forming, multivariate shape models, local shape model, and the application of the quality assessment framework.

8.4.1 Mechanistic simulation

The finite element model adopted in this thesis used a multi-step implicit contact approach. Sheet metal assembly is a complex process involving many contact interactions, and capturing contact behaviour with an implicit approach can prove difficult with convergence issues often arising. Quasi-static explicit simulation, which employs a finite difference approach, could be more suitable for modelling sheet metal assemblies to

greater levels of accuracy due to its ability to deal with very complex contact interactions. A major limitation of this approach however is computational time, which could prove overwhelming due to the many cycles present in an assembly process.

8.4.2 Virtual assembly and metal forming

This thesis only explored the virtual assembly of a single station assembly process with simple theoretical variation modes such as bow and twist used to simulate possible physically occurring variation modes. A logical extension to the analysis of sheet metal assembly variation would be to use sheet metal forming simulation to generate more realistic variation patterns. This would provide more valid component inputs for single and multi-station modelling, and allow for more accurate variation propagation analysis and better designs for the dimensional control of these variation patterns.

8.4.3 Stochastic simulation

Stochastic simulation is often combined with assembly simulation to predict tolerance stack-up. While Monte Carlo approaches can be readily combined with linearized mechanistic simulation methods, they do not combine well with more time intensive contact simulation methods due to the massive computational requirement. In this thesis, a method for reducing the need for costly finite element simulation via parametric modelling was demonstrated. Here, a mapping between component and assembly shapes was developed from simulation data with differing levels of variation modes (such as bow or twist). Once this relationship was established, stochastic modelling could be readily adopted using the model. While a fairly simple method was used to establish the component to assembly response, this concept could be extended to utilise methods such as backpropagation neural networks, multivariate splines, and gaussian processes to develop multiple-input multiple-response models. Xiong et al. present one such method (Xiong et al., 2007) that appears particularly well suited.

8.4.4 Multivariate shape model

The kernel density estimate/point distribution model (KDE-PDM) presented in this thesis is one approach for the statistical modelling of shapes with a mixture of kernels (in this case a multivariate gaussian). A natural extension to this method is to use a smaller mixture of gaussians to estimate a multivariate density using an Expectation-Maximisation approach. Further alternatives are discussed in chapter 6. Another area of investigation of the multivariate model is the dimensional reduction method. In this thesis, principal components analysis was used to extract a smaller set of uncorrelated, linear components to describe most of the information in a data set. Other methods, such as Kernel PCA (Muller et al., 2001), are able to extract non-linear components

that might have the potential to accurately describe a data set with a smaller set of components than traditional PCA.

8.4.5 Localized shape model

The key area of extension required for the localised shape model is to develop a generalised approach that can assess surfaces that are not nominally planar. As mentioned in chapter 7, techniques developed in the field of computer vision such as non-rigid point set registration could allow for such a generalisation of the local shape characterisation approach, as they would be able to capture and register entire surfaces, rather than a predefined set of coordinates which only cover a subset of the total surface area.

8.4.6 Application of quality assessment framework

This thesis has developed a number of tools for the analysis of assembly process variation and quality assessment, and outlined possible avenues of application. The use of these approaches within an industry context to provide real world dimensional control improvements is the ultimate goal of this research.

Appendix A

Experimental assembly setup

A.1 Channel section fabrication

Channel sections used for the experimental setup in this thesis were made from sheet metal 0.85 mm thick. A laser cutter was used to cut the blanks to size and cut out the locating hole and slot for each channel. A CNC bender was then used to fold the channels into shape. Figure A.1 shows some example channel samples after the cutting and folding process, but before a bow was induced. The following sections will proceed to illustrate the bending tool, formed channels with bow, the assembly rig, and built assemblies.

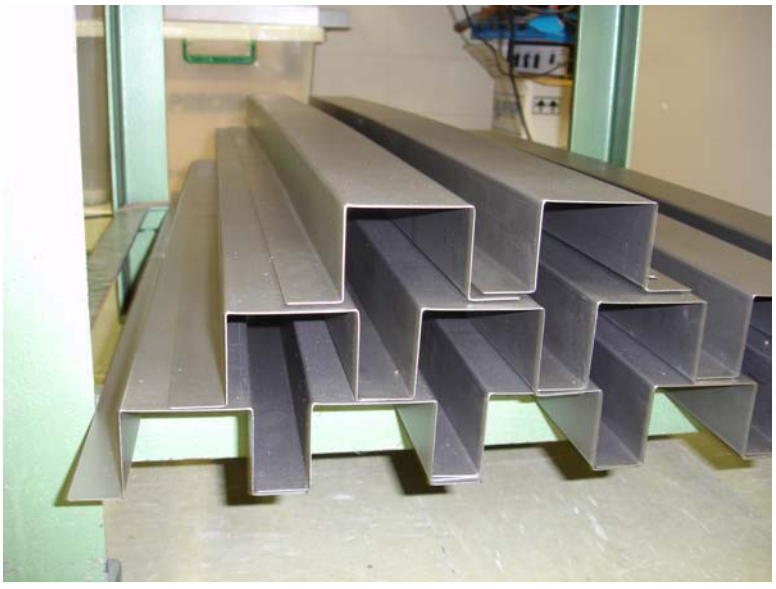

Figure A.1: Laser cut and folded channels.

A.2 Bending tool

Figure A.2 shows an image of the tooling setup used to create a bow in the top hat section (ie, for inducing an artificial variation mode). The tool was fashioned from eight 31.75 mm thick aluminium plates, and a hydraulic press was used to apply the required loads for forming the hat section.

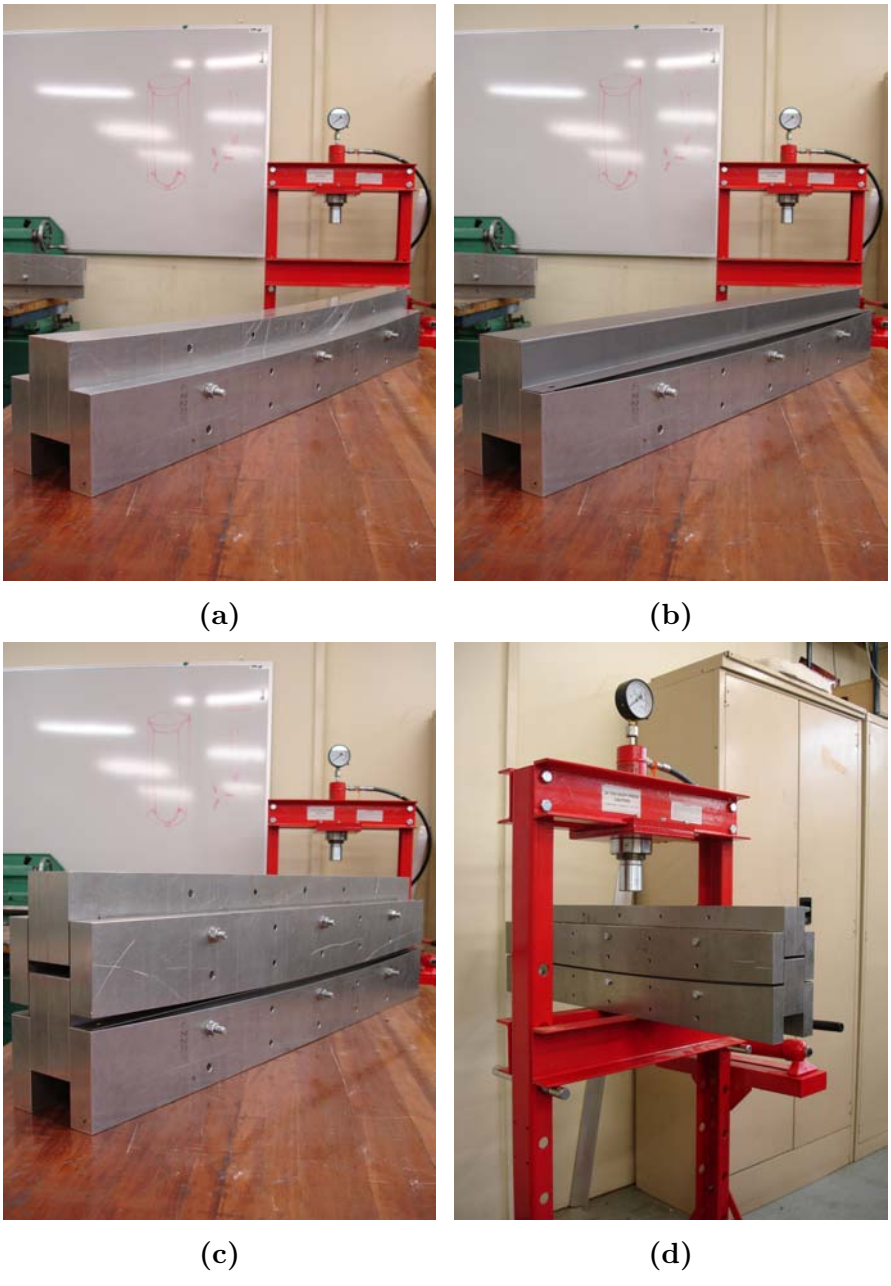

(a) **(b)**

(c) **(d)**

Figure A.2: Images show the lower bending tool (a), the folded and laser cut channel (b), the upper bending tool (c), and the hydraulic press (d).

A.3 Channel with bow

In Figure A.3, channels with and without bow are laid side by side. Figure A.4 shows another image of the bending tool used to induce a bow in the channels. An example scanned channel investigated in chapters 5 and 7 is illustrated in Figure A.5.

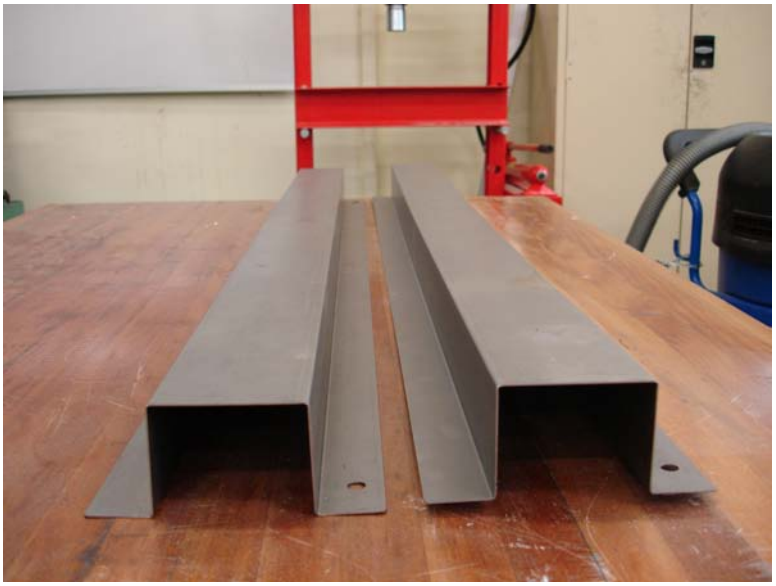

Figure A.3: A flat channel (left) and a channel with a slight bow (right).

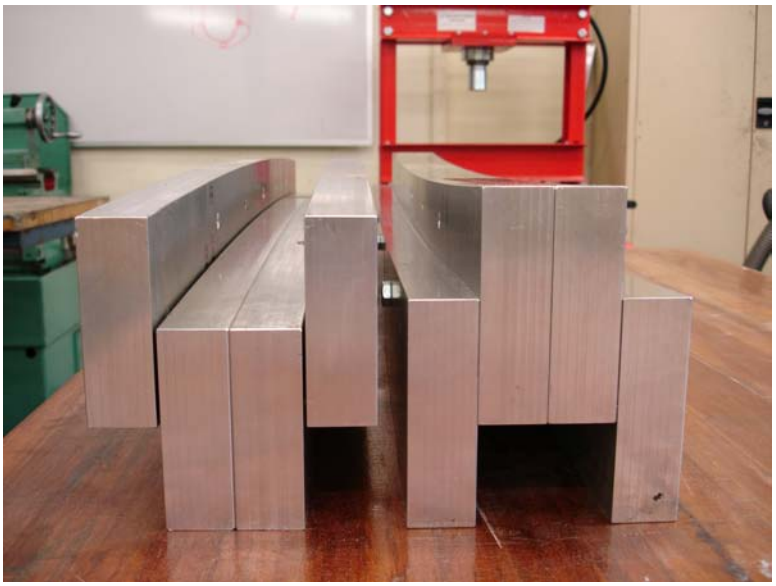

Figure A.4: The bending tool.

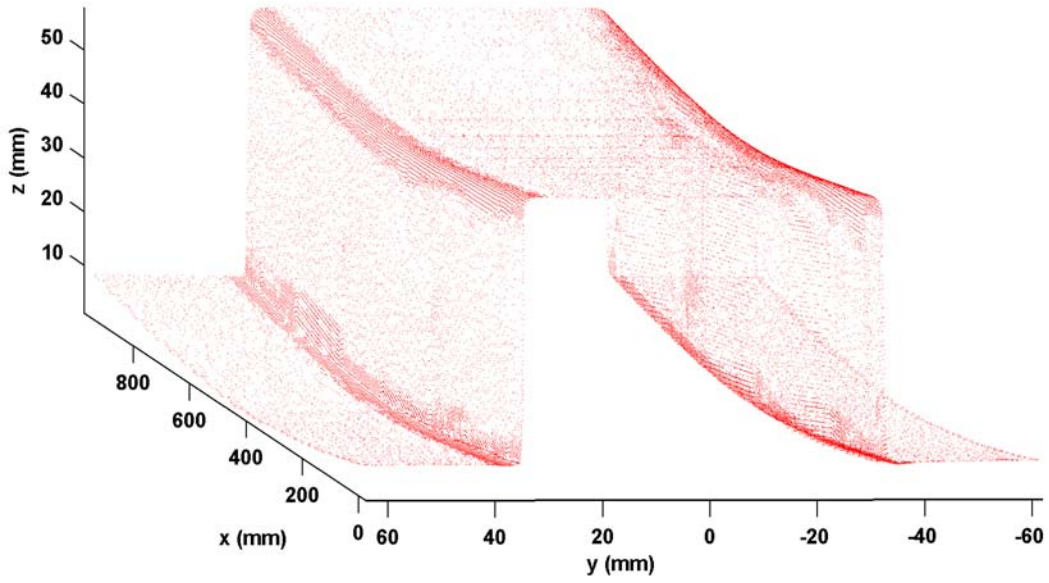

Figure A.5: Channel with negative bow (point cloud from 3D scan).

A.4 Assembly rig

In Figure A.6, a CAD model of the experimental assembly rig is shown. Figure A.7 shows an image of the actual assembly rig. Channel sections with bow were attached to a flat bottom plate through a place, clamp, fasten, release cycle. Here, a set of rest surfaces and locating pins were used to place the components for assembly. Toggle clamps were then applied to hold the components in position for assembly. A series of resistance spot welds were then made down each flange to join the components together. Finally, the welded assembly was released by the toggle clamps. Built assemblies were then clamped and measured using a FARO Arm Platinum/3D Scanners Model Maker X70 combination. Figure A.8 shows one assembly built with clamp sequence 1, and one assembly built with clamp sequence 2, as described in Section 5.2.1. Differences between the final shape of the two assemblies can be seen through close inspection.

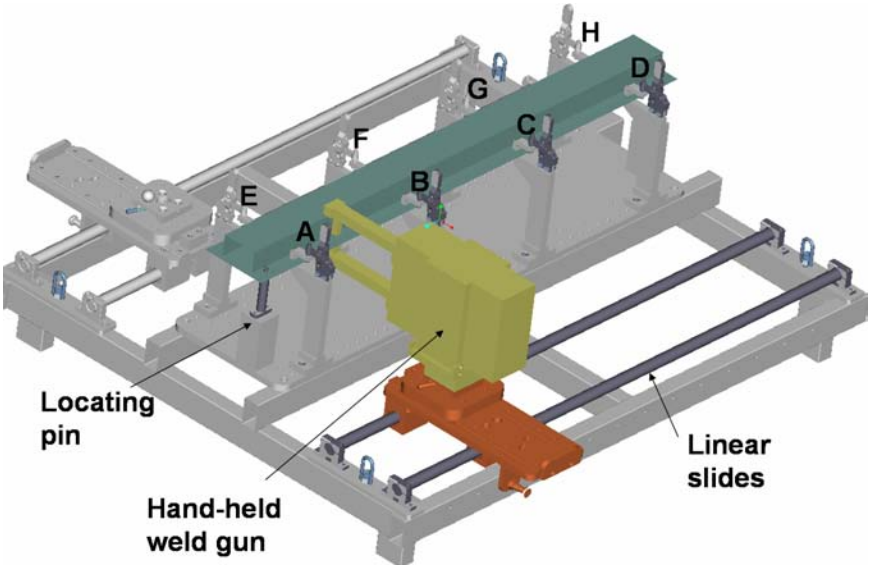

Figure A.6: CAD model of the experimental assembly rig.

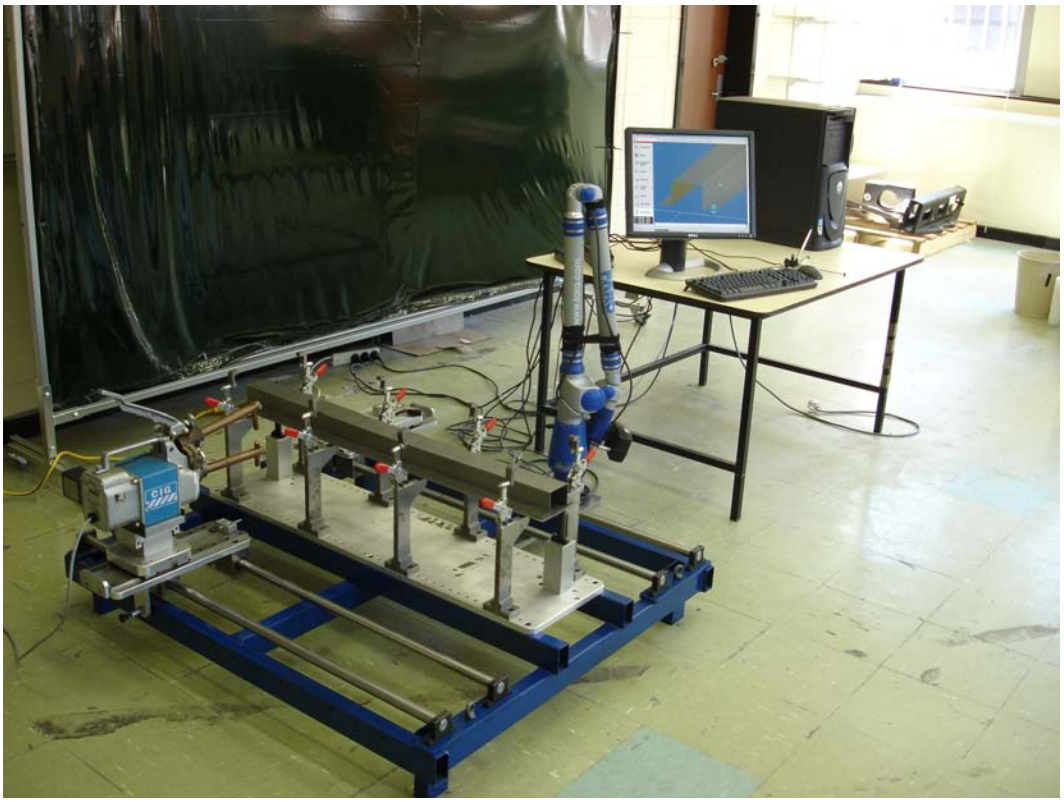

Figure A.7: Image of the actual experimental setup.

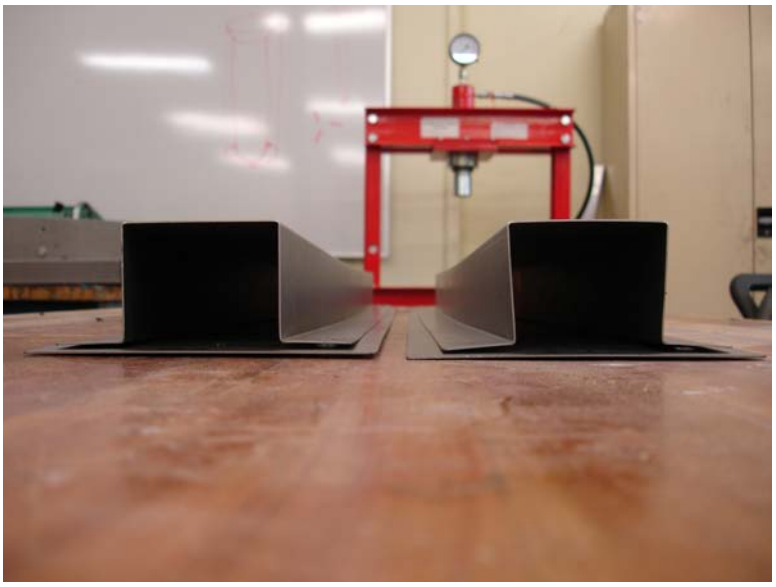

Figure A.8: Image of two assemblies built with different clamping sequences. Note how the left wall on the right-hand-side assembly is pushed further inwards than the corresponding wall on the left-hand-side assembly.

Appendix B

Virtual assembly

B.1 Nonlinear finite element model

As already mentioned in the previous chapters, a number of mechanistic simulation approaches have been used to model the sheet metal assembly process. These have included simple beam models (Shiu et al., 1997), linear finite element approaches (Chang and Gossard, 1997), linearized contact models (Liu and Hu, 1997a), non-linear contact models (Cao and Rastogi, 2001), and even thermo-mechanical models (Fan et al., 2007). All of these approaches are based around the place, clamp, fasten, release cycle presented in chapter 1. There are two main finite element methods: static implicit and dynamic explicit simulations. In this thesis, only static implicit simulation is considered to model the sheet metal assembly process. This is because the process can be modelled as a series of static implicit steps, with the starting conditions of each step defined by the outcomes of the previous step. Linearized finite element simulation approaches require all contact locations between components and tooling to be pre-defined. Here, clamp and weld locations are the logical choices for contact points. This approach does not consider the possible effects of deformation induced contact, where contact between components occurs at regions other than weld and clamp locations. The static implicit approach implemented in this thesis seeks to capture these effects, however, the result is that the analysis is no longer linear due to contact interactions. The drawback here is that while a more accurate representation of the physical process can be achieved by this approach, computation effort increases significantly. Figure B.1 presents an example nonlinear load-displacement curve that could result due to consideration of contact effects in assembly. Solving nonlinear problems involves a combination of incremental and iterative procedure. An analysis step is broken down into increments so that the nonlinear solution path can be estimated. To solve each increment, the displacement of mesh nodes is updated according to a Newton iterative search of the statics equation

$$\Delta\vec{u}^{(i+1)} = \Delta\vec{u}^{(i)} + K_t^{-1}.(\vec{F}^{(i)} - I^{(i)}) \tag{B.1}$$

where K_t is the current tangent stiffness matrix, $\vec{F}$ is the applied load vector, u is the nodal displacement, and $\vec{I}$ is the internal force vector.

The sheet metal assembly process is a complex process involving component-to-component and component-to-tooling interactions, and often very small time increments are required for a solution to converge, and in some cases, convergence is not possible. For a more detailed about the static implicit approach for nonlinear contact problems please refer to Lee 1999.

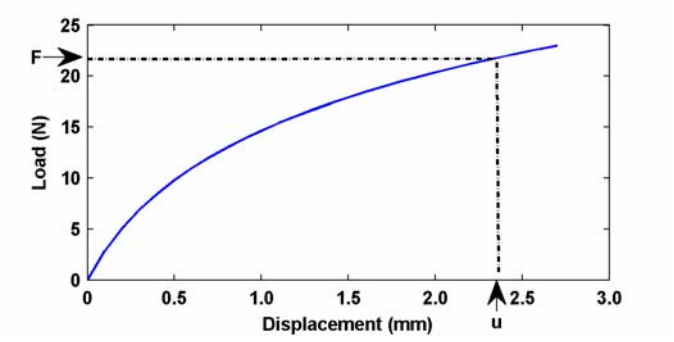

Figure B.1: Example nonlinear load-displacement curve.

B.2 Finite element model mapping

The nonlinear contact assembly model adopted in this thesis is quite computationally intensive. The analysis of variation propagation in sheet metal assemblies often involves the use of Monte Carlo simulations, where hundreds or thousands of random component shapes are used as inputs for assembly functions (the FE simulation approach) to observe the final assembly variation distribution. Directly using an FE model for each of the hundreds or thousands of simulations is not practical for nonlinear contact assembly models. Therefore, a simple approach was used to reduce the required number of FE simulations to perform Monte Carlo studies of variation propagation in this thesis. This approach will be described in the following. Here, only the variation of a single input component in a two piece assembly was considered (the top hat). Furthermore, the variation modes investigated in the component could be described by a single parameter: for example, a bow could be characterised purely by its middle deflection, and twist could be described completely by twist angle. A parametric study, which involved the simulation of a selection of variation modes over a range of magnitudes, was then conducted. These results provided an indicator of the relationship between each

variation mode, and the final assembly shape (or position of each MP): cubic spline interpolation was then used to provide a model of this relationship (see Appendix F for a description of the spline method). For example, each final assembly measurement point was plotted against the range of variation mode magnitudes, and a cubic spline interpolant used to model this relationship as indicated in Figure B.2. These cubic spline models could then be used in place of FE simulation for detailed Monte Carlo simulation. In the illustrated example, only 9 FE simulations across a range of different levels of bow were required to develop a spline model, after which Monte Carlo simulations with hundreds of samples could be run. Using a direct method, hundreds of computationally intensive FE simulations would be required to conduct an equivalent study. While a fairly simple approach was adopted for this thesis, this concept could be extended to include advanced multiple-input multiple-response regression methods for more complex assembly cases.

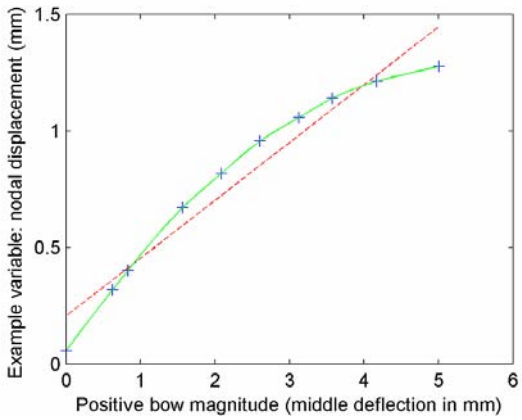

Figure B.2: Plot of an example non-linear relationship between the input variation mode (Positive bow middle deflection) and final assembly nodal displacement. The spline model passes through all data points, whereas the linear model (dotted line) is a poor approximation.

Appendix C

Clamp sequence study

Table C.1: Average displacement from nominal of the final assembly for each input variation mode example and clamp sequence combination.

Clamp sequence	Negative bow -2.6mm	Positive bow 2.6mm	Negative twist -3°	Positive twist 3°	Row total (mm)
611	0.36	0.35	0.13	0.08	0.91
612	0.32	0.36	0.09	0.11	0.88
613	0.33	0.25	0.14	0.15	0.87
614	0.36	0.26	0.16	0.15	0.93
621	0.27	0.43	0.10	0.09	0.89
622	0.30	0.27	0.24	0.22	1.03
623	0.27	0.43	0.10	0.10	0.89
624	0.30	0.27	0.22	0.24	1.03
631	0.27	0.24	0.18	0.23	0.93
632	0.28	0.25	0.23	0.18	0.93
633	0.31	0.30	0.27	0.21	1.09
634	0.31	0.29	0.21	0.28	1.09
641	0.34	0.22	0.11	0.18	0.84
642	0.33	0.23	0.23	0.17	0.95
643	0.35	0.22	0.17	0.11	0.84
644	0.34	0.24	0.16	0.22	0.95
Min	0.27	0.22	0.09	0.08	0.84
Max	0.36	0.43	0.27	0.28	1.09
Range	0.09	0.21	0.19	0.21	0.25
Max/Min-1(%)	34.41%	96.28%	221.14%	275.10%	29.99%

Table C.1 was used to select a smaller subset of clamping sequences for detailed investigation in section 4.3.1. Note the clamp sequence number consists of three digits: the first digit is 6 which indicates the number of clamps, the second digit indicates a

logical clamp sequence grouping (ie, 1 = Down one flange and back, 2 = Middle to outer, 3 = One end to the other, and 4 = Out to middle), and the final digit indicates a variant of a logical grouping (ie, start at the locating pin vs the locating slot, clockwise vs anti-clockwise).

Appendix D

Local shape descriptors

D.1 Continuous wavelet transform: Signal extension

For the continuous wavelet-based local shape characterisation approach, the average power of a series of lengthwise cross sections are used to see what scale features are present on a surface. Some signal preparation was required to ensure that the average power figures were actually capturing features of interest. The first step in this process involved artificially extending each processed signal, by a local linear least square fit at each end (see section F.1). This process is illustrated in Figure D.1.

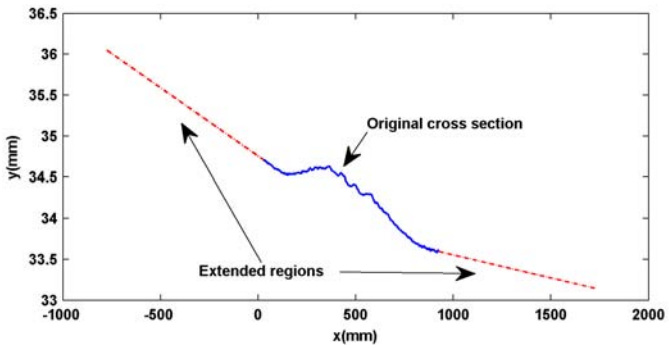

Figure D.1: An example of the signal extending procedure.

The reasoning for this signal extension can be seen in Figure D.2, the corresponding wavelet transform of the extended signal. It can be seen that at the end of each signal, there are very high magnitude regions. When taking the average power of a series of scales of the entire extended signal, these high power regions would cloud the presence of any local features of interest. Therefore, by extending the original signal, performing the wavelet transform on the extended signal, and then only considering the component of the wavelet transform corresponding to the original signal, the high magnitude regions at the end of each signal can be avoided. The higher magnitude

regions on this sub-section of the transform will then be able capture the local features of interest, as illustrated in Figure D.3.

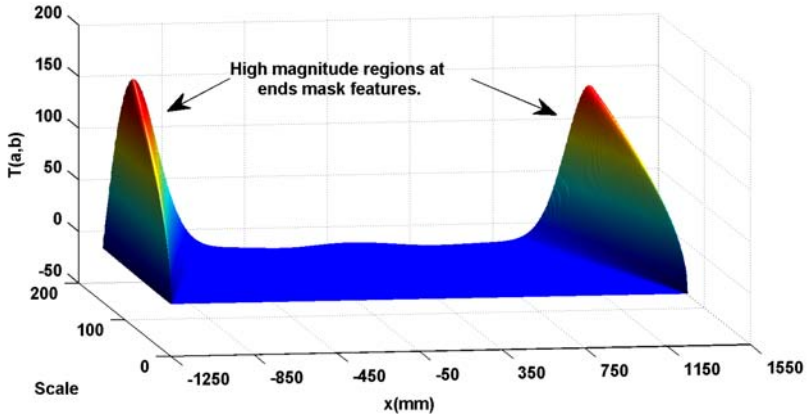

Figure D.2: The wavelet transform plot for the extended signal. Note how at either end of the extended signal there are very high magnitude regions. These high magnitude regions would dwarf any local features captured on the original signal.

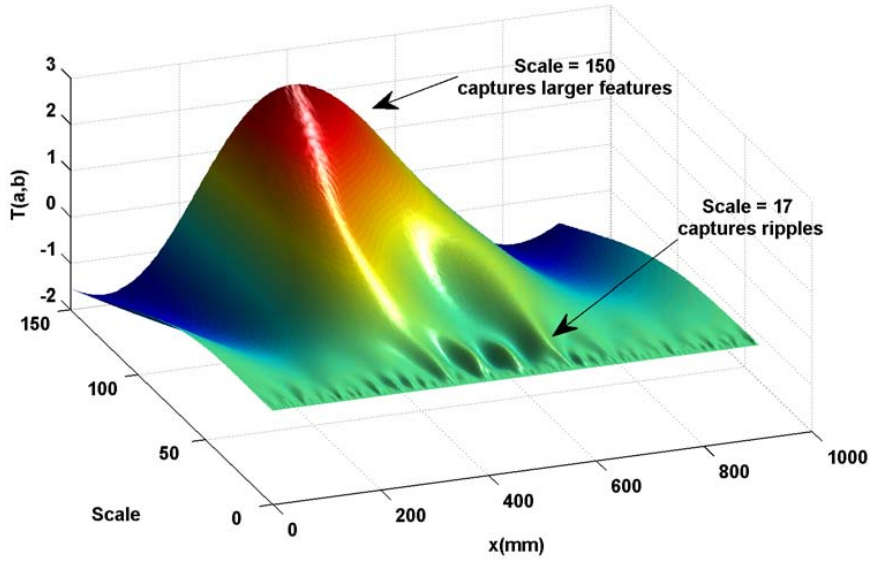

Figure D.3: Corresponding continuous wavelet transform of a lengthwise cross section of the wall at $z = 44.5$ mm, with scale ranging from 0.1 to 150.

Appendix E

Statistical tools

E.1 Statistical inference

The comparison of two populations forms an important part of understanding and selecting assembly processes. For example, when looking to identify the effect of a process parameter (such as clamping sequence) on the dimensional outcomes of an assembly, it is of interest to see whether adjustment of this parameter results in shifts in the mean or variance of the process. The mean and variance of corresponding MP s from two populations can be investigated using a two sample T-test, and an F-test for ratio of variances. For more detailed desriptions of the methods, see Keller and Warrack [1997].

E.1.1 Comparison of means

In order to determine whether there is a difference between the means of two populations, μ_1 and μ_2, the null hypothesis H_0 must be tested against the alternative hypothesis H_A

$$H_0 : (\mu_1 - \mu_2) = 0, \qquad H_A : (\mu_1 - \mu_2) \neq 0 \tag{E.1}$$

where the corresponding test statistic is

$$t = \frac{(\bar{x}_1 - \bar{x}_2) - (\mu_1 - \mu_2)}{\sqrt{s_1^2/n_1 + s_2^2/n_2}} \tag{E.2}$$

with the degrees of freedom equal to

$$d.f. = \frac{\left(s_1^2/n_1 + s_2^2/n_2\right)}{\left(\frac{\left(s_1^2/n_1\right)}{n_1 - 1} + \frac{\left(s_2^2/n_2\right)}{n_2 - 1}\right)} \tag{E.3}$$

where s_1 and s_2 are the sample standard deviations, n_1 and n_2 are the sample sizes, and $\bar{x}_1$ and $\bar{x}_2$ are the sample means. The rejection region at a significant level α is

$$|t| \leq t_{\alpha/2,d.f.} \tag{E.4}$$

If the value of the test statistic falls in the rejection region, the alternative hypothesis (that the means are different) is accepted. If the value of the test statistic falls outside the rejection region, then the null hypothesis (the means are the same) is accepted. It should be noted that the two populations and the test statistic are assumed to be normally distributed.

E.1.2 Comparison of variances

A primary goal of quality engineers is the control of variability: it is a key interest to identify processes that result in lower levels of variance. The ratio of two population variances can be investigated to reveal such differences. In this case, we are looking to test the null hypothesis H_0 that the variances are equal, against the alternative hypothesis H_A that the variance of population 1 is greater than that of population 2

$$H_0 : \sigma_1^2 = \sigma_2^2, \qquad H_A : \sigma_1^2 > \sigma_2^2 \tag{E.5}$$

The corresponding test statistic is F-distributed

$$F = s_1^2/s_2^2 \tag{E.6}$$

with $v_1 = n_1 - 1$ and $v_2 = n_2 - 1$ degrees of freedom. Here, s_1 and s_2 are the sample standard deviations, and n_1 and n_2 the sample sizes. The rejection region at a significance level α is

$$F > F_{1-\alpha,v_1,v_2} \tag{E.7}$$

Again, if the value of the test statistic falls in the rejection region, the alternative hypothesis (that the variance of population 1 is higher than that of population 2) is accepted. If the value of the test statistic falls outside the rejection region, then the null hypothesis (the variances are the same) is accepted.

Appendix F

Data fitting

Data fitting is the process of estimating an underlying function of a set of data points. In this thesis there are three main data fitting methods used. Linear least squares regression is applied in chapter 7 as a preprocessing step where a signal is extrapolated. Cubic piece-wise splines are adopted in chapters 4 and 5 to find a mapping between component and assembly shapes from a parametric FE simulation data set. Thin-plate splines are applied in chapter 5 to estimate surface measurement points from an FE mesh: the approach is particularly suited as the data being interpolated is thin-sheet metal, which the TPS emulates. These methods are described in the following.

F.1 Simple linear regression

In simple linear regression, it is assumed that an underlying data set can be modelled by a function of the following form

$$y = \beta_0 + \beta_1 x \tag{F.1}$$

where y is a linear function of the unknown parameters β_0 and β_1. The parameters for any linear model can be found through the method of least squares, where the solution for Equation F.1 is as follows

$$\beta = (X^T X)^{-1} X^T Y \tag{F.2}$$

where

$$\beta = \begin{bmatrix} \beta_0 \\ \beta_1 \end{bmatrix}, \quad X = \begin{bmatrix} 1 & x_1 \\ 1 & x_2 \\ \vdots & \vdots \\ 1 & x_n \end{bmatrix}, \quad Y = \begin{bmatrix} y_1 \\ y_2 \\ \vdots \\ y_n \end{bmatrix} \tag{F.3}$$

Figure F.1 shows a simple linear regression fit of a set of data points.

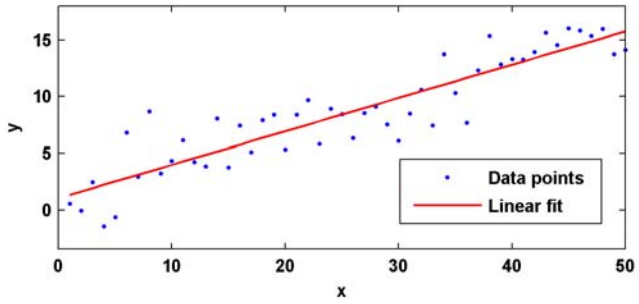

Figure F.1: Simple linear regression for a set of data points: $y = \beta_0 + \beta_1 x$, where $\beta_0 = 1.03$ and $\beta_1 = 0.29$.

F.2 Cubic piece-wise splines

Cubic spline interpolation is a popular approach for interpolating a set of data points with a smooth curve. The approach connects data values with a set of piece-wise cubic curves. This can be expressed in the following:

$$S(x) = \begin{cases} S_1(x) & \text{if} \quad x_1 \leq x \leq x_2 \\ S_2(x) & \text{if} \quad x_2 \leq x \leq x_3 \\ & \downarrow \\ S_{n-1}(x) & \text{if} \quad x_{n-1} \leq x \leq x_n \end{cases} \tag{F.4}$$

where S_i is a cubic polynomial defined by:

$$S_i(x) = a_i(x - x_i)^3 + b_i(x - x_i)^2 + c_i(x - x_i) + d_i \tag{F.5}$$

for i = 1,2,...,n-1.

There are n-1 intervals, each with four coefficients, so a total of 4(n-1) parameters are required to define the spline, and therefore 4(n-1) conditions to solve for the parameters. The spline interpolant must pass through each data point, giving two conditions for each interval:

$$S_i(x) = y_i, \quad S_{i+1}(x) = y_{i+1} \tag{F.6}$$

The first and second derivatives at each point are also set to be continuous to ensure a continuous and smooth piecewise interpolation:

$$S'_{i-1}(x_i) = S'_i(x_i), \quad S''_{i-1}(x_i) = S''_i(x_i) \tag{F.7}$$

This leaves us needing two more end conditions to solve the linear system. There are many different possible end conditions. For cubic run-out splines, the second derivatives at each endpoint depend on the two corresponding nearest points.

$$S''(x_1) = 2S''(x_2) - S''(x_3), \quad S''(x_n) = 2S''(x_{n-1}) - S''(x_{n-2}) \tag{F.8}$$

An example cubic piecewise spline fit with a cubic run-out is presented in Figure F.2. There are 6 data points, and 5 corresponding piecewise cubic polynomial segments. Note how the cubic spline interplant fits the data with a smooth continuous curve.

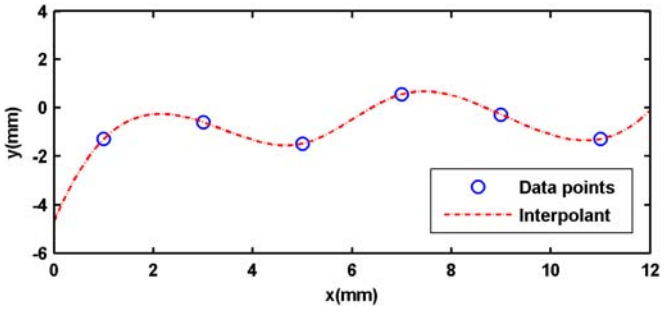

Figure F.2: Example cubic spline fit of randomly generated data points.

F.3 Thin-plate splines

A radial basis function is a real-valued function that depends only on the distance from its centre, (x_i, y_i). The thin-plate spline radial basis function is given in equation (F.13).

$$\phi(x, y) = \begin{cases} r^2 \log r^2 & \text{if} \quad r > 0 \\ 0 & \text{if} \quad r = 0 \end{cases} \tag{F.9}$$

where,

$$r^2 = (x - x_i)^2 + (y - y_i)^2 \tag{F.10}$$

A plot of the TPS radial basis function with $x_i = 0$ and $y_i = 0$ is shown in Figure F.3. It can be seen that the function is radially symmetric about its centre.

Radial basis functions are often used to build approximating functions. The two dimensional thin plate spline interpolation function has the following form

$$f(x, y) = \beta_0 + \beta_1 x + \beta_2 y + \sum_{i=1}^{N} \alpha_i \phi(x, y) \tag{F.11}$$

The TPS interpolating function mimics the deflection of an infinite thin plate, by minimizing the energy functional

$$E(f) = \int\int \left(\frac{\partial^2 f}{\partial x^2}\right) + 2\left(\frac{\partial^2 f}{\partial xy}\right) + \left(\frac{\partial^2 f}{\partial y^2}\right) dxdy \tag{F.12}$$

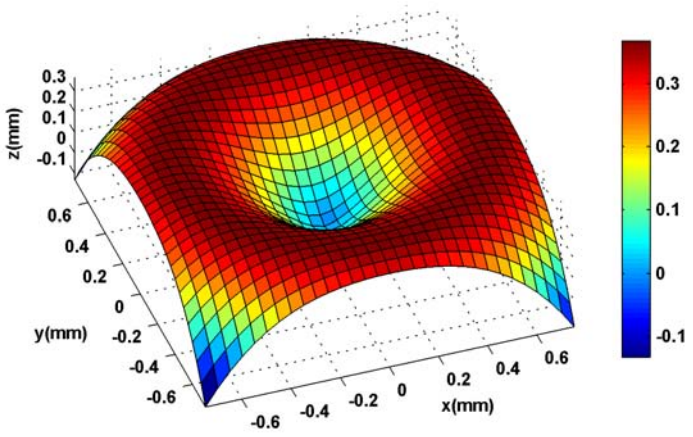

Figure F.3: Thin plate spline radial basis function with a centre at (0,0)

where the coefficents of the radial basis interpolant can be found by solving the following system of linear equations

$$\begin{bmatrix} K & P^T \\ P & 0 \end{bmatrix} \begin{bmatrix} \alpha \\ \beta \end{bmatrix} = \begin{bmatrix} f \\ 0 \end{bmatrix} \tag{F.13}$$

where

$$K_{ij} = \phi_i(x_j, y_j) \tag{F.14}$$

$$P = \begin{bmatrix} 1 & 1 & ... & 1 \\ x_1 & x_2 & ... & x_N \\ y_1 & y_2 & ... & y_N \end{bmatrix} \tag{F.15}$$

The thin-plate spline (TPS) is the two-dimensional equivalent of the natural cubic spline, and can be seen to find the smoothest fit of the underlying point set. Figure F.4 illustrates a TPS interpolation of a randomly generated data set.

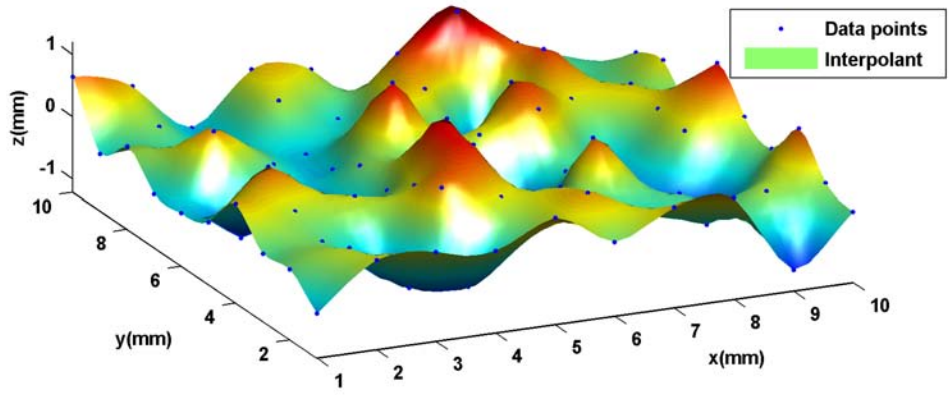

Figure F.4: Thin plate spline interpolation of a randomly generated set of data points.

Appendix G

Mean shifts

Figure G.1 shows a simplified representation of the mean shifts between the two weld sequences explored in chapter 3, within the Body Co-ordinate System. Figure G.2 shows the corresponding directional movement between weld sequence means in the 2D PCA plot. Note how a single vector in the PCA plot can represent a complicated correlated variation pattern in the Body Co-ordinate System.

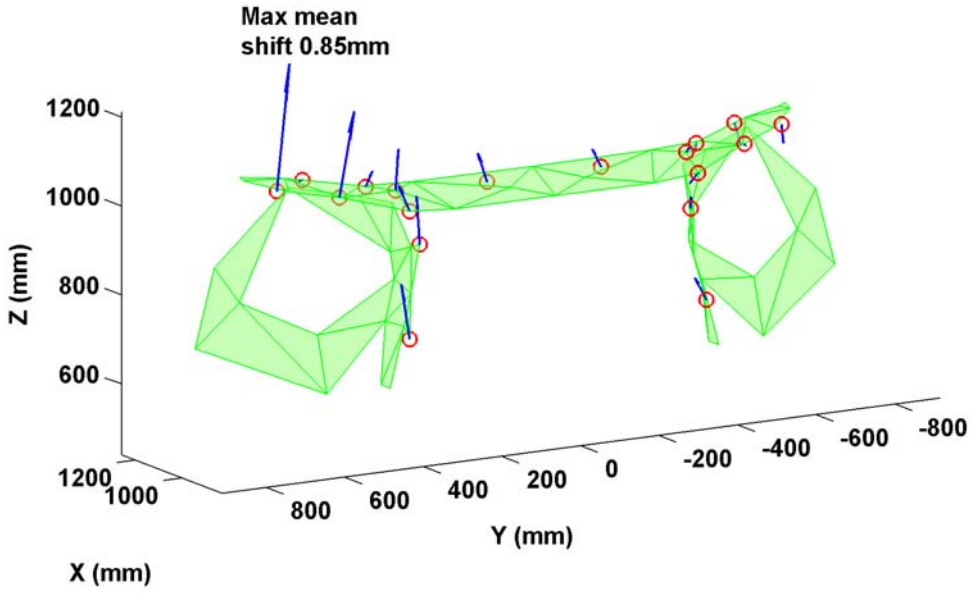

Figure G.1: Simplified representation of the assembly investigated. Vector plots show the mean shift between weld sequences.

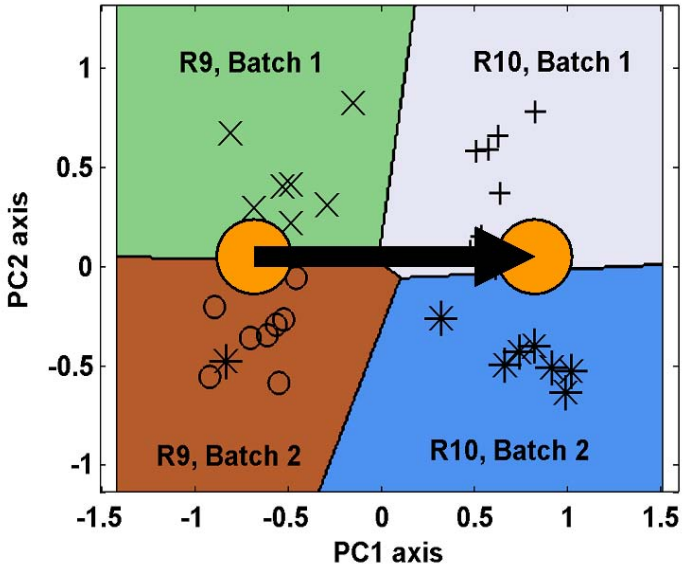

Figure G.2: Corresponding mean shifts between weld sequences in a 2D PCA space.

Appendix H

Other methods

H.1 Linear discriminant analysis

Fisher s linear discriminant analysis (LDA), like PCA, is a dimensional reduction technique that is useful for describing important information in an underlying data set with a smaller number of variables. It is also an orthogonal change of basis method, however, its goals differ from PCA in that it aims to find the best representation for providing discrimination between different specified classes within a data set. For LDA, the aim is to find a transformation matrix that maximises the ratio of between-class scatter to the within-class scatter. Suppose there is a set of n d-dimensional samples x_1,...,x_n, and c classes with n_1 in the subset D_1, n_2 in the subset D_2, through to n_c in the subset D_c. We seek $(c-1)$ projections $y = [y_1, ..., y_{c-1}]$ through $(c-1)$ projection vectors w_i, which are arranged in the projection matrix $W = [w_1|\ w_2|\ ...|\ w_{c-1}|]$

$$y = W^T x \tag{H.1}$$

In order to find a projection that seeks to maximise between-class scatter and minimise within-class scatter, we need to maximise the following scalar objective function

$$J(W) = \frac{|W^T S_B W|}{|W^T S_W W|} \tag{H.2}$$

Here, the within class scatter matrix is defined as

$$S_W = \sum_{i=1}^{c} S_i \tag{H.3}$$

where

$$S_i = \sum_{x \in D_i} (x - \mu_i)(x - \mu_i)^T \tag{H.4}$$

and

$$\mu_i = \frac{1}{n_i} \sum_{x \in D_i} x \tag{H.5}$$

The between-class scatter matrix is defined as

$$S_B = \sum_{i=1}^{c} n_i (\mu_i - \mu)(\mu_i - \mu)^T$$

where

$$\mu = \frac{1}{n} \sum_{x} x = \frac{1}{n} \sum_{i=1}^{c} n_i \mu_i \tag{H.6}$$

It can be shown that the optimal projection matrix W is the one whose columns are the eigenvectors corresponding to the largest eigenvalues of the following generalized eigenvalue problem

$$(S_B - \lambda_i S_W)\, w_i = 0 \tag{H.7}$$

Figure H.1 shows a classification example from chapter 4 highlighting the the ability of LDA to provide discrimination between different classes.

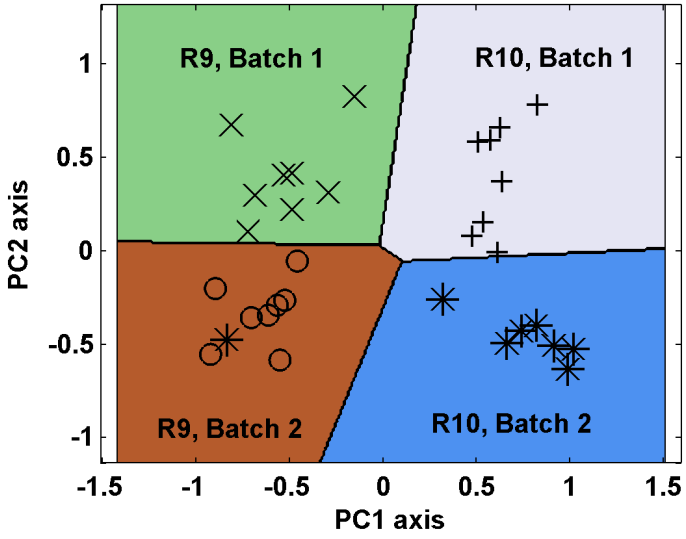

Figure H.1: Black lines show multi-class LDA decision boundaries separating the four classes: (R9, Batch 1), (R9, Batch 2), (R10, Batch 1), and (R10, Batch 2). It should be noted that there is one outlier in the data set.

H.2 Discrete cosine transform

The Discrete Cosine Transform (DCT), like the related Discrete Fourier Transform (DFT), represents a signal by a sum of underlying sinusoids with different frequencies and amplitudes. It differs from the DFT in that it only deals with real numbers. A key application of the DCT has been for image compression, due to its ability to represent the majority of a signal s power in a few low frequency components. In chapter 7, a 2D version of the DCT is used to denoise 3D scan data. Firstly, the 2D DCT is calculated on an M by N surface grid as:

$$B_{pq} = \alpha_p \alpha_q \sum_{m=0}^{M-1} \sum_{n=0}^{N-1} A_{mn} \cos \frac{\pi(2m+1)p}{2M} \cos \frac{\pi(2n+1)q}{2N}, \qquad \begin{matrix} 0 \leq p \leq M-1 \\ 0 \leq q \leq N-1 \end{matrix} \tag{H.8}$$

where,

$$\alpha_p = \begin{cases} 1/\sqrt{m}, & p = 0 \\ \sqrt{2/M}, & 1 \leq p \leq M-1 \end{cases} \qquad \alpha_q = \begin{cases} 1/\sqrt{n}, & q = 0 \\ \sqrt{2/N}, & 1 \leq q \leq N-1 \end{cases}$$

Each entry in the DCT matrix represents the contribution of a particular basis function to the original surface shape. The basis functions with low power levels, and therefore a small contribution to the overall shape of the surface, are set to zero. This effectively removes low level noise. An inverse transform is then applied to reveal the denoised surface.

Bibliography

Amaratunga, K. (1999). Analysis and classification of surface variation error using a geometry-adapted discrete wavelet transform. *Proceedings of SPIE - The International Society for Optical Engineering*, 3723:310 318.

Apley, D. W. and Shi, J. (1998). Diagnosis of multiple fixture faults in panel assembly. *Journal of Manufacturing Science and Engineering*, 120:793 801.

Apley, D. W. and Shi, J. (2001). Factor-analysis method for diagnosing variability in multivariate manufacturing processes. *Technometrics*, 43(1):84 95.

Apley, D. W. and Zhang, F. (2007). Identifying and visualizing nonlinear variation patterns in multivariate manufacturing data. *IIE Transactions (Institute of Industrial Engineers)*, 39(6):691 701.

Bellman, R. (1961). *Adaptive Control Processes: A Guided Tour*. Princeton University Press.

Bernard, A., Ammar-Khodja, S., Perry, N., and Laroche, F. (2007). Virtual engineering based on knowledge integration. *Virtual and Physical Prototyping*, 2(3):137 154.

Bishop, C. M. (2007). *Pattern Recognition and Machine Learning*. Springer, 1st edition.

Bylund, N. (2005). Adrian: A software for computing the stiffness of automotive joints and its application in the product development process. *Journal of Computing and Information Science in Engineering*, 5(4):388 393.

Camelio, J. and Hu, S, J. (2003). Modeling variation propagation of multi-station assembly systems with compliant parts. *Journal of Mechanical Design*, 125:673 681.

Camelio, J., Hu, S. J., and Zhong, W. (2004a). Diagnosis of multiple fixture faults in machining processes using designated component analysis. *Journal of Manufacturing Systems*, 23(4):309 315.

Camelio, J. A., Hu, S. J., and Ceglarek, D. (2004b). Impact of fixture design on sheet metal assembly variation. *Journal of Manufacturing Systems*, 23(3):182 193.

Camelio, J. A., Hu, S. J., and Marin, S. P. (2004c). Compliant assembly variation analysis using component geometric covariance. *Journal of Manufacturing Science and Engineering, Transactions of the ASME*, 126(2):355 360.

Camelio, J. A., Hu, S. J., and Yim, H. (2005). Sensor placement for effective diagnosis of multiple faults in fixturing of compliant parts. *Journal of Manufacturing Science and Engineering, Transactions of the ASME*, 127(1):68 74.

Cao, J., Lai, X., Jin, S., and Lin, Z. (2007). A systematic method of adaptive joint design considering different assembly sequence in sheet metal product. *International Journal of Advanced Manufacturing Technology*, 34(5-6):457 463.

Cao, T. and Rastogi, Chetan., a. C. H. (2001). Application of variation simulation in body assembly process design. In *SAE 2001-01-3064*.

Ceglarek, D. and Shi, J. (1996). Fixture failure diagnosis for auto body assembly using pattern recognition. *Journal of Engineering for Industry*, 118:55 66.

Chang, M. and Gossard, D. C. (1997). Modeling the assembly of compliant, non-ideal parts. *CAD Computer Aided Design*, 29(10):701 708.

Chang, S. and Ravathur, J. (2005). Computer vision based non-contact surface roughness assessment using wavelet transform and response surface methodology. *Quality Engineering*, 17(3):435 451.

Chapman, C, B. and Pinfold, M. (1999). Design engineeringa need to rethink the solution using knowledge based engineering. *Knowledge-Based Systems*, 12:257 267.

Chapman, C, B. and Pinfold, M. (2001). The application of a knowledge based engineering approach to the rapid design and analysis of an automotive structure. *Advances in Engineering Software*, 32:903 912.

Chen, G., Chen, J., Zhao, Z., and Ruan, X, Y. (2005). An object-oriented hierarchical case representation of automotive panels in a computer-aided process planning system. *International Journal of Advanced Manufacturing Technology*, 26:1323 1330.

Chen, G., Zhou, J., Cai, W., Lai, X., Lin, Z., and Menassa, R. (2006a). A framework for an automotive body assembly process design system. *CAD Computer Aided Design*, 38(5):531 539.

Chen, K. S., Huang, M. L., and Li, R. K. (2001). Process capability analysis for an entire product. *International Journal of Production Research*, 39(17):4077 4087.

Chen, Q., Yang, S., and Li, Z. (1999a). Surface roughness evaluation by using wavelets analysis. *Precision Engineering*, 23(3):209 212.

Chen, Q., Yang, S., and Li, Z. (1999b). Surface roughness evaluation by using wavelets analysis. *Precision Engineering*, 23:209 212.

Chen, S., Lin, Z., Zhang, Yizhu, and Li, Y. (2006b). A parametric study of sheet metal joints for dimensional integrity. *International Journal of Advanced Manufacturing Technollogy*, 29:446 452.

Choi, S. W., Park, J. H., and Lee, I.-B. (2004). Process monitoring using a gaussian mixture model via principal component analysis and discriminant analysis. *Computers and Chemical Engineering*, 28(8):1377 1387.

Clements, J, A. (1989). Process capability calculations for non-normal distributions. *Quality Progress*, 22:95 100.

Cootes, T. F., J, T. C., H, C. D., and J, G. C. (1992). A trainable method of parametric shape description. *Image and Vision Computing*, 10(5):289 294.

Cootes, T. F. and Taylor, C. J. (1999). A mixture model for representing shape variation. *Image and Vision Computing*, 17:567 73.

Cootes, T. F., Taylor, C. J., Cooper, D. H., and Graham, C. J. (1995). Active shape models - their training and application. *Computer Vision and Understanding*, 61:38 59.

Corporation, C. R. (1998). Estimating economic impacts of new dimensional control technology applied to automobile body manufacturing. *Journal of Technology Transfer*, 23(2):53 60.

Cox, N. D. (1979). Tolerance analysis by computer. *Journal of Quality Technology*, 11(2).

Craig, Roy, R. J. (1999). *Mechanics of Materials*. Wiley.

Dahlstrom, S. and Lindkvist, L. (2007). Variation simulation of sheet metal assemblies using the method of influence coefficients with contact modeling. *Journal of Manufacturing Science and Engineering, Transactions of the ASME*, 129(3):615 622.

Daniel, B. T., West, G. A. W., and Cardew-Hall, M. J. (1997). *Spatial computing: Issues in vision, multimedia, and visualization techniques. Chap. Geometric Variations: Analysis, Optimization and Control.* Singapore: World Scientific.

Daniel, B, T. (1998). Inspecting 3d objects using deformable shape models. Master s thesis, Curtin University of Technology.

Daubechies, I. (1992). *Ten Lectures on Wavelets*. Number 61 in CSMS/NSF Series in Applied Mathematics. SIAM Publications.

Ding, Y., Ceglarek, D., and Shi, J. (2002a). Fault diagnosis of multistage manufacturing processes by using state space approach. *Journal of Solar Energy Engineering, Transactions of the ASME*, 124(2):313 322.

Ding, Y., Shi, J., and Ceglarek, D. (2002b). Diagnosability analysis of multi-station manufacturing processes. *Journal of Dynamic Systems, Measurement and Control, Transactions of the ASME*, 124(1):1 13.

Duda, R, O., Hart, P, E., and Stork, D, G. (2001). *Pattern Classification*. John Wiley & Sons, Inc.

Fan, X., Masters, I., Roy, R., and Williams, D. (2007). Simulation of distortion induced in assemblies by spot welding. *Proceedings of the Institution of Mechanical Engineers, Part B: Journal of Engineering Manufacture*, 221(8):1317 1327.

Ferrari, D., West, G., Rolfe, B, F., and Cardew-Hall, M. (2006). Free-form feature representation and comparison. *Proceedings of the ASME 2006 International Design and Engineering Technical Conference, September 10-13, Philadelphia, Pennsylvania, USA, DETC2006-99066*.

Gao, J., Chase, K. W., and Magleby, S. P. (1995). Comparison of assembly tolerance analysis by the direct linearization method and modified monte carlo simulation methods. *Proceedings of the ASME Design Engineering Technical Conference*, pages 353 360.

Garcia Guzman, L., Hammet, P., and Herrin, G. (2004). Understanding multivariate components - sheet metal assembly relationships using dimensional slow build studies. *International Journal of Production Research*, 42(13):2651 2666.

Gershenfeld, N. (1998). *The Nature of Mathematical Modeling*. Cambridge University Press.

Gerth, R. (2006). Virtual functional build: A case study. In *Virtual Engineering, Virtual/Digital Technology and Rapid Prototyping or SAE Technical paper series (SP-2000)*.

Gerth, R. J. and Baron, J. (2003). Integrated build: a new approach to building automotive bodies. *International Journal of Automotive Technology and Management*, 3(3/4):185 201.

Girolami, M. and He, C. (2003). Probability density estimation from optimally condensed data samples. *IEEE Transactions on Pattern Analysis and Machine Intelligence*, 25(10):1253 1264.

Glancy, C. G. and Chase, K. W. (1999). A second order method for assembly tolerance analysis. In *Proceedings of the 1999 ASME Design Engineering Technical Conferences, September 12-15, Las Vegas, Nevada, DETC99/DAC-8707*, pages 1 8.

Greegard, L. and Strain, J. (1991). The fast gauss transform. *Journal of Scientific Computing (SIAM)*, 2:79 94.

Gresham, R., Hodgson, P., Smith, J., and Cardew-Hall, M. (2001). Data capture and analysis system for sheet metal forming problems. *Proceedings of Sheet Metal 2001 9th International Conference, ACCO C.V., Belgium*, pages 521 527.

Hall, P. (1987). On kullback-leibler loss and density estimation. *The Annals of Statistics*, 15(4):1491 1519.

Hammet, P., Baron, J., and Smith, D. (1999). Automotive body measurement system capability. Technical report, Auto/Steel Partnerships online database.

Han, C, P. (2006). Effect of testing normality on estimating process capability indices. *Quality Engineering*, 18:391 395.

Hill, A., F, C. T., and J, T. C. (1993). Model-based interpretation of 3d medical images. *British Machine Vision Conference, BMVA Press*, 2:339 348.

Hoffman, K. and Santosa, F. (2003). A simple model of sheet metal assembly. *SIAM Review*, 45(3):558 573.

Hu, M., Lin, Z., Lai, X., and Ni, J. (2001). Simulation and analysis of assembly processes considering compliant, non-ideal parts and tooling variations. *International Journal of Machine Tools and Manufacture*, 41(15):2233 2243.

Hu, S. and Wu, S. (1992). Identifying sources of variation in automobile body assembly using principal component analysis. *Transactions for NAMRI/SME*, 20.

Hu, S. J. (1997). Stream of variation theory for automotive-body assembly. *CIRP Ann. Manuf. Technol.*, 46(1):1 6.

Huang, W., Ceglarek, D., and Zhou, Z. (2004). Tolerance analysis for design of multistage manufacturing processes using number-theoretical net method (nt-net). *International Journal of Flexible Manufacturing Systems*, 16(1):65 90.

Jiang, X, Q., Blunt, R., and Stout, K, J. (2001). Lifting wavelet for three-dimensional surface analysis. *International Journal of Machine Tools & Manufacture*, 41:2163 2169.

Jin, J. and Shi, J. (1999). State space modelling of sheet metal assembly for dimensional control. *Transactions of the ASME*, 121:756 762.

Josso, B. and Burton, D, R. a. L. M. J. (2001). Wavelet surface roughness analysis and characterisation. *Computer methods in applied mechanics and engineering*, 191:829 842.

Keller, G. and Warrack, B. (1997). *Statistics for Management and Economics*. Duxbury Press.

Keller, M. (1989). *Rude Awakening: The Rise, Fall and Struggle for Recovery of General Motors.* Morrow, New York.

Khan, A., Ceglarek, D., Shi, J., Ni, J., and Woo, T. C. (1999). Sensor optimization for fault diagnosis in single fixture systems: A methodology. *Journal of Manufacturing Science and Engineering*, 121:109 117.

Kung, S., Diamantaras, K., and Taur, J. (1994). Adaptive principal component extraction (apex) and applications. *IEEE Transactions on Signal Processing*, 42(5):1202 1271.

Lavoue, G., Dupont, F., and Baskurt, A. (2005). A new cad mesh segmentation method, based on curvature tensor analysis. *CAD Computer Aided Design*, 37(10):975 987.

Lee, S, W., Yoon, J, W., and Yang, D, Y. (1999). Comparative investigation into the dynamic explicit and the static implicit method for springback of sheet metal stamping. *Engineering Computations*, 16:347 373.

Lian, J., Lai, X, M., Lin, Z, Q., and Yao, F, S. (2002). Application of data mining and process knowledge discovery in sheet metal assembly variation diagnosis. *Journal of Materials Process Technology*, 129:315 320.

Liao, G. (2006). Clamp shimming optimization for minimizing sheet-metal assembly deformation. *Proceedings of the Institution of Mechanical Engineers, Part B: Journal of Engineering Manufacture*, 220(5):707 713.

Liao, G. Y. (2003a). A genetic algorithm approach to weld pattern optimization in sheet metal assembly. In *American Society of Mechanical Engineers, Mechanical Engineering Division Publication (MET)*, volume 3, pages 53 58, Washington, DC, United States.

Liao, G. Y. (2007). Employing shimming for clamping compliant sheet-metal parts. *International Journal of Computer Applications in Technology*, 28(1):46 51.

Liao, X. and Wang, G. (2005a). Employing fractals and fem for detailed variation analysis of non-rigid assemblies. *International Journal of Machine Tools & Manufacture*, 45:445 454.

Liao, X. and Wang, G. (2005b). Wavelets-based method for variation analysis if non-rigid assemblies. *International Journal of Machine Tools & Manufacture*, 45:1551 1559.

Liao, Y. G. (2003b). A genetic algorithm-based fixture locating position and clamping schemes optimization. *Proceedings of the IMechE Part B. Journal of Engineering Manufacture*, 217(8):1075 1083.

Liao, Y. G. (2005). Optimal design of weld pattern in sheet metal assembly based on a genetic algorithm. *International Journal of Advanced Manufacturing Technology*, 26(5):512 516.

Liu, C. and Hu, J. (1995a). An offset finite element model and its applications in predicting sheet metal assembly variation. *International Journal of Machining, Tools and Manufacturing*, 35(11):1545 1557.

Liu, C. S. (1995). *Variation simulation for deformable sheet metal assembly.* PhD thesis, University of Michigan.

Liu, S. C. and Hu, S, J. (1997a). Variation simulation for deformable sheet-metal assemblies using finite element methods. *Transactions of the ASME*, 119:368 374.

Liu, S. C. and Hu, S. J. (1995b). Spot weld sequence in sheet metal assembly: Its analysis and synthesis. In *American Society of Mechanical Engineers, Manufacturing Engineering Division (MED)*, volume 2-2, pages 1145 1156, San Francisco, CA, USA.

Liu, S. C. and Hu, S. J. (1997b). Parametric study of joint performance in sheet metal assembly. *International Journal of Machine Tools & Manufacture*, 37(6):873 884.

Ma, J. (2005). Towards artifact-free characterization of surface topography using complex wavelets and total variation minimization. *Applied Mathematics and Computation*, 170:1014 1030.

Magid, E., Soldea, O., and Rivlin, E. (2007). A comparison of gaussian and mean curvature estimation methods on triangular meshes of range image data. *Computer Vision and Image Understanding*, 107:139 159.

Majeske, K. D. and Hammett, P. C. (2000). The functional build approach to tolerance development. *IEEE Transactions on Engineering Management*, 47(4):493 496.

Manarvi, I. A. and Juster, N. P. (2004). Framework of an integrated tolerance synthesis model and using fe simulation as a virtual tool for tolerance allocation in assembly design. *Journal of Materials Processing Technology*, 150(1-2):182 193.

Marron, J. S. (1988). Automatic smoothing parameter selection: A survey. *Empirical Economics (EMPEC)*, 13:187 208.

Merkley, K. G. (1998). *Tolerance analysis of compliant assemblies*. PhD thesis, Department of Mechanical Engineering, Brigham Young University.

Muller, K., Mika, S., Ratsch, G., Tsuda, K., and Scholkopf, B. (2001). An introduction to kernel-based learning algorithms. *IEEE Transactions on neural networks*, 12(2):181 201.

Placek, C. (1989). Motorola, westinghouse nuclear fuel unit, globe metallurgical named malcolm bridge national quality award winners. *Quality*, pages 13 14.

Rathi, Y., Dambreville, S., and Tannenbaum, A. (2006). Statistical shape analysis using kernel pca. In *Proceedings of SPIE - The International Society for Optical Engineering*, San Jose, CA, United States.

Rolfe, B. F., Cardew-Hall, M. J., Abdallah, S. M., and West, G. A. W. (2003). A shape error metric for sheet metal forming and its application to springback. *Journal of Manufacturing Science and Engineering, Transactions of the ASME*, 125(3):468 475.

Rong, Q., Ceglarek, D., and Shi, J. (2000). Dimensional fault diagnosis for compliant beam structure assemblies. *Journal of Manufacturing Science and Engineering*, 122:773 780.

Sain, S. R. (2002). Multivariate locally adaptive density estimation. *Computation Statistical and Data Analysis*, 39:165 86.

Sain, S. R., Baggerly, K. A., and Scott, D. W. (1994). Cross-validation of multivariate densities. *Journal of the American Statistical Association, Theory and Methods*, 49(427):807 817.

Scott, D. W. (1992). *Multivariate density estimation. Theory, Practice and visualization*. John Wiley & Sons, Inc.

Shapiro, S, S. and Wilk, M, B. (1965). An analysis of variance test for normality (complete samples). *Biometrika*, 52:591 611.

Shapiro, S. S. and Gross, A. J. (1981). *Statistical Modeling Techniques*. Marcel Dekker, Inc., New York.

Sheffer, A. and de Sturler, E. (2001). Parameterization of faceted surfaces for meshing using angle-based flattening. *Engineering and Computers*, 17:326 337.

Shewart, W, A. (1931). *Economic control of quality of manufactured product*. Van Nostrad.

Shiu, B., Shi, J., and Tse, K. (2000). Dimensional quality of sheet metal assembly with welding-induced internal stress. *Proceedings of the Institution of Mechanical Engineers, Part D: Journal of Automobile Engineering*, 214(7):693 704.

Shiu, B. W., Li, B., Fu, X. Y., and Liu, Y. (2002). Tolerance allocation of sheet metal assembly using a finite element model. *JSME International Journal, Series C: Mechanical Systems, Machine Elements and Manufacturing*, 45(1):258 266.

Shiu, B, W., Apley, D, W., Ceglarek, D., and Shi, J. (2003). Tolerance allocation for compliant beam structure assemblies. *IEEE Transactions*, 35:329 342.

Shiu, B, W., Ceglarek, D., and Shi, J. (1997). Flexible beam-based modeling of sheet metal assembly for dimensional control. *Transactions of NAMRI/SME*, 25:49 54.

Sirovich, L. and Kirby, M. (1987). A low-dimensional procedure for the characterization of human faces. *J. Opt. Soc. Amer. A*, 4(3):519 524.

Smith, J., Cardew-Hall, M. J, P. V., and Hodgson, P. (2004). Design, implementation and use of a knowledge acquisition tool for sheet metal forming. *24th ASME Computers In Engineering Conference, Salt Lake City, USA*.

Smith, W. A. P. and Hancock, E. R. (2006). Face recognition using 2.5d shape information. In *CVPR '06: Proceedings of the 2006 IEEE Computer Society Conference on Computer Vision and Pattern Recognition*, pages 1407 1414, Washington, DC, USA. IEEE Computer Society.

Soderberg, R., Linkvist, L., and Dahlstrom, S. (2006). Computer-aided robustness for compliant assemblies. *Journal of Engineering Design*, 17(5):411 428.

Somerville, S. and Montgomery, D. (1996). Process capability indices and non-normal distributions. *Quality Engineering*, 19(2):305 316.

Sozou, P. D., Cootes, T. F., and Di Mauro, E. C. (1994). A nonlinear generalization of pdms using polynomial regression. *British Machine Vision Conference*, pages 397 406.

Sozou, P. D., Cootes, T. F., and Di Mauro, E. C. (1995). A nonlinear point distribution model using a multi-layer perceptron. *British Machine Vision Conference*, pages 107 116.

Taguchi, G. (1986). *Introduction to quality engineering.* Asian Productivity Organization, Tokyo.

Takezawa, N. (1980). An improved method for establishing the process-wise quality standard. *Reports of Statistical Application Research, JUSE*, 27:63 75.

Theodoridis, S. and Koutroumbas, K. (2006). *Pattern Recognition.* Academic Press, USA, 3rd edition.

Trucco, E. and Fisher, R, B. (1995). Experiments in curvature-based segmentation of range data. *IEEE Transactions on Pattern Analysis and Machine Intelligence*, 17(2):177 182.

Vieira, M. and Shimada, K. (2005). Surface mesh segmentation and smooth surface extraction through region growing. *Computer Aided Geometric Design*, 22(8):771 792.

Wahba, G. (1990). *Spline models for observational data.* Society for Industrial and Applied Mathematics.

Watanabe, C. and Ane, Bernadetta, K. (2004). Constructing a virtuous cycle of manufacturing agility: concurrent roles of modularity in improving agility and reducing lead time. *Technovation*, 24:573 583.

Wu, S. M. and Hu, S. (1990). Impact of 100 percent in-process measurement on statistical process control in automobile body assembly. *American SOC of Mechanical Engineer, Production Engineering Division,*, 44:433 448.

Wu, Y., Zhou, Z., Cui, G., and Peng, H. (2006). Assembly variation analysis for deformable sheet metal based on pseudo random numbers. *WSEAS Transactions on Systems*, 5(6):1510 1516.

Xie, L. S. and Hsieh, C. (2002). Clamping and welding sequence optimization for minimizing cycle time and assembly deformation. *International Journal of Materials and Product Technology*, 17(5/6):389 399.

Xiong, C., Rong, Y., Koganti, R, P., Zaluzec, M, J., and Wang, N. (2002). Geometric variation prediction in automotive assembling. *Assembly Automation*, 22(3):260 269.

Xiong, Y., Chen, W., Apley, D., and Ding, X. (2007). A non-stationary covariance-based kriging method for metamodelling in engineering design. *International Journal for Numerical Methods in Engineering*, 71(6):733 756.

Yang, K. (1996). Improving automotive dimensional quality by using principal component analysis. *Quality and Reliability Engineering International*, 12(6):401 409.

Yi, P., Liang, F., and Hseih, C. (2005). Clamp shimming optimisation for minimising assembly deformation. *SAE technical paper series, 2005-01-0824*.

Yue, J., Camelio, J. A., Chin, M., and Cai, W. (2007). Product-oriented sensitivity analysis for multistation compliant assemblies. *Journal of Mechanical Design, Transactions of the ASME*, 129(8):844 851.

Zhang, B. and Ni, J. (2003). Adaptive product, process and tooling design strategy for optimal dimensional quality of automotive body assemblies. *Journal of Manufacturing Science and Engineering, Transactions of the ASME*, 125(4):835 843.

Zitova, B. and Flusser, J. (2003). Image registration methods: a survey. *Image and Vision Computing*, 21:977 1000.